Soviet Physics

CRYSTALLOGRAPHY

Vol. 1, No. 2, pp. 113-204

March-April, 1956

Digitized by the Internet Archive
in 2023

https://archive.org/details/crystallography-reports_march-april-1956_1_2

SOVIET PHYSICS – CRYSTALLOGRAPHY VOL. 1, NO. 2 MAR.-APR., 1956

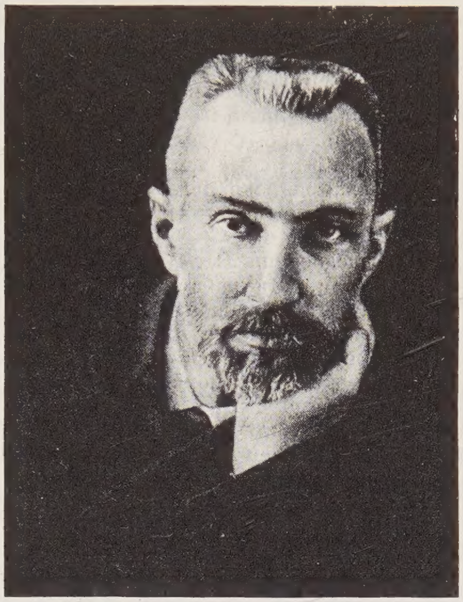

PIERRE CURIE
(On the Fiftieth Anniversary of His Death)

April 19, 1956, is the 50th anniversary of the tragic death of the outstanding French scientist Pierre Curie.

Pierre Curie was born in 1859 in Paris into the family of a doctor. His early education for middle school was obtained at home. His striking ability at mathematics, especially solid geometry, enabled him to obtain his baccalaureate in natural sciences at the age of sixteen; he became a student in the physics department at the Sorbonne.

At the age of 19 he became an assistant in the department of experimental physics at the University of Paris; this marked the start of his scientific career. His first paper was on the determination of the wavelengths of thermal radiation. Shortly afterwards he took up crystallography, with emphasis on crystal symmetry. Crystallography was his sole interest from 1879 to 1891, especially crystal physics; later, he worked on radioactivity, but remained interested in crystals.

Pierre and his elder brother, Jacques (a mineralogist), concluded that deformation should produce electrical polarization in certain crystals. This was strikingly confirmed shortly afterwards; in 1880 they discovered piezoelectricity, which they studied in great detail on quartz crystals. They established Curie's first and second laws for the longitudinal and transverse piezoelectric effects in quartz, which remain accepted even today. They also observed the inverse effect predicted by Lippman, namely deformation of a crystal linearly dependent on the applied electric field.

The piezoelectric effect proved to be of considerable scientific importance; the brothers Curie used a quartz plate to measure small charges and currents, and the device they developed for this purpose proved of value in the work on radioactivity. Piezoelectricity is now widely used in radio, electronics, hydroacoustics, and instruments generally.

Pierre Curie's papers on symmetry form a major part of his contribution to crystallography; these he wrote mainly from 1883 onwards, after he had been appointed professor in the school of physics and chemistry. He derived the limiting point-symmetry groups for crystals, which correspond to the symmetries of homogeneous anisotropic media with axes of infinite order. The derivation of these groups enabled him to give a rational classification of crystals on the basis of the possible presence of various physical properties. He linked his work on symmetry closely to these physical properties, as when he stated that "I consider that it would be of interest in the study of physical phenomena to bear in mind the considerations of symmetry so familiar to the crystallographer."

His work over many years led to the formulation of the general principle of symmetry, which he gave in its final form in 1893-95, as follows: "When certain causes give rise to known consequences,the symmetry elements of the causes must be reproduced in the consequences. When known consequences contain a known dissymmetry, this latter must lie in the causes giving rise to the consequences. Propositions contrary to these two are incorrect, at least in practice, i.e., that consequences can be more symmetrical than the causes giving rise to them."

Pierre Curie also made a major contribution to the theory of crystal growth, which had been founded by Gibbs previously, though this was unknown to him at the time. The basic concept was that a crystal in equilibrium with a solution must have a shape such as to correspond to minimum surface energy subject to constant volume.

In 1891, Pierre Curie began a long series of studies on the magnetic properties of bodies as functions of temperature; these formed the basis of a dissertation submitted in 1895. His results on paramagnetic, ferromagnetic, and diamagnetic bodies were of considerable importance; the results for paramagnetic bodies are known under the name Curie's law (susceptibility inversely proportional to the absolute temperature). He also observed that iron has a special point above which it ceases to be ferromagnetic (the Curie point). Similar relationships have since been deduced for ferroelectrics.

He also participated in researches by his wife, Maria Curie-Sklodowska, on radioactivity; this led to their joint discovery of polonium and radium in 1898, and in 1899 to the first observation of colors produced by irradiation (in glass and porcelain acted on by radium rays). They also showed that these rays affect the cells of organisms. In 1903, Pierre Curie observed the spontaneous production of heat by radium salts, which proved that radioactivity is accompanied by the release of much energy; this pointed the way to the idea that radioactivity is a result of atomic transformations. The Curies made a detailed study of this radiation, and showed that the decay was not detectably dependent on the external conditions. This led Pierre Curie to state that decay constants could serve as time standards and could be used to determine the ages of rocks. In 1903, the Curies and Becquerel were awarded the Nobel prize for their work on radioactivity.

In 1904, a new department was set up for Pierre Curie in the University of Paris (a resolution of the French parliament was required to do this); his post in the school of physics and chemistry was taken over by one of his students,Paul Langevin, who later also became a famous physicist. In 1905, Pierre Curie was made a member of the Paris Academy of Sciences.

The work on radioactivity was continued after his death (April 19, 1906) by his wife, who replaced him as professor at the Sorbonne. Later, this department was headed by their daughter,Irene Joliot-Curie, who died in March of this year. The work of Frederic and Irene Joliot-Curie together led to a most important discovery, artificial radioactivity, which further increased the scientific fame associated with the name of Curie.

The name of Pierre Curie is eternally recorded in the annals of science. In addition to being an energetic and exceptionally capable scientist, Pierre Curie was a warm and humane man. A good indication of this is given by his words on receiving the Nobel prize: "It is not difficult to foresee that radium in the wrong hands could be extremely dangerous; this raises the question whether it is best for mankind to know the secrets of nature, whether man is sufficiently adult to use them properly, or whether such knowledge will only do him harm. Nobel's discovery is here characteristic. Powerful explosives have enabled men to perform great works, but they are also a fearful means of destruction in the hands of great evildoers who drive men to war. I am one of those who, like Nobel, consider that all new discoveries will, in the end, bring mankind greater happiness than harm."

SOVIET PHYSICS – CRYSTALLOGRAPHY VOL. 1, NO. 2 MAR.-APR., 1956

KINEMATIC THEORY OF INTENSITIES IN ELECTRON-DIFFRACTION PATTERNS

Part 2. Patterns from Textures and Polycrystalline Aggregates

B. K. Vainshtein

Institute of Crystallography, Academy of Sciences of the USSR

Translated from Kristallografiya, Vol. 1, No. 2,
pp. 150-158, March-April, 1956
Original article submitted December 23, 1955

Formulas are deduced for the intensities in texture and polycrystalline patterns from the distribution function of the angles taken up by the crystallites. This function has two components in the case of a texture: a density of $n/2\pi$ constant at all angles (n is the number of crystallites in the specimen) and a distribution $f(\alpha)$ of the axes of the crystallites around the texture axis. An expression is derived for the integral intensity of arcs, this being independent of the form of $f(\alpha)$, and also one for the intensity at the center of the arcs, which is dependent on $f(\alpha)$. The distribution-function concept is used to discuss the intensities of the rings given by a polycrystalline aggregate.

Angular Distribution Function for Crystallites

Part 1 [1] dealt with the intensities of spot patterns from ideal or mosaic single crystals. The reflection intensities were deduced by reference to an angular distribution function for the crystallites (and hence for the reflecting planes in them). The same concept is used here. Let $f(\alpha)$ be the angular density of the normals to a given plane; the range α to $\alpha + d\alpha$ contains $f(\alpha)d\alpha$ crystallites, and the integral over all possible positions equals the number of crystallites in the specimen:

$$\int f(\alpha)\,d\alpha = n = V'/V, \tag{1}$$

where V is the volume of a crystallite and V' is the volume of the specimen.[1]

It is convenient in calculating the intensity to express the distribution over solid angles in terms of components over plane angles; condition (1) applies to each such component.

Texture patterns are widely used in electron diffraction [2, 3], specimens with platy textures being most common, in which the crystallites have some major crystallographic face parallel to the substrate but are disordered in azimuth. The direction of the normal to this face is the texture axis. Needle textures are relatively rare [4]; in these the texture axis is a direction common to the axes of all the needles, which are randomly rotated around that direction. The axis of a platy texture is normal to the substrate and coincides with one of the axes of the reciprocal lattice; the axis of a needle texture lies in the plane of the substrate and coincides with one of the axes of the atomic lattice [3]. The reciprocal lattice for a texture of either type is a set of concentric rings and has cylindrical symmetry; the texture axis is an axis of infinite order.

We have seen in Part 1 that the distribution function can be expressed in terms of components for plane angles that correspond to rotation around certain specified axes.

The first such component is $f(\alpha_1)$, the density around the texture axis (range 2π); this is constant and is given by (1) as

$$f(\alpha_1)\int_0^{2\pi} d\alpha_1 = n, \quad f(\alpha_1) = n/2\pi. \tag{2}$$

A real specimen is imperfect, so the special directions in the crystallites (all parallel in the ideal case) are spread over a certain solid angle (Fig. 1a), whose magnitude defines the deviation

---

[1] V' is, of course, the volume of the specimen traversed by the electron beam, and n is the number of crystallites in that volume.

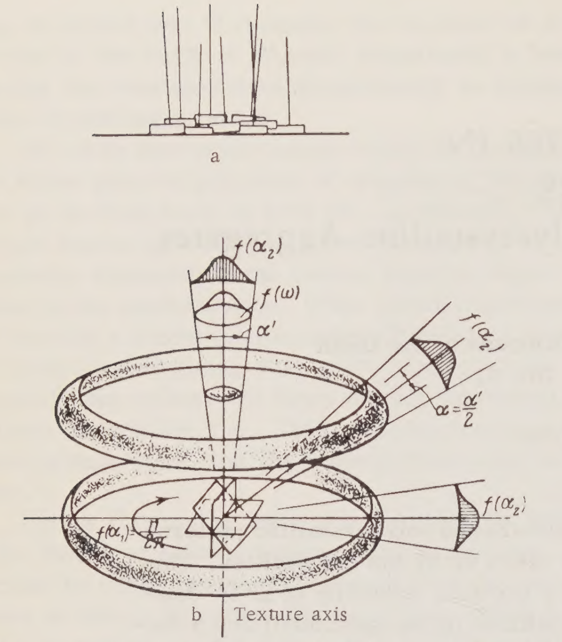

Fig. 1. a) Structure of a textured specimen, and b) component distribution functions $f(\alpha_1)$ and $f(\alpha_2)$ for the angles of the normals with respect to different planes.

from perfection. This spread is responsible for the conversion of the reciprocal lattice rings (infinitely thin) into spherical belts (Fig. 1b), so the reflections corresponding to the latter take the form of short arcs [2, 3]. The spread is not uniform, i.e., is characterized by a second distribution $f(\omega)$. It is convenient to replace this spread in the solid angle α by $f(\alpha_2)$, the projection of this distribution on some plane angle α_2 (the cylindrical symmetry makes the choice arbitrary), which (Fig. 1b) defines the form of the nodes on the texture axis and of the cross sections of the other ring nodes. Let α' be the angular range in which $f(\alpha_2)$ is finite; then formula (21) of [1] shows that the density at the peak is about twice the mean of $f(\alpha_2)$, i.e., that

$$f(\alpha_2)_{\max} \approx 2\frac{1}{\alpha'}\int f(\alpha_2)\,d\alpha_2 = \frac{2n}{\alpha'} = \frac{n}{\alpha}, \tag{3}$$

where $\alpha = \alpha'/2$ is the effective angular width of $f(\alpha_2)$.

It is a matter of no importance how the intensity in an arc is distributed if we are interested only in the integral intensity; the angular spread around the texture axis is then unimportant, and $f(\alpha_2)$ should not appear in the formula for the integral intensity. But another approach is to measure the intensity at the center of the arc (i.e., over a small area); this local intensity will be dependent on $f(\alpha_2)$.

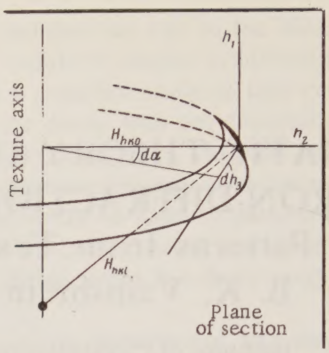

Fig. 2. Scheme for calculating the intensity of a reflection for a straight texture.

The distribution function for a polycrystalline specimen is as follows. The crystallites take up all spatial orientations at random, and the normals to any reflecting plane are uniformly distributed throughout a solid angle of 4π. The distribution function with respect to solid angle is then constant at $n/4\pi$.

Integral Intensities in Texture Patterns[2]

Straight Textures. By this is meant the pattern from a needle texture with the specimen at right angles to the beam ($\varphi = 0$), and also the pattern from a platy texture in reflection. The texture axis is perpendicular to the beam in both cases. Such texture patterns would also occur with platy textures in transmission for $\varphi = 90°$, but this cannot be realized.

The integral intensity is calculated precisely as in [1] for mosaic specimens, by taking the integral of the interference function over two directions in the plane of the screen, which in this case coincide with directions h_1 and h_2 in the reciprocal lattice, which is represented on a scale $L\lambda$ on the screen (Fig. 2). Then formula (11) of [1] applies:

$$I_{hkl} = J_0\lambda^2\left|\frac{\Phi}{\Omega}\right|^2\frac{A_1A_2}{a_1^2a_2^2}G. \tag{4}$$

Formula (13) of [1] gives

$$G = \int f(\alpha)\frac{\sin^2\pi A_3h_3}{(\pi\alpha_3h_3)^2}\,d\alpha, \tag{5}$$

which is defined by the integral of the interference function in the third direction, as modified by the distribution function. Only the first component in (2) is important for the integral intensity of an arc, so by $d\alpha$ in (5) we should understand an element of rotation around the texture axis. This elementary angle is dependent solely on the distance of the reflection from the texture axis in the pattern, which corresponds in reciprocal space to the horizontal component of the reciprocal-lattice vector H_{hkl} (Fig. 2), if, as is usual, we denote the texture axis by c^*. This horizontal component is H_{hk0} for an orthogonal lattice. The formulas may be applied to oblique lattices if by H_{hk0} (or d_{hk0}) is understood the corresponding horizontal component. Then,

---

[2] See [5] for some preliminary evidence on this.

$$d\alpha = \frac{dh_3}{H_{hk0}} = d_{hk0}\cdot dh_3 = \frac{dh_3\cdot L\lambda}{R}, \tag{6}$$

where R is the distance of the reflection from the vertical axis of the pattern (a quantity that is measured). From (2), since the integral of the interference function is, from (7) of [1], equal to A_3/a_3^2, etc.,

$$G = \frac{A_3 n}{a_3^2}\,\frac{d_{hk0}}{2\pi} = \frac{A_3 n}{a_3^2}\,\frac{L\lambda}{2\pi R}. \tag{7}$$

It is of interest to compare (7) with the analogous expression (16) of [1], where $d_{hk0}/2\pi$ is replaced by d_{hkl}/α, the other first factors being the same. The replacement of d_{hkl} by d_{hk0} reflects the fact that the angular spread in a mosaic is the same for all directions, i.e., occurs around the 000 point in the reciprocal lattice, whereas, in a texture it occurs around a special direction (the texture axis). The small quantity α (the effective angular spread in a mosaic, about $^1/_{15}$ radian) is replaced by a large one, 2π, so the reflection arises from far fewer crystals (about $^1/_{100}$).

Only a very small part is effective out of the complete circle produced from the node; the intensities in texture patterns are therefore very small fractions of the initial intensity, so kinematic scattering applies very closely provided, of course, that the blocks do not exceed the critical size. Dynamic effects may occur in rare cases, but these are far more common in mosaic materials. The reason is that a textured or polycrystalline specimen must contain much smaller blocks than does a mosaic one of the same volume if the distribution over all orientations is to be uniform.

Substituting (7) into (4), and using (2), we have

$$I_{hkl} = J_0\lambda^2\left|\frac{\Phi}{\Omega}\right|^2 V'\,\frac{d_{hk0}\,p}{2\pi} \tag{8a}$$

and

$$\frac{I_{hkl}}{J_0 S} = \lambda^2\left|\frac{\Phi}{\Omega}\right|^2 t\,\frac{d_{hk0}}{2\pi}\,p, \tag{8b}$$

where V', S, and t are the volume, area, and thickness of the film, p being the repeat factor (see below). R may be measured directly on the pattern, in which case the d_{hk0} of (8a) and (8b) should be replaced by $L\lambda/R$.

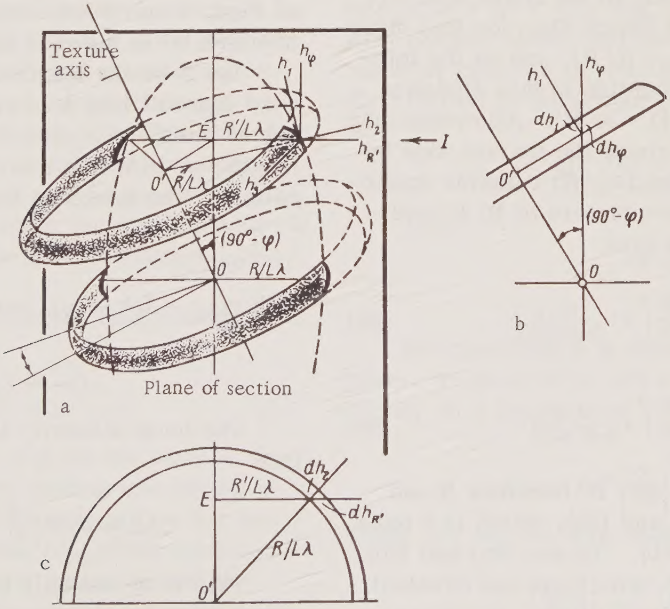

Fig. 3. Calculation of the intensity of a reflection in an oblique-texture pattern. a) Inclined section of ring; b) form of this section on direction I; c) form in ring on arrow II.

The $00l$ reflections (on the texture axis) do not obey these formulas, because they have R equal to 0 and $d_{hk0} = d_{000} = \infty$; their integral intensities may be calculated by noting that the angular spread of these planes over 2π is unimportant (the planes reflect without relation to their azimuthal position). But they appear in the reflecting position on account of $f(\alpha_2)$, α_2 here being reckoned perpendicular to the screen; but this means that formula (18) of [1] (for a mosaic single crystal) is applicable to the $00l$ reflections, so the $d_{hk0}/2\pi$ of (8a) and (8b) should be replaced by d_{00l}/α, where α is the effective angular spread of the texture axis; p = 1.

Oblique Texture. An oblique-texture pattern is obtained when a platy texture is inclined at an oblique angle φ (usually about 60°); the reflections lie on ellipses [2,3]. Figure 3a illustrates the intersection of the rings in the reciprocal lattice by a plane (the reflection sphere). The following points are important here. The integration for (4) was taken over two directions in the plane of the screen coincident with the h_1 and h_2 directions of the reciprocal lattice. An inclined specimen gives an element of length in the vertical direction on the pattern (Fig. 3) of dh_φ as $dh_1/\sin\varphi$, so the integral of the interference function in this direction will not be A_1/a_1^2 [one of the factors in (4)], but $A_1/a_1^2 \sin\varphi$. The horizontal direction also does not coincide with h_2; Fig. 3c shows that, if the horizontal coordinate R' of the reflection is known, together with the minor semiaxis R of the ellipse (i.e., the radius of the ring in the reciprocal lattice), then the element of length $dh_{R'}$ for this direction is given by $dh_{R'}/dh_2 = R/R'$, and so the integral of the interference function in this direction will take the value $(A_1/a_2^2) \cdot R/R'$. Allowance may be made for the spread around the texture axis by integrating with respect to $d\alpha_1$; (7) remains applicable. Then we must insert factors of R/R' and $1/\sin\varphi$ in (8a) and (8b) to give

$$I_{hkl} = J_0 \lambda^2 \left| \frac{\Phi}{\Omega} \right|^2 V' \frac{L\lambda \cdot p}{2\pi R' \sin\varphi} \tag{9a}$$

and

$$\frac{I_{hkl}}{J_0 S} = \lambda^2 \left| \frac{\Phi}{\Omega} \right|^2 t \frac{L\lambda \cdot p}{2\pi R' \sin\varphi}. \tag{9b}$$

But $\sin\varphi = 1$ for $\varphi = 90°$; R' becomes R and (9a) and (9b) become (8a) and (8b), which is a particular case of (9a) and (9b). To use (9a) and (9b), we need to know φ and R', which are not constant for the reflections on a given ellipse, but decrease as l increases. We can reduce (9a) and (9b) to a form analogous to (8a) and (8b) by introducing the fictitious interplanar distance

$$d' = \frac{L\lambda}{R' \sin\varphi}, \tag{10}$$

which is greater than d_{hk0} for an oblique texture, but becomes equal to it at $\varphi = 90°$.

Reflections on the vertical axis of the pattern do not obey (9a) and (9b), because R' is 0; in principle, these intensities could be calculated from $f(\alpha_2)$, as for the $00l$ reflections of straight textures, but there is no need for this complicated calculation, because rotation of the specimen will remove the reflection from the region with R' = 0 and split it into two arcs with R' ≠ 0.

We may convert from relative integral intensities for arcs on texture patterns to relative moduli $|\Phi|$ via

$$|\Phi_{hkl}^{\mathrm{rel}}| = \sqrt{I_{hkl}^{\mathrm{rel}} \cdot R' / p}, \tag{11}$$

where R' varies along an ellipse for an oblique texture but is constant for the vertical direction for a straight texture, in which case it can be replaced by $R \sim H_{hk0} = 1/d_{hk0}$.

Local Intensity in a Texture Pattern

The local intensity is the best quantity to measure if the arcs are very broad, namely, I'_{hkl} at the center of an arc. Consider first the case $\varphi = 90°$, where the angular width is governed by the form of $f(\alpha_2)$. The effective angular width of an arc (which is the effective angular width of the spherical belts of Figs. 1 and 2 for a straight texture) is $\alpha \approx \alpha'/2$, in which α' is the real angular width; see (3).

Let Δ be the length of the small part of the arc used (the slit length in microphotometry). The integral intensity is distributed, in effect, over a length $r\alpha$, in which r is the radius of the arc on the pattern. The intensity localized in Δ is then

$$I'_{hkl} = I_{hkl} \frac{\Delta}{r\alpha} \tag{12}$$

with $r_{hkl} = L\lambda/d_{hkl}$, so

$$I'_{hkl} = I_{hkl} \cdot \frac{\Delta \cdot d_{hkl}}{\alpha \cdot L\lambda}. \tag{13}$$

The local intensity at the center of an arc is then

$$I'_{hkl} = J_0 \lambda^2 \left| \frac{\Phi}{\Omega} \right|^2 V' \frac{d_{hkl} d_{hk0}}{\alpha \cdot 2\pi L\lambda} \cdot p. \tag{14}$$

This is so not only for $\varphi = 90°$, but also for any other φ, and so is general, as we now show.

The effective angular width α'' of an arc on an oblique-texture pattern is not equal to α (Fig. 4),

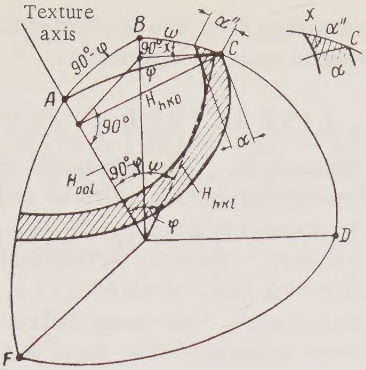

Fig. 4. Determination of α".

but is given by

$$\alpha'' = \alpha / \sin \chi, \tag{15}$$

where χ is a complicated function of φ [5]. The spherical right-angled triangle ABC of Fig. 4 implies that $\cos \varphi = \cos \chi \sin \psi$; $\cos \psi = \cos \omega \sin \varphi$; these transform to $\sin \chi \sin \psi = \sin \varphi \sin \omega$. But $\sin\omega = H_{R'}/H_{hkl}$ and $\sin \psi = H_{hk0}/H_{hkl}$, so (15) and (10) give

$$\alpha'' = \alpha \frac{H_{hk0}}{H_{R'} \sin \varphi} = \alpha \frac{d'}{d_{hk0}}. \tag{16}$$

Then I'_{hkl} is, as in (12),

$$I'_{hkl} = I_{hkl} \frac{\Delta}{r\alpha''} = I_{hkl} \frac{\Delta \cdot d_{hk0}}{r\alpha\, d'} . \tag{17}$$

We substitute (9a) and use (10) to get (14) again, because d' and $\sin \varphi$ cancel, and the dependence on the angle of rotation is lost. This result is entirely in order: a measurement of the local intensity is essentially one of the density of the interference function for a reciprocal-lattice ring, and this cannot be dependent on the angle of rotation of the specimen. The local intensity can also be measured for hk0 reflections without inclining the specimen ($\varphi = 0$) when the reflections take the form of rings; $d_{hk0}d_{hkl}$ in (14) then becomes d^2_{hk0}.

The relative local intensity is then converted to $|\Phi|$ via

$$|\Phi^{\mathrm{rel}}_{hkl}| = \sqrt{I^{\mathrm{rel}}_{hkl} / d_{hkl}\, d_{hk0}\, p}. \tag{18}$$

See [5] on the question of p for the texture method; a general technique for finding this factor is examination of the point reciprocal lattice for the crystal with allowance for the $|\Phi_{hkl}|^2$ for each node (i.e., consideration of the structure factor) together with calculation of the number of point nodes that fuse into a ring node for the given orientation of the texture axis.

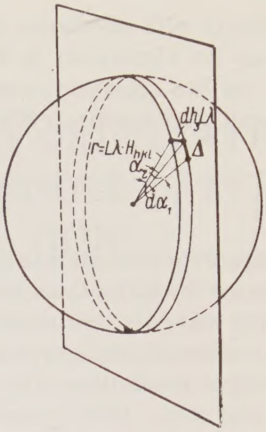

Fig. 5. Scheme for calculation of the local intensity from a polycrystalline aggregate.

Note should be made of the cases characteristic of the hemihedral classes in which a ring node contains crystallographically distinct point nodes, for the electron-diffraction pattern can give only the mean value $(|\Phi_{hkl}|^2 + |\Phi_{\bar{h}kl}|^2)/2$.

Intensities from Polycrystalline Films

The distribution over solid angles is $n/4\pi$ for a polycrystalline film; (4) is found by integration over two directions in the plane of the pattern. The point of interest is usually the local intensity in a ring over a short length Δ. The angular width of this is $\alpha_2 = \Delta/r = \Delta/H_{hkl}L\lambda$ (Fig. 5). Integration with respect to $d\alpha_1$ and multiplication by the plane angle α_2 gives us G, which relates the solid-angle distribution to the product of the two plane ones:

$$G = \frac{n}{4\pi} \frac{d_{hkl} \cdot \Delta}{L\lambda} \int \frac{\sin^2 \pi A_3 h_3}{(\pi a_3 h_3)^2}\, d\alpha_1, \quad d\alpha_1 = \frac{dh_3}{H_{hkl}} . \tag{19}$$

Thus,

$$G = \frac{n\Delta\, d^2_{hkl} \cdot A_3}{4\pi a_3^2} . \tag{20}$$

Incorporating p (a different value is needed here), we have from (19) and (20) that the local intensity in a length Δ is

$$I'_{hkl} = J_0 \lambda^2 \left| \frac{\Phi}{\Omega} \right|^2 V' \frac{d^2_{hkl} \cdot \Delta \cdot p}{4\pi L\lambda} . \tag{21}$$

Then, for the relative values,

$$|\Phi^{\mathrm{rel}}_{hkl}| = \sqrt{I^{\mathrm{rel}}_{hkl} / d^2_{hkl} \cdot p} . \tag{22}$$

Formula (21) is the only intensity formula for electron diffraction that can be derived from an x-ray powder formula with allowance for the small scattering angles for electrons. In this case (and this one only), the two situations are identical: a scattering volume with randomly distributed crystallites.

Conclusions

The kinematic approximation is used to derive intensity formulas for the reflections in electron diffraction from textures and polycrystalline aggregates.A texture pattern containing short arcs is best measured in terms of integral intensities, the $|\Phi|$ being found via (9a), (9b), and (11). More extended arcs make it preferable to measure the local intensity at the center of each arc, the $|\Phi|$ here being found via (14) and (18). The local intensity of a powder ring is given by (21). Textured and polycrystalline specimens, as used in electron diffraction, have small crystallites, so they are much less prone to give dynamic scattering than are mosaic single crystals; the scattering is usually kinematic.

LITERATURE CITED

1. B.K. Vainshtein, "The kinematic theory of electron-diffraction intensities. I. Spot patterns," Kristallografiya, 1 (1956).
2. Z.G. Pinsker, Electron Diffraction [in Russian](1949), pp. 100-105.
3. B.K. Vainshtein, "Electron-diffraction patterns from textures," Tr. Inst. Kristallogr., 6, 174-192 (1951).
4. A.N. Lobachev, Z.G. Pinsker, and B.K. Vainshtein, "The rotation method in electron diffraction," Tr. Inst. Kristallogr., 11, 75-77 (1955).
5. B.K. Vainshtein, "Intensities in oblique-texture electron-diffraction patterns," Tr. Inst. Kristallogr., 6, 193-202 (1951).

DETERMINATION OF THE LAUE CLASS AND ORIENTATION FOR AN UNFACETTED CRYSTAL FROM A SINGLE PATTERN RECORDED WITH POLYCHROMATIC RADIATION FROM THE CRYSTAL AT REST

A. I. Zaslavskii and D. L. Rogachev

Zhdanov University, Leningrad

Translated from Kristallografiya, Vol. 1, No. 2,
pp. 159-164, March-April, 1956
Original article submitted November 1, 1955

It has been usual to deduce the Laue class and orientation of an unfacetted crystal from three patterns recorded on flat film. A new method is proposed for crystals giving highly detailed patterns that employs only a single cylindrical film. The spherical coordinates of reflections and of points of intersection of zonal curves are deduced from a set of curves for ρ = const and φ = const. The results are marked in directly on the stereographic projection, which simplifies and shortens the operations.

Any x-ray study of a structure by oscillation, rotation, etc., is preceded by the setting of the crystal in the correct position in the goniometer. This may be a simple matter if the crystal is euhedral, for all that is required is optical adjustment sometimes followed by final adjustment from Laue patterns [1].

The operation becomes much more difficult if the crystal has no faces, or only very poor ones; the only means of identifying the crystallographic directions may then be to record patterns with polychromatic radiation.

The main line of development has so far been based on the use of flat films with the crystal at rest; but the flat-film method has a major but not always obvious, drawback, for it records only diffraction directions lying at angles between 3-4 and 60-70° to the primary beam.

The stereographic projection given by these reflections is far from complete. Umanskii and Kvitka [2] have used three Laue patterns with crystal settings differing by 60°, the three being used together in the stereographic projection and in the deduction of all reciprocal-lattice nodes. However, rather a large volume of work is involved in processing three Laue patterns.

Komkov and Frank-Kamenetskii [3] have used a single pattern in the zone-occurrence method to determine the orientation. We consider that the conclusions drawn from a few reflections on a single flat film may be ill-defined or wrong; our own experience confirms this.

A crystal giving a complex pattern (minerals, inorganic, and intermetallic compounds) can readily be made to yield more reflections by using a cylindrical film with a tube operated at about 40 kV and having an anode of Mo, Ag, or W together with a beryllium or other such window.

This combination (fixed crystal, cylindrical film) has so far not been used in this country, because it has been considered more difficult to construct a stereographic projection from a cylindrical film; but this is very greatly simplified by a net of the curves for ρ = const and $(90 - \varphi)$ = const drawn up by Rösch [4] as long ago as 1926, and described by Schiebold and Schneider [5].

Henry et al. [6] have given a net of these curves on a scale suitable for practical use; Fig. 1 reproduces this in a more convenient form.

The curves for ρ = const may be represented as the result of projecting onto a cylinder the lines of intersection of the Ewald sphere with cones of

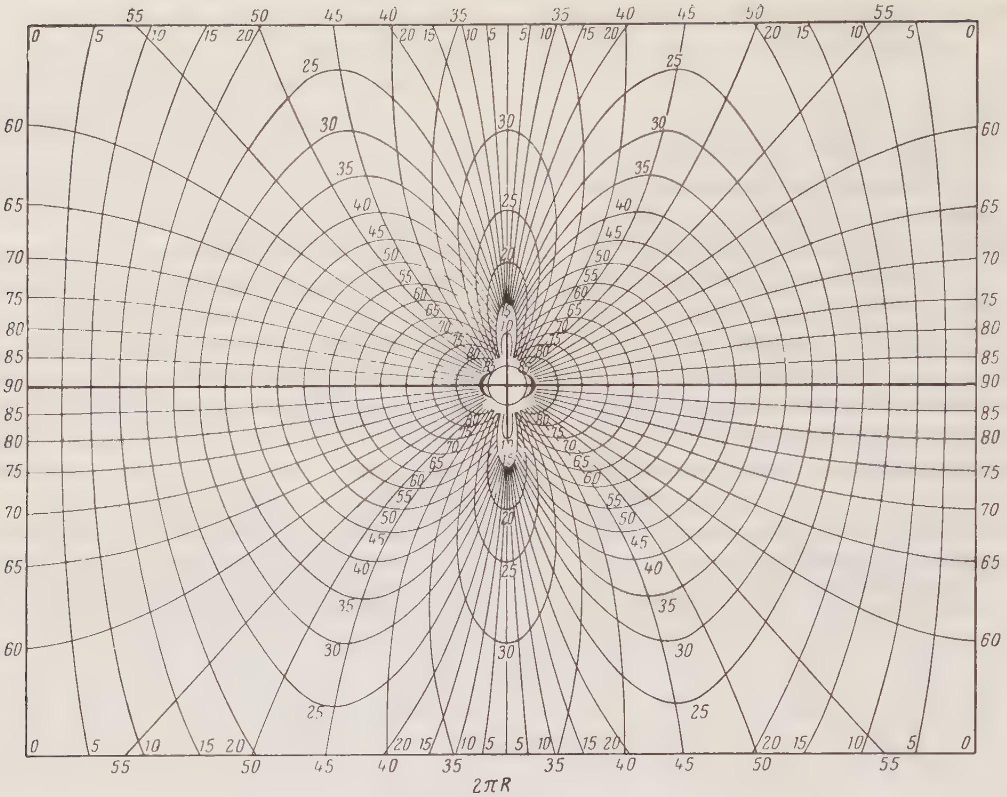

Fig. 1. Net of curves for ρ = const and $(90 - \varphi)$ = const for a cylindrical film of radius 30 mm.

semivertex angle ρ. These lines are somewhat similar to the digit 8 in shape, and they retain much the same form on projection onto a cylinder.

The curves ρ = const may be represented analytically as

$$\cos\frac{x}{R} = -\frac{1}{2\cos\rho}\cdot\frac{\frac{y}{R}}{\sqrt{1+\left(\frac{y}{R}\right)^2}} + \sqrt{1+\left(\frac{y}{R}\right)^2}.$$

The second type of curve, $(90 - \varphi)$ = const, results from projection onto the cylinder of sections of the Ewald sphere by a series of vertical planes at various angles to the primary beam.

The $(90 - \varphi)$ curves may be represented as

$$\cos\left(\frac{x}{R} - \varphi\right) = \cos\varphi\sqrt{1+\left(\frac{y}{R}\right)^2}.$$

The two sets of curves together give the spherical coordinates of reflections recorded on the cylindrical film, and these coordinates enable us to construct a stereographic projection, which gives a complete picture of the diffraction symmetry, because the points fill a large part of the projection.

If necessary, ρ and φ can be calculated from the coordinates x and y on the film:

$$\cos\rho = \frac{1}{2}\,\frac{B}{(1+B^2) - \sqrt{1+B^2}\cos A},$$

$$\tan\varphi = \frac{\sqrt{1+B^2} - \cos A}{\sin A},$$

where $A = x/R$, $B = y/R$, and R is the radius of the film.

The array of spots in the stereographic projection gives a reliable identification of the Laue class as well as the angular adjustments needed to bring the axis of rotation into coincidence with any given crystallographic direction.

We consider it much more convenient to use a projection constructed directly on a stereographic sphere for this purpose.

The method may be illustrated by our work on the orientation and Laue class of a new mineral, which was found and passed to us by M. D. Dorfman of the Kola Branch of the Academy of Sciences, which so far has been called pink platy Fe silicate. Figure 2 shows the Laue pattern recorded on a cylindrical film with the crystal in a random position;

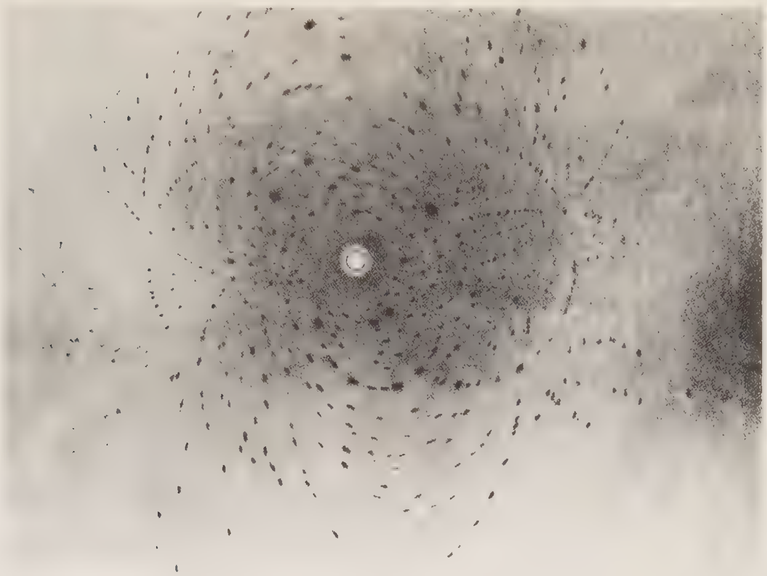

Fig. 2. Pattern from a crystal of "pink platy Fe silicate" recorded on a cylindrical film (radius 30 mm) with the crystal in a random position (Mo anode).

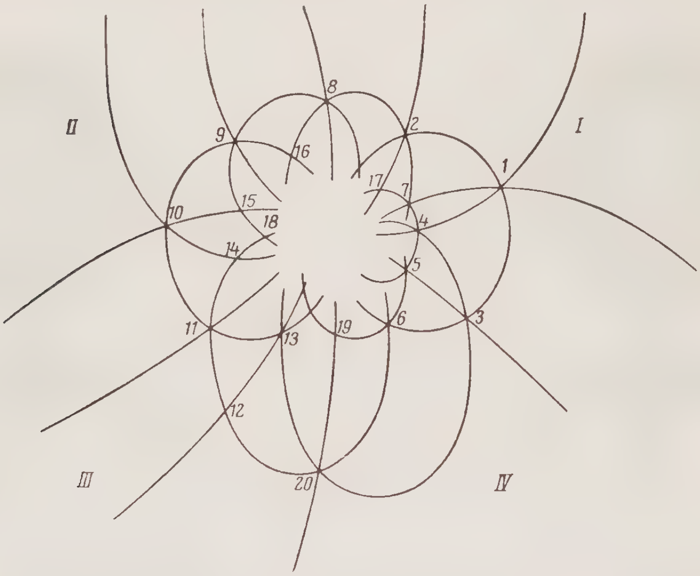

Fig. 3. Scheme for the Laue pattern from a crystal of "pink platy Fe silicate" recorded on a cylindrical film; the zonal curves are shown, together with the numbering of the spots and the quartering.

Fig. 3 shows a scheme for this, with the zonal curves and numbering of the main points.

A tracing from this scheme was superimposed on the net to give the coordinates of the main points, which are listed in the table.

These results were used to mark in the principal crystallographic directions on the stereographic projection (Fig. 4) and also on a stereographic sphere (Fig. 6a).

The array on the sphere revealed at once a symmetry plane, with a two-fold axis perpendicular to it; the crystal therefore belongs to Laue class C_{2h}–$2/m$. It is also easy to establish the angular movements of the sphere needed to bring any crystallographic direction to the vertical position, e.g., the two-fold b axis (Figs. 5 and 6b). The usual x-ray methods, e.g., that of [1], may be used to perform the final adjustment.

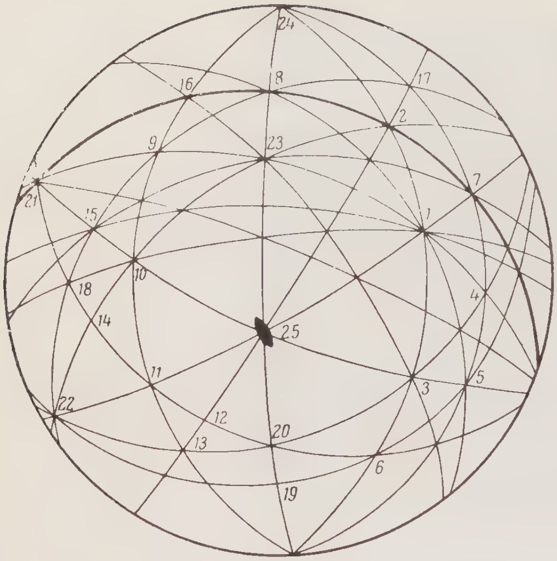

Fig. 4. Initial stereographic projection for the crystal.

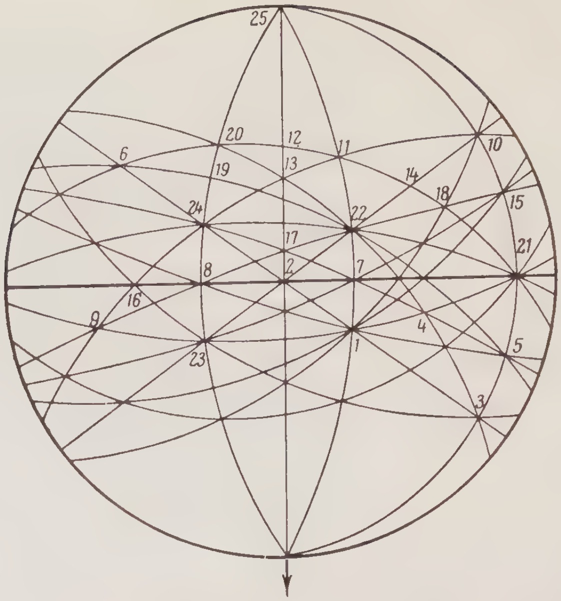

Fig. 5. Result of analysis of the initial stereographic projection from a crystal of "pink platy Fe silicate" recorded on a cylindrical film.

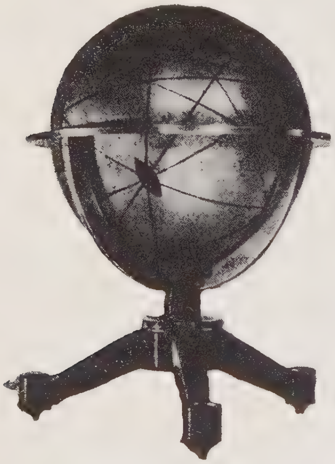

Fig. 6a. Projection of the crystal on a stereographic sphere.

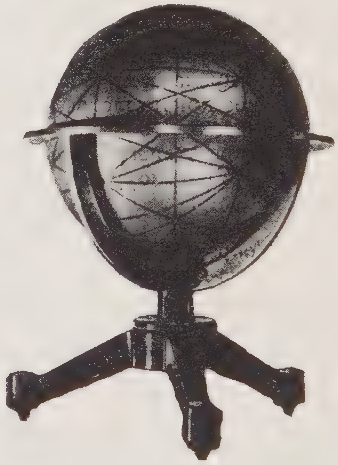

Fig. 6b. Projection of the crystal on a stereographic sphere with identification of a symmetry plane.

Conclusions

A convenient method of determining the orientation and Laue class is as follows.

1. The Laue pattern is recorded on a cylindrical film with the crystal in a random position; the zonal curves and points of intersection of these are identified.

2. A net of curves for ρ and $(90 - \varphi)$ is used to determine the spherical coordinates of these points of intersection, which correspond to major directions in the reciprocal lattice.[1]

3. These directions and zonal curves are entered directly on the stereographic sphere or on the stereographic projection.[2]

4. The symmetry elements relating these points are deduced, as well as the angular displacements needed to bring any given crystallographic direction into coincidence with the axis of rotation.

---

[1] Analytic computation is best for points with ρ and φ less than 30°.

[2] The stereographic sphere can also be used to advantage in the three-patterns method.

TABLE 1. Data for Stereographic Projection Derived from X-ray Pattern of Pink Platy Fe Silicate Crystal

Spot	ρ	$(90-\varphi)$	Quarter
1	75	54	I
2	40	54	I
17	47	73	I
7	66	73	I
8	22	10	II
16	31	56	II
9	49	56	II
10	84	56	II
15	75	69	II
18	90	75	II
4	88	72	IV
5	62	72	IV
3	59	54	IV
6	35	55	IV
19	18	5	IV
20	29	5	III
13	35	54	III
12	41	38	III
11	56	55	III
14	80	70	III

5. The adjustment is refined by the method of Kvitka et al.

The work is simplified if the crystal has some faces, because the crystal can be given a reasonable initial orientation.

This method is a rapid, convenient, and reliable way of identifying the Laue class and orientation for a crystal lacking faces. The method is especially convenient if the camera does not allow a flat film to be used, especially in Weissenberg goniometers.

We are indebted to M. D. Dorfman for providing the crystal for examination.

LITERATURE CITED

1. S. S. Kvitka, Yu. N. Sokurskii, and M. M. Umanskii, "X-ray methods of adjusting crystals," Zavodsk. lab., 16, 696 (1950).
2. M. M. Umanskii and S. S. Kvitka, "Laue patterns as a method of goniometry for crystals," Transactions, 1949 Fedorov Meeting [in Russian] (1951).
3. A. I. Komkov and V. A. Frank-Kamenetskii, "Identification of the orientation of an unfaceted crystal from a single Laue pattern by the zone-occurrence method," Uch. zap. Leningr. Gos. 11, No. 178, Ser. Geol. Nauk, 4, 255 (1954).
4. S. Rösch, "Über die Reflexphotographie," Abhandlungen der matem.-phys. Klasse der Sächsischen Akademie der Wissenschaften, 39, 6 (1926); "Ein Diagramm mit den Kurven ν = const und den Schichtlinien 1. Art (Vgl. S. 651) benutzen S. Hermann und M. Ruhemann," Z. Krist., 83, 136 (1932).
5. E. Schiebold and E. Schneider, "Internationale Tabellen zur Bestimmung von Kristallstrukturen," Zweiter, Vol. 2, Ch. 12, p. 637 (1935).
6. N. F. M. Henry, H. Lipson, and W. A. Wooster, The Interpretation of X-Ray Diffraction Photographs (London, 1953).

SOVIET PHYSICS – CRYSTALLOGRAPHY VOL. 1, NO. 2 MAR.-APR., 1956

STRUCTURE TYPES WITH ATOMIC CLOSE PACKING: POSSIBLE STRUCTURE TYPES FOR THE COMPOSITION AB_3

N. L. Smirnova

M. V. Lomonosov State University, Moscow

Translated from Kristallografiya, Vol. 1, No. 2,
pp. 165-170, March-April, 1956
Original article submitted June 9, 1955

The possible structure types are deduced on the assumption that close packing allows only structures in which an A atom is surrounded only by B atoms, while each B atom has at least one A atom in its coordination sphere. Two different models for the structure type are proposed for ε-Cu_3Sn, which has hexagonal close packing and a superlattice, for which the space group and repeat distances are known.

Here we consider the structure types for binary compounds[1] in which the A and B atoms together form a close-packed array; minor distortions are neglected. Many intermetallic compounds are of this type; all[2] except Ag_3Sb [1] are such that an A atom lies at the center of a cube–octahedron of B atoms, while each B atom has A atoms in its coordination sphere. On this basis we assume that close packing allows only structures in which an A atom is surrounded only by B atoms, while each B atom has at least one A atom in its coordination sphere. Determination of the possible structure types then amounts to determination of the array of A and B atoms.

Let P_B be the reciprocal of the number of A atoms in the coordination sphere of a B atom, and let P_A be the sum of the P_B for all B atoms in the coordination sphere of an A atom; P_A is then the number of B atoms per A atom.

Figure 1 shows the possible coordination of the A and B atoms in a layer; P_B can be $1/3$, $1/2$, or 1. A B atom in the layer may be surrounded by B atoms alone. An atom with $P_B = 1/3$ in a layer also has $P_B = 1/3$ in space, because only B atoms occur at the six points 1, 2, 3, 4, 5, and 6 in cubic close packing and at the three points 1, 2, and 3 in the layers above and below in hexagonal close packing (Fig. 2). A B atom with $P_B = 1$ in a layer, and also surrounded by B atoms alone, will have a P_B in space not less than $1/3$, because, at most two of the six atoms above and below it can be A atoms. A B atom with $P_B = 1/2$ in a layer will have in space a P_B either of $1/4$ (Fig. 3) or $1/3$; P_B in space cannot be less than $1/4$, so P_A in space cannot be less than $1/4 \cdot 12 = 3$, i.e., there must be not less than three B atoms per A atom. Each A atom cannot be completely surrounded by B atoms for A : B > 1 : 3.[3]

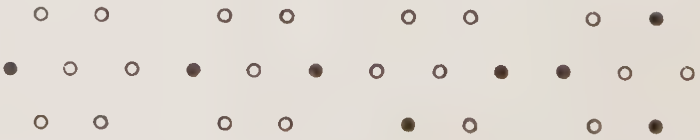

Fig. 1. Possible coordination of A atoms (●) and B atoms (○) in a layer.

---

[1] I consider structure types, not particular compounds, for the latter may be of variable composition, which may not even include the composition corresponding to the given structure type.

[2] The range of compositions with B : A < 3 is not considered here.

[3] The range of compositions with B : A < 3 is not considered here.

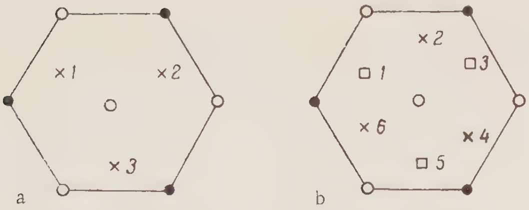

Fig. 2. a) ×, layers above and below; ○, middle layer; b) ×, lower layer; ○, middle layer; □, upper layer; ●, A atoms.

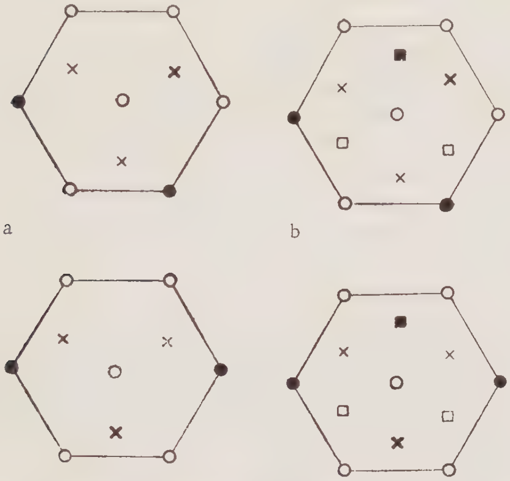

Fig. 3. Possible coordination of A atoms (●, ×, ■) around a B atom for $P_B = \frac{1}{4}$ for (a) hexagonal close packing, (b) cubic close packing. a) ○, middle layer; ×, lower and upper layers. b) ×, lower layer; ○, middle layer; □, upper layer.

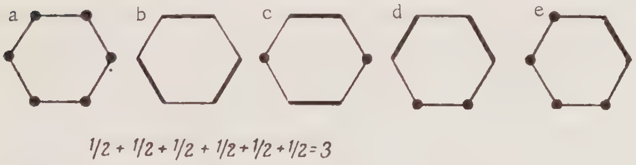

Fig. 4. Possible linking of hexagons of B atoms for $P_B = \frac{1}{2}$ in a layer. ●, links via vertices; –, links via sides.

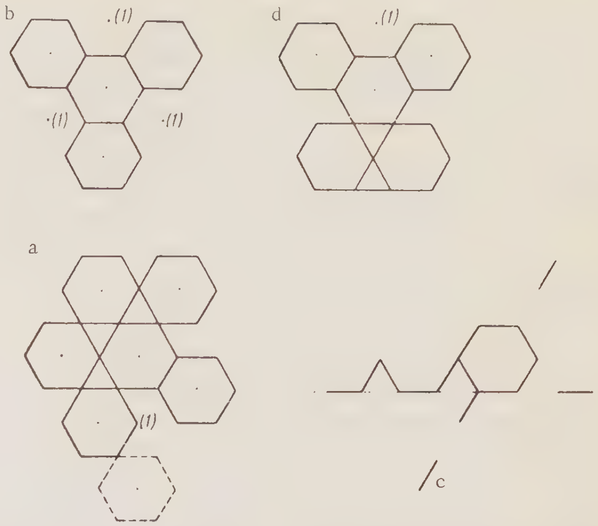

Fig. 5. P_B can take only the value 1 at points marked (1). The vertices of the hexagons are B atoms, an A atom being at the center of each.

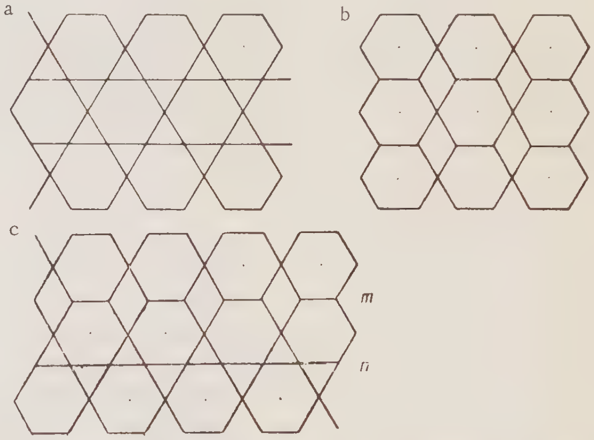

Fig. 6. Possible linking of hexagons in a layer when P_B in space is $\frac{1}{4}$. The vertices of the hexagons are B atoms, an A atom being at the center of each.

Here we consider the case $P_B = \frac{1}{4}$ for all B atoms, which are equivalent (the array of A atoms in the coordination sphere of B is not considered). All the P_A are then 3, the compound having the composition AB_3. We have seen that P_B in space cannot be less than $\frac{1}{3}$ for atoms with $P_B = \frac{1}{3}$ or 1 in a layer, so all the B atoms in each layer must have $P_B = \frac{1}{2}$. This corresponds to linking of hexagons of B atoms, each of which has an A atom at the center; the links are via vertices and via edges not having a vertex in common (Fig. 4). Linking as in b and d, or combination of b or d with the other types, is impossible because there would be B atoms with $P_B = 1$ (Fig. 5b, d). For the same reason, the hexagons cannot link via vertices along a line through an edge joining them (Fig. 5a). This figure shows that linking along such a line occurs with a gap equal to the length of an edge. Such sequences do not occur if the lines are not parallel (Fig. 5c), so linking along lines that are not parallel is impossible. Figure 6 shows three possible types of link. Layers of a different type may be obtained by taking different combinations of links of types m and n.

A space lattice can consist only of a layer of the same type placed on a given layer, and this can be done in only one way. Figure 7 shows possible arrays (three types only) in hexagonal close pack-

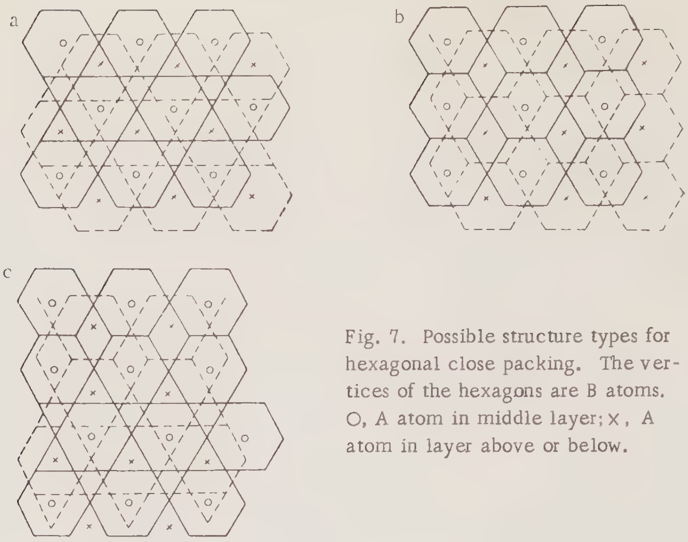

Fig. 7. Possible structure types for hexagonal close packing. The vertices of the hexagons are B atoms. ○, A atom in middle layer; ×, A atom in layer above or below.

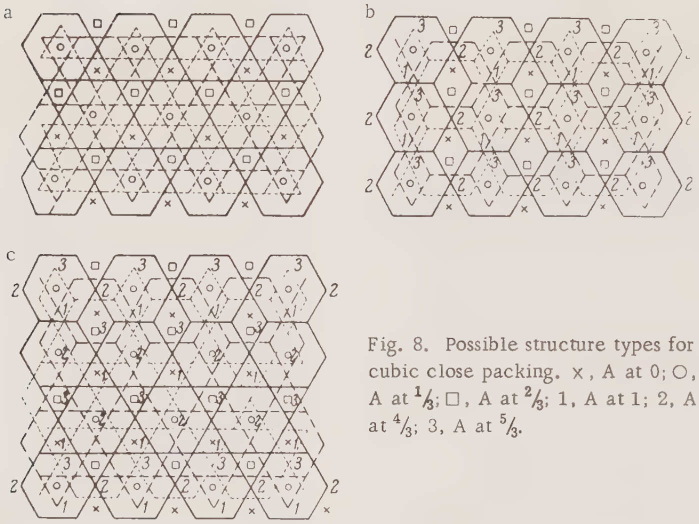

Fig. 8. Possible structure types for cubic close packing. ×, A at 0; ○, A at $^1/_3$; □, A at $^2/_3$; 1, A at 1; 2, A at $^4/_3$; 3, A at $^5/_3$.

ing; the other types may be derived from layers with a different type of link.

Mg_3Cd crystallizes in type *a* [1], as do some other compounds, while type b occurs in the γ phase of Cu–Al [2]. No representatives of the other types have been found in the literature; they should have orthorhombic unit cells with $a = 2a_{hex}$, $c = c_{hex}$, $b = a_{hex}\sqrt{3}$, $3a_{hex}\sqrt{3}$, $4a_{hex}\sqrt{3}$, and so on. For ε-Cu_3Sn [3,4], we have $a = 2a_{hex}$, $c = c_{hex}$, and $b = 8a_{hex}\sqrt{3}$, etc.; the space group is Cmcm, and two models may be proposed for the structure (Fig. 9).[4]

Figure 8 shows the layer stacking for cubic packing; Cu_3Au is of type *a* [1], as are some other compounds. Types b and c have the A atoms in the fourth layer above the points 1, those in the fifth above points 2, and those in the sixth above points 3. Only three types are shown; the others may be derived from layers with a different type of link. All structures, apart from those of type *a*, consist of six layers along the 3 axis. $TiAl_3$ is a representative of type b [1]; $ZrAl_3$ is also a representative of this series of structure types [1]. All of these

---

[4] The structure of ε-Cu_3Sn has been determined [Z. Metallkunde, 46, 9, 692 (1955)]; *a* and c correspond to [3,4], while b = $= 10a_{hex}\sqrt{3}$. The principle is that of Fig. 8a. The same workers have discovered several new compounds that fit the above treatment, which have cubic close packing and superlattices. (Note added in proof.)

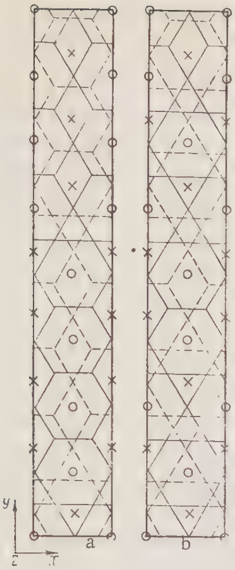

Fig. 9. Possible structure types for ε-Cu_3Sn. O, Sn in middle layers; ×, Sn in layer above or below. The vertices of the hexagons are Cu atoms.

types arise from the possibility of placing the cube–octahedra of the next layer on the square tops of cube–octahedra in the previous layer, or on square sections of octahedra [5].

The arrays in multilayer structures may be found by superimposing layers of types *a*, b, c, etc. (Fig. 6) as in d and i. For instance, the $TiNi_3$ structure type [1] occurs by superposition of type *a* layers in the order ABAC.

We are indebted to Academician N. V. Belov and to Professor G. B. Bokii for valuable comments and advice.

LITERATURE CITED

1. G. B. Bokii, Introduction to Chemical Crystallography [in Russian] (1954).
2. G. Kurdyumov, V. Miretskii, and T. Stelletskaya, "Transformations in eutectoid alloys. V. Structure of the γ' martensite phase and the mechanism of the $\beta_1 \rightarrow \gamma'$ transformation," ZhÉTF, 8, 22-23 (1938).
3. J. D. Bernal, "The complex structure of the copper–tin intermetallic compounds," Nature, 122, 54 (1928).
4. O. Carlsson and G. Hägg, "Zur Kenntnis des Kristallbaues einiger Kupfer-Zinnphasen," Z. Krist., 83, 308 (1932).
5. N. V. Belov, Structures of Ionic Crystals and Metallic Phases [in Russian] (1947), p. 194.

SOVIET PHYSICS – CRYSTALLOGRAPHY VOL. 1, NO. 2 MAR.-APR., 1956

CRYSTAL STRUCTURE OF ZOISITE

E. G. Fesenko, I. M. Rumanova,
and N. V. Belov

Institute of Crystallography, Academy of Sciences of the USSR

Translated from Kristallografiya, Vol. 1, No. 2,
pp. 171-196, March-April, 1956
Original article submitted January 24, 1956

The crystal structure of zoisite $Ca_2Al_3[Si_2O_7][SiO_4]O(OH)$ is completely analyzed through a direct determination of the structure-amplitude signs by statistical equations. A method of separating out the key group of signs for this determination is developed in detail.

Zoisite, $Ca_2Al_3Si_3O_{12}(OH)$, is the third mineral of the epidote group [1,2] which has been analyzed in the Institute of Crystallography. It is related to the first of these, ilvaite [$CaFe^{\cdot\cdot\cdot}Fe_2^{\cdot\cdot}Si_2O_8(OH)$], by the common Fedorov group D_{2h}^{16} = Pnma, and to the monoclinic epidote $Ca_2Al_2FeSi_3O_{12}(OH)$ by a similar formula, Al replacing Fe. Characteristic of the three minerals is one short period (5.5 to 5.9 kX), along which passes a screw axis 2_1, and perpendicular to which is a mirror plane. Along this direction in both ilvaite and epidote stretch columns of Fe or Al octahedra, linked by common edges, the atoms being disposed in only four levels; a repetition of this may be expected in zoisite, also. In ilvaite and epidote, despite the orthosilicate formulas, one finds the radicals [Si_2O_7], predicted for minerals of the epidote group by Sobolev [3]. Whereas, however, in ilvaite all the Si are in diortho-groups [Si_2O_7], in epidote one orthosilicate group [SiO_4] corresponds to each [Si_2O_7].

Considering zoisite as a microtwinned epidote, Ito [4] calculated the coordinates of the atoms in his first epidote structure, obtained by trial and error. The failings of the latter were critically analyzed in [2]. In order to justify his coordinates of zoisite, Ito confined himself to a table giving the similarity of the intensities of 50 arbitrarily selected *hkl* reflections, among which 16 were not observed; the corresponding coordinates led to unacceptable distances. Some Si–O distances proved to be 1.45, 1.90 to 1.97, and even 2.10 kX; the lengths of the O–O edges in the Si tetrahedra were 2.39 and 3.26 kX, etc. (cf. [2]).

Experimental X-ray Data from Zoisite, and Its Preliminary Analysis

The specimens for examination consisted of crystals from the Khorutanii region, obtained from the Mineralogical Museum of the Academy of Sciences of the USSR. The crystals had a well-developed zone of elongation, along which their dimensions were 1.5 to 2 mm (0.2-0.3 mm across). The observation of transparent, colorless crystals made it possible to neglect the Fe content and regard the formula of zoisite as $Ca_2Al_3Si_3O_{12}(OH)$.

Unit Cell. Fedorov Group. The parameters of the orthorhombic cell (from rotation x-ray photographs and from pinacoids far out on zero layers of oscillation patterns) were a = 16.20 kX, b = 5.50 kX, c = 10.14 kX, in agreement with earlier data [5]. From the specific gravity of the colorless (i.e., iron-free) crystals (3.25) and the "molecular weight" (454.3), we obtain the number of "molecules" (formula units) in the cell as 4 (3.90).

We had available oscillation patterns of the zero and three-layer lines from rotation around b using Cu and Mo radiation, and the zero lines from oscillation patterns around a and c in Cu radiation only.

From the Laue class and the extinctions observed, we arrived at x-ray group No. 17 [6], mmmPn-a, which includes the two Fedorov groups C_{2v}^{9} = Pn2_1a and D_{2h}^{16} = Pnm$a$.

As indicated, zoisite is a member of a family of minerals characterized by a mirror plane perpendicular to the shortest period. Further evidence, given subsequently, leads us, with the earlier authors, to the holohedral group $D_{2h}^{16} = Pnma$.

The general positions are eightfold and the special positions fourfold, divided into the following groups: two groups of four at centers of symmetry (at levels of 0 and b/2) without parameters, and positions in the mirror planes (at heights ¼ and 3b/4). In the unit cell we must put eight atoms of Ca, 12 Al, 12 Si, 48 O, 4 OH. There is no doubt but that the Al and Si atoms and OH groups fall in groups of four in particular special positions.

The extremely strong (040) reflection, with the short axis b = 5.50 kX, indicates that all the atoms are located in only four levels, as in the case of epidote and ilvaite, and also in Al_2SiO_5, $BaSO_4$, Mg_2SiO_4, Sb_2S_3, and a number of others. The "stencil" nature of the arrangement of the atoms in four levels along the short b axis (on account of the wide "forbidden bands" due to the large ionic radius of oxygen) has been repeatedly mentioned, for example in [1,2], where it was shown that this is an argument in favor of the holohedral group D_{2h}^{16}. The arrangement of the atoms in only four levels also followed from the first "lateral" xy Patterson synthesis.

Intensities of Reflections and Structure Amplitudes. On the x-ray diffraction patterns, the intensities were estimated visually by comparison with 17 blackening marks [7], which differed by a factor of $\sqrt{2}$ and completely covered the range of the film emulsion. From the relative intensities, taking account of polarization and kinematical factors, values of the structure-amplitude moduli were obtained in [8]. On dividing by the sum of the atomic factors for corresponding $\sin\vartheta/\lambda$, all the $|F_{hkl}|$ were converted, apart from an unknown multiplier, into unitary structure amplitudes $|\hat{F}_{hkl}|$, required for the statistical method of structural analysis [9].

Comparison of the experimental material obtained from the Cu and Mo radiation patterns indicates the considerable quantitative and qualitative advantage of the latter (Table 1).

The number of h0l and h1l reflections in the Mo patterns was almost three times greater than for Cu; the Mo lacked only nine of the reflections available in the Cu patterns: (200), (201), (002), (102), (202), (112), (311), (312), and (411).

The advantage of the Mo patterns also appears in the fact (important for the statistical method) that, among the reflections with large indices, those for which the unitary amplitudes are large occur relatively often. The distribution of approximately a third of the h0l and h1l reflections with the largest unitary amplitudes in the Cu and Mo patterns is given in Table 2.

TABLE 1

Radiation	No. of reflections on patterns	
	h0l	h1l
CuK_α	139	96
MoK_α	402	273
Total different	407	277

TABLE 2

Radiation	Distribution of reflections with greatest unitary amplitudes	
	h0l	h1l
CuK_α	17	31
MoK_α	137	92

The number 137 includes two reflections, the (16.0.7) and (17.0.6) which, although $(\sin\vartheta)/\lambda < 1/\lambda$ Cu,[1] are absent from the Cu pattern, probably due to strong absorption.

Statistical Method of Determining the Signs of the Structure Amplitudes

Determination of the structure-amplitude signs by direct methods in earlier investigations [10,2, 11] was divided into two stages. In the first, which (as it seemed to the authors) made subsequent steps more reliable, the Harker–Kasper inequalities [9] were used to establish the signs of a small number of maximum unitary amplitudes $\hat{F}_{hkl}$. Starting from this "key" group of signs, the signs of other unitary amplitudes were found successively at the second stage by means of the statistical equation of Zachariasen [10] (for centrosymmetric crystals)

$$S_{hkl} = S\,(\overline{S_{h_i k_i l_i}\cdot S_{h+h_i,\,k+k_i,\,l+l_i}}) \qquad (1)$$

or

$$S_H = S\,(\overline{S_{K_i}\cdot S_{H+K_i}}).$$

The keys S_{K_i} and S_{H+K_i} found from the inequalities were supplemented as work proceeded by the signs of other amplitudes with large unitary values.

The method of inequalities demands the reduction of the experimental amplitudes to absolute values; although this can be effected either experimentally or by calculation [12,13], it involves a great deal of work. More troublesome are difficulties of principle, since a number of factors in structural analysis (absorption, temperature, extinction) are hard to evaluate and, furthermore, it is general practice to use atomic factors calculated for free atoms. The main failing of the method of inequalities is the fact that it is only suitable for large unitary amplitudes,[2] and the number of these is extremely small when there are large numbers of atoms in the cell (no heavy atom among them).

---

[1] Strictly speaking, the construction of the cassette made it possible to record reflections with $\sin\vartheta/\lambda$ inside the following limits: $0.127 \le \sin\vartheta/\lambda_{Mo} \le 1.360$ for Mo radiation and $0.059 \le \sin\vartheta/\lambda_{Cu} \le 0.626$ for Cu radiation.

This justified an attempt to eliminate the stage with the inequalities and to establish the key group in another way. One of such ways [15], discussed later in detail for the group D_{2h}^{16} = Pnm*a*, consists of constructing a chain of signs (for example $S_{H_1} = S_{H_2} = -S_{H_3}$, etc.) from individual equalities between S_{H_A} and S_{H_B} (in the present case, $S_{H_1} = S_{H_2}$; $S_{H_2} = -S_{H_3}$). The individual equalities may be obtained statistically, using, in conjunction with relation (1), those relationships between the signs of the amplitudes F_{hkl}, $F_{\bar{h}kl}$, $F_{h\bar{k}l}$, $F_{hk\bar{l}}$ which characterize the given Fedorov group. Each chain includes S_{hkl} with indices of a definite type. As shown later, for a correct choice of three chains, in general one may arbitrarily assign one sign to each, and so fix all the signs in the chains. The signs obtained serve as key signs for finding the remaining S_{hkl} with merely the help of relation (1).

Comparison of Structure-Amplitude Signs. Having selected a pair of reflections from among those strongest in unitary amplitude[3] ("comparison" reflections), we match these with such pairs of ("determining") reflections that, as a result of the addition or subtraction of corresponding indices (independently of the two others) of the determining pair, the indices of the two comparison reflections are obtained, after which we write out the two corresponding Zachariasen equalities. By means of relations characteristic of each Fedorov group, it is easy to decide whether the signs of the comparison reflections are the same or opposite. For the group D_{2h}^{16} = Pnm*a*, such relations are [16]:

a) for $\begin{matrix} h+l=2n \\ k=2n \end{matrix}$ $F_{hkl} = F_{\bar{h}\bar{k}\bar{l}} = F_{\bar{h}kl} = F_{h\bar{k}l} = F_{hk\bar{l}}$.

b) for $\begin{matrix} h+l=2n \\ k=2n+1 \end{matrix}$ $F_{hkl} = F_{\bar{h}\bar{k}\bar{l}} = -F_{\bar{h}kl} = -F_{h\bar{k}l} = F_{hk\bar{l}}$.

c) for $\begin{matrix} h+l=2n+1 \\ k=2n \end{matrix}$ $F_{hkl} = F_{\bar{h}\bar{k}\bar{l}} = -F_{\bar{h}kl} = F_{h\bar{k}l} = -F_{hk\bar{l}}$.

d) for $\begin{matrix} h+l=2n+1 \\ k=2n+1 \end{matrix}$ $F_{hkl} = F_{\bar{h}\bar{k}\bar{l}} = F_{\bar{h}kl} = -F_{h\bar{k}l} = -F_{hk\bar{l}}$.

(2)

Let us take an example. For the comparison reflections 808 and 8.0.20, we find the determining pairs

1) $30\bar{6}$	5.0.14	5) $17.1.\bar{6}$	$9.1.\overline{14}$
2) 29.0.14	$21.0.\bar{6}$	6) 18.1.14	$10.1.\bar{6}$
3) $37.0.\bar{6}$	$\overline{29}.0.14$	7) 25.1.14	$17.1.\bar{6}$
4) $38.0.\bar{6}$	$\overline{30}.0.14$		

Then,

$$\begin{aligned}
&1)\ S_{808} = S_{30\bar{6}} \times S_{5.0.14} = -S_{306} \times S_{5.0.14} \\
&\quad S_{8.0.20} = S_{306} \times S_{5.0.14} \\
&2)\ S_{808} = S_{21.0.6} \times S_{29.0.14} \\
&\quad S_{8.0.20} = S_{21.0.\bar{6}} \times S_{29.0.14} = -S_{21.0.6} \times S_{29.0.14} \\
&3)\ S_{808} = S_{37.0.\bar{6}} \times S_{\overline{29}.0.14} = -S_{37.0.6} \times S_{\overline{29}.0.14} \\
&\quad S_{8.0.20} = S_{37.0.6} \times S_{\overline{29}.0.14} \\
&4)\ S_{808} = S_{38.0.\bar{6}} \times S_{\overline{30}.0.14} = S_{38.0.6} \times S_{\overline{30}.0.14} \\
&\quad S_{8.0.20} = S_{38.0.6} \times S_{\overline{30}.0.14} \\
&5)\ S_{808} = S_{17.1.\bar{6}} \times S_{9.1.\overline{14}} = -S_{17.1.6} \times S_{9.1.\overline{14}} \\
&\quad S_{8.0.20} = S_{17.1.6} \times S_{9.1.\overline{14}} \\
&6)\ S_{808} = S_{18.1.14} \times S_{10.1.6} \\
&\quad S_{8.0.20} = S_{18.1.14} \times S_{10.1.\bar{6}} = S_{18.1.14} \times S_{10.1.6} \\
&7)\ S_{808} = S_{25.1.14} \times S_{17.1.6} \\
&\quad S_{8.0.20} = S_{25.1.14} \times S_{17.1.\bar{6}} = -S_{25.1.14} \times S_{17.1.6}
\end{aligned}$$

With a "probability" of 0.72, the signs of the amplitudes of 808 and 8.0.20 are different.

Relation (1) is statistical, and in comparing the signs it is desirable to have the largest possible numbers of pairs for determining whether the signs of the comparison pair are like or unlike, remembering, of course, that any application of (1) determines the signs of the H amplitudes with a greater probability, the greater the unitary amplitudes of K_i and $H + K_i$.

Method of Selecting the Comparison and Determining Pairs. For an arbitrary selection of the comparison pairs with positive indices $h_1k_1l_1$ and $h_2k_2l_2$, the indices of the determining pairs, in the case of the D_{2h}^{16} group, are found from the conditions:

$$\begin{aligned} &h_1 = h_i - h_j, \quad k_1 = k_i - k_j, \quad l_1 = l_i - l_j, \\ &h_2 = h_i \mp h_j, \quad k_2 = k_i \mp k_j, \quad l_2 = l_i \mp l_j, \end{aligned} \qquad (3)$$

where h_i, h_j, k_i, k_j, l_i, l_j (the indices of the determining pairs) may be positive and negative. It was shown earlier [15] that the greatest number of determining pairs is obtained on comparing amplitudes with two equal analogous indices. For one of such indices we chose k, taking $k_1 = k_j = k_0$, and

---

[2] If we use inequalities including a small number (3 or 4) of amplitudes [9, 14].

[3] We shall everywhere replace the unitary amplitudes by quantities proportional to them.

TABLE 3

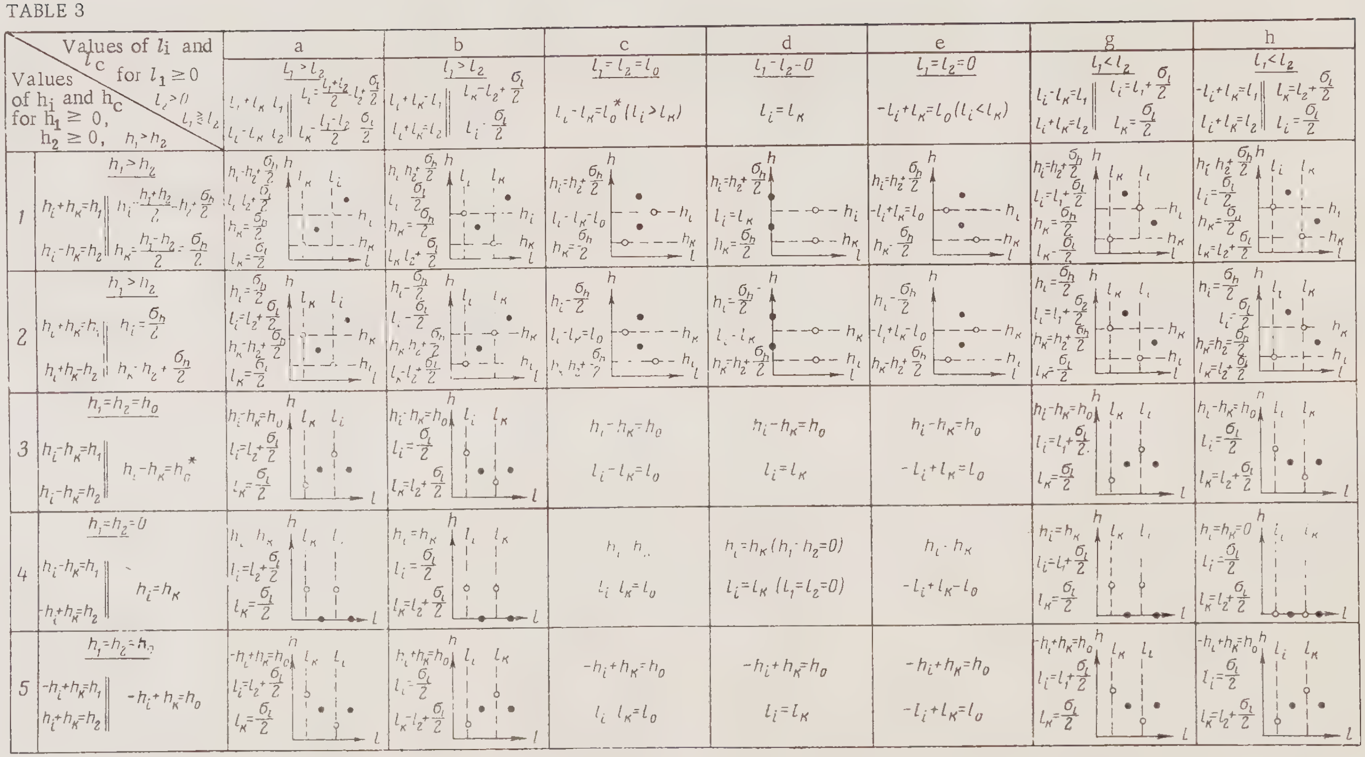

	Values of l_i and l_c for $l_1 \geq 0$, $l_2 > 0$, $l_1 \geq l_2$ / Values of h_i and h_c for $h_1 \geq 0$, $h_2 \geq 0$, $h_1 > h_2$	a	b	c	d	e	g	h
		$l_1 > l_2$ $l_i + l_\kappa = l_1$ ‖ $l_i = \frac{l_1+l_2}{2} = l_2 + \frac{\sigma_l}{2}$ $l_i - l_\kappa = l_2$ ‖ $l_\kappa = \frac{l_1-l_2}{2} = \frac{\sigma_l}{2}$	$l_1 > l_2$ $l_i + l_\kappa = l_1$ ‖ $l_\kappa = l_2 + \frac{\sigma_l}{2}$ $l_i + l_\kappa = l_2$ ‖ $l_i = \frac{\sigma_l}{2}$	$l_1 = l_2 = l_0$ $l_i - l_\kappa = l_0^* \ (l_i > l_\kappa)$	$l_1 = l_2 = 0$ $l_i = l_\kappa$	$l_1 = l_2 = 0$ $-l_i + l_\kappa = l_0 \ (l_i < l_\kappa)$	$l_1 < l_2$ $l_i - l_\kappa = l_1$ ‖ $l_i = l_1 + \frac{\sigma_l}{2}$ $l_i + l_\kappa = l_2$ ‖ $l_\kappa = \frac{\sigma_l}{2}$	$l_1 < l_2$ $-l_i + l_\kappa = l_1$ ‖ $l_\kappa = l_2 + \frac{\sigma_l}{2}$ $l_i + l_\kappa = l_2$ ‖ $l_i = \frac{\sigma_l}{2}$
1	$h_1 > h_2$ $h_i + h_\kappa = h_1$ ‖ $h_i = \frac{h_1+h_2}{2} = h_2 + \frac{\sigma_h}{2}$ $h_i - h_\kappa = h_2$ ‖ $h_\kappa = \frac{h_1-h_2}{2} = \frac{\sigma_h}{2}$	$h_i = h_2 + \frac{\sigma_h}{2}$ $l_i = l_2 + \frac{\sigma_l}{2}$ $h_\kappa = \frac{\sigma_h}{2}$ $l_\kappa = \frac{\sigma_l}{2}$	$h_i = h_2 + \frac{\sigma_h}{2}$ $l_i = \frac{\sigma_l}{2}$ $h_\kappa = \frac{\sigma_h}{2}$ $l_\kappa = l_2 + \frac{\sigma_l}{2}$	$h_i = h_2 + \frac{\sigma_h}{2}$ $l_i - l_\kappa = l_0$ $h_\kappa = \frac{\sigma_h}{2}$	$h_i = h_2 + \frac{\sigma_h}{2}$ $l_i = l_\kappa$ $h_\kappa = \frac{\sigma_h}{2}$	$h_i = h_2 + \frac{\sigma_h}{2}$ $-l_i + l_\kappa = l_0$ $h_\kappa = \frac{\sigma_h}{2}$	$h_i = h_2 + \frac{\sigma_h}{2}$ $l_i = l_1 + \frac{\sigma_l}{2}$ $h_\kappa = \frac{\sigma_h}{2}$ $l_\kappa = \frac{\sigma_l}{2}$	$h_i = h_2 + \frac{\sigma_h}{2}$ $l_i = \frac{\sigma_l}{2}$ $h_\kappa = \frac{\sigma_h}{2}$ $l_\kappa = l_2 + \frac{\sigma_l}{2}$
2	$h_1 > h_2$ $h_i + h_\kappa = h_1$ ‖ $h_i = \frac{\sigma_h}{2}$ $h_i + h_\kappa = h_2$ ‖ $h_\kappa = h_2 + \frac{\sigma_h}{2}$	$h_i = \frac{\sigma_h}{2}$ $l_i = l_2 + \frac{\sigma_l}{2}$ $h_\kappa = h_2 + \frac{\sigma_h}{2}$ $l_\kappa = \frac{\sigma_l}{2}$	$h_i = \frac{\sigma_h}{2}$ $l_i = \frac{\sigma_l}{2}$ $h_\kappa = h_2 + \frac{\sigma_h}{2}$ $l_\kappa = l_2 + \frac{\sigma_l}{2}$	$h_i = \frac{\sigma_h}{2}$ $l_i - l_\kappa = l_0$ $h_\kappa = h_2 + \frac{\sigma_h}{2}$	$h_i = \frac{\sigma_h}{2}$ $l_i = l_\kappa$ $h_\kappa = h_2 + \frac{\sigma_h}{2}$	$h_i = \frac{\sigma_h}{2}$ $-l_i + l_\kappa = l_0$ $h_\kappa = h_2 + \frac{\sigma_h}{2}$	$h_i = \frac{\sigma_h}{2}$ $l_i = l_1 + \frac{\sigma_2}{2}$ $h_\kappa = h_2 + \frac{\sigma_h}{2}$ $l_\kappa = \frac{\sigma_l}{2}$	$h_i = \frac{\sigma_h}{2}$ $l_i = \frac{\sigma_l}{2}$ $h_\kappa = h_2 + \frac{\sigma_h}{2}$ $l_\kappa = l_2 + \frac{\sigma_l}{2}$
3	$h_1 = h_2 = h_0$ $h_i - h_\kappa = h_1$ ‖ $h_i - h_\kappa = h_0^*$ $h_i - h_\kappa = h_2$ ‖	$h_i - h_\kappa = h_0$ $l_i = l_2 + \frac{\sigma_l}{2}$ $l_\kappa = \frac{\sigma_l}{2}$	$h_i - h_\kappa = h_0$ $l_i = \frac{\sigma_l}{2}$ $l_\kappa = l_2 + \frac{\sigma_l}{2}$	$h_i - h_\kappa = h_0$ $l_i - l_\kappa = l_0$	$h_i - h_\kappa = h_0$ $l_i = l_\kappa$	$h_i - h_\kappa = h_0$ $-l_i + l_\kappa = l_0$	$h_i - h_\kappa = h_0$ $l_i = l_1 + \frac{\sigma_l}{2}$ $l_\kappa = \frac{\sigma_l}{2}$	$h_i - h_\kappa = h_0$ $l_i = \frac{\sigma_l}{2}$ $l_\kappa = l_2 + \frac{\sigma_l}{2}$
4	$h_1 = h_2 = 0$ $h_i - h_\kappa = h_1$ ‖ $h_i = h_\kappa$ $-h_i + h_\kappa = h_2$ ‖	$h_i = h_\kappa$ $l_i = l_2 + \frac{\sigma_l}{2}$ $l_\kappa = \frac{\sigma_l}{2}$	$h_i = h_\kappa$ $l_i = \frac{\sigma_l}{2}$ $l_\kappa = l_2 + \frac{\sigma_l}{2}$	$h_i = h_\kappa$ $l_i - l_\kappa = l_0$	$h_i = h_\kappa \ (h_1 = h_2 = 0)$ $l_i = l_\kappa \ (l_1 = l_2 = 0)$	$h_i = h_\kappa$ $-l_i + l_\kappa = l_0$	$h_i = h_\kappa$ $l_i = l_1 + \frac{\sigma_l}{2}$ $l_\kappa = \frac{\sigma_l}{2}$	$h_i = h_\kappa = 0$ $l_i = \frac{\sigma_l}{2}$ $l_\kappa = l_2 + \frac{\sigma_l}{2}$
5	$h_1 = h_2 = h_0$ $-h_i + h_\kappa = h_1$ ‖ $-h_i + h_\kappa = h_0$ $h_i + h_\kappa = h_2$ ‖	$-h_i + h_\kappa = h_0$ $l_i = l_2 + \frac{\sigma_l}{2}$ $l_\kappa = \frac{\sigma_l}{2}$	$h_i + h_\kappa = h_0$ $l_i = \frac{\sigma_l}{2}$ $l_\kappa = l_2 + \frac{\sigma_l}{2}$	$-h_i + h_\kappa = h_0$ $l_i - l_\kappa = l_0$	$-h_i + h_\kappa = h_0$ $l_i = l_\kappa$	$-h_i + h_\kappa = h_0$ $-l_i + l_\kappa = l_0$	$-h_i + h_\kappa = h_0$ $l_i = l_1 + \frac{\sigma_l}{2}$ $l_\kappa = \frac{\sigma_l}{2}$	$-h_i + h_\kappa = h_0$ $l_i = \frac{\sigma_l}{2}$ $l_\kappa = l_2 + \frac{\sigma_l}{2}$

Note: The cases $h_i + h_c = h_0$ and $l_i + l_c = l_0$ give nothing essentially new

Arbitrary notation: ● – Comparison
○ – Determining

then the k indices of the determining reflections will be any pair of numbers corresponding to the conditions $k_i = k_j = k_0$. The two triplets of indices of the determining pair each correspond in reciprocal space to one lattice point in the planes $y^* = k_i$ and $y^* = k_j$, and the triplets of indices of the comparison pair to points in the plane $y^* = k_0$. If in reciprocal space we separate out all possible pairs of planes ($y^* = k_i$, $y^* = k_j$) with the condition $k_i - k_j = k_0$, then each such pair gives determining pairs (or their lattice points) for the comparison pair, the points of which lie in the plane $y^* = k_0$. The rules for choosing the pairs are found by considering all possible values of $(h_i, l_i)_{k_i}$ and $(h_j, l_j)_{k_j}$ as functions of the values of $(h_1, l_1)_{k_0}$ and $(h_2, l_2)_{k_0}$. We distinguish three cases:

1) $h_1 \neq h_2$; $l_1 \neq l_2$ (see Table 3, 1a, 1b, 1g, 1h, 2a, 2b, 2g, 2h);

2) A $h_1 \neq h_2$; $l_1 = l_2$ (1c, 1d, 1e, 2c, 2d, 2e);
B $h_1 \neq h_2$; $l_1 \neq l_2$ (3a, 4a, 5a, 3b, 4b, 5b, 3g, 4g, 5g, 3h, 4h, 5h);

3) $h_1 = h_2$; $l_1 = l_2$ (degeneracy condition).

The results of this consideration are shown in Table 3, where for each case we give rules for the geometric choice of pairs in three superposed planes ($y^* = k_0$, $y^* = k_i$, $y^* = k_j$) of the reciprocal lattice.

We see from Table 3 that the maximum number of determining pairs is obtained on comparison of reflections with two equal analogous indices.

For $h_1 \neq h_2$, $l_1 = l_2 = l_0$ (A), the indices of the determining pairs, according to condition (3), will be

$$h_i = \frac{h_1 + h_2}{2} = h', \quad h_j = \frac{h_1 - h_2}{2} = h''\,,^4 \quad l_0 = l_i - l_j,$$

and the indices of the comparison pair are formed from those of the determining pair by the formulas

$$(h_1, k_0, l_0) = (h', k_i, l_i) - (\overline{h}'', k_j, l_j),$$
$$(h_2, k_0, l_0) = (h', k_i, l_i) - (h'', k_j, l_j).$$

For $h_1 = h_2 = h_0$, $l_1 \neq l_2$ (B),

$$h_0 = h_i - h_j, \quad l_i = \frac{l_1 + l_2}{2} = l', \quad l_j = \frac{l_1 - l_2}{2} = l''$$

and, clearly,

$$(h_0, k_0, l_1) = (h_i, k_i, l') - (h_j, k_j, \overline{l}''),$$
$$(h_0, k_0, l_2) = (h_i, k_i, l') - (h_j, k_j, l'').$$

If as determining reflections we could have chosen those with any unitary amplitudes, then, on the basis of relations (2), the same number of determining pairs would support both the identity and the opposition of the signs for the comparison pair of reflections (for example, $S_{h_0k_0l_1} = S_{h_0k_0l_2}$ for $h_j + l'' = 2n$, $k_j = 2n$, and $S_{h_0k_0l_1} = -S_{h_0k_0l_2}$ for $h_j + l'' = 2n + 1$, $k_j = 2n$).

Our problem, however, is the selection of determining pairs with maximum unitary amplitudes, the statistics of which lead to one definite sign. The scheme for the geometric choice of such pairs is shown in Fig. 1a (scheme A) and Fig. 1b (scheme B). Here, in the square $(h, l)_k$ networks, lattice points with large unitary amplitudes are separated out, and by simple superposition the three networks ($y^* = k_0$, $y^* = k_i$, $y^* = k_j$) are placed together in one figure. The $H_1(h_1, k_0, l_0)$, $H_2(h_2, k_0, l_0)$ and, correspondingly, $L_1(h_0, k_0, l_1)$, $L_2(h_0, k_0, l_2)$ are the points of the comparison pair; $H_i(h', k_i, l_i)$, as also $L_i(h_i, k_i, l')$, is one of the points of the determining pair; each of the points $H_j(h'', k_j, l_j)$ and $H_k(h'', k_j, l_k)$, just as $L_j(h_j, k_j, l'')$ and $L_k(h_k, k_j, l'')$, is the second in the determining pair [use of the points $H_k(L_k)$ in the determining pairs corresponds to choice of reflections with negative indices $l_k(h_k)$]. In the schemes, AB belongs to the k_i network, and A_1B_1 to the k_j network; we may, however, take AB for the k_j and A_1B_1 for the k_i, which corresponds to the condition $k_0 = \overline{k}_i - \overline{k}_j$.

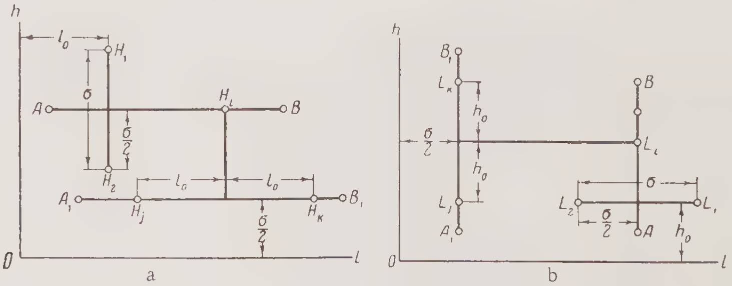

a b

Fig. 1. Schemes for selecting determining pairs. a) For condition $h_1 > h_2$, $l_1 = l_2$. b) For condition $h_1 = h_2$, $l_1 > l_2$.

---

[4] In Table 3 and in the figures, h'' and l'' are indicated by $\sigma/2$, and h' and l' by $h_1 + (\sigma/2)[l_2 + (\sigma/2)]$.

Any of the so-chosen combinations H_iH_j, H_iH_k, and L_iL_j, L_iL_k gives a determining pair for the comparison pairs H_1H_2 or L_1L_2. It is not hard to see that selection according to schemes A and B gives all possible determining pairs for the given pair of planes $y^* = k_i$, $y^* = k_j$. In order to obtain the maximum number of determining pairs, choice is made according to these schemes for all possible pairs of planes satisfying the condition $k_0 = k_i - k_j$.[5]

Construction of Chains and Choice of Initial Signs. Pairs for which the identity or opposition of the signs is substantiated statistically are connected in a chain of signs through reflections common to different pairs. Reflections with indices belonging to only one of the eight groups 1) h = 2n, k = 2n, l = 2n; 2) 2n + 1, 2n, 2n; 3) 2n, 2n, 2n + 1; 4) 2n, 2n + 1, 2n; 5) 2n + 1, 2n, 2n + 1; 6) 2n + 1, 2n + 1, 2n; 7) 2n, 2n + 1, 2n + 1; 8) 2n + 1, 2n + 1, 2n + 1, can enter into each chain.

Out of the set available, we may assign signs arbitrarily to three reflections [10,17,18] and by this fix the origin of the cell in one of the eight translationally nonidentical centers of symmetry of the unit cell. Let us, in fact, denote the coordinates of the centers of symmetry in the primitive cell by $(\varepsilon_1, \varepsilon_2, \varepsilon_3)$, where ε can only take the values 0 and $\frac{1}{2}$; then the structure factor

$$F_{hkl} = 2\sum_{j=1}^{N/2} f_j \cos 2\pi (hx_j + ky_j + lz_j)$$

on transition to an origin in any other center of symmetry, transforms into

$$F'_{hkl} = \cos 2\pi (h\varepsilon_1 + k\varepsilon_2 + l\varepsilon_3) F_{hkl},$$

where, for $\cos 2\pi (h\varepsilon_1 + k\varepsilon_2 + l\varepsilon_3)$ either +1 or −1 are possible values, i.e., the sign of F'_{hkl} changes or remains the same, depending on the choice of coordinates for the new origin and the parity of the indices h, k, l.

For reflections of the first group, the sign of the amplitude does not depend on the choice of origin at one center of symmetry or another, and is determined exclusively by the structure. Signs may be assigned to the amplitudes of the remaining groups quite arbitrarily. In fact, since the signs of the amplitudes of the second group with even k and l and odd h change on transferring the origin to any of the four centers with $\varepsilon_1 = \frac{1}{2}$, on assigning the sign of a structure amplitude of this type we fix the value of ε_1. By assigning the sign of an amplitude from the third or fourth groups, we fix ε_3 and, correspondingly, ε_2. A fixed sign for an amplitude of the fifth group determines whether the sum $\varepsilon_1 + \varepsilon_3$ is integral or fractional. In order to fix the origin in one of the eight centers of symmetry, we must assign the signs of three amplitudes of different groups in such a way that the sign of one of them is not a consequence of the assignment of the other two.

An origin in one of the four centers of symmetry of a primitive projection of the cell on, for example, the xz plane, is fixed by the assignment of signs for two structure amplitudes F_{h0l} of different groups (excluding the first group).

Selection of the Key Group of Amplitudes and Determination of Signs. Experimental values of F_{h0l} were reduced to quantities proportional to $\hat{F}_{h0l}$, allowing for the temperature factor $\exp[-B(\sin\vartheta/\lambda)^2]$ [10,19,22]. According to [13], for the comparatively refractory silicates (beginning of the endothermic process in zoisite is at 1000°C, compare muscovite, 860°C), the factor $B \leq 1$ [kX]^2. With some reserve, we took B = 0.7[kX]^2.

Initially we selected 50% of the reflections with the greatest $\hat{F}_{h0l}$. Choice of the determining pairs from this group, despite their relatively large number, led to unsatisfactory statistics, and the key group was reduced to 30% (137 reflections in all). Since this number was small for obtaining a sufficient number of determining pairs, to the key group were added 30% of the strongest $\hat{F}_{h1l}$ (92 reflections), which were used only for forming the determining pairs. All the h0l reflections taken into the key group, and also the auxiliary h1l, were set out in two square networks (simplified h0l and h1l planes of the reciprocal lattice), and with the help of these the selection of the comparison and determining pairs was made by schemes A and B. The statistics proved satisfactory, and it was possible to compare approximately 60 pairs of reflections. For three or four determining pairs, the difference or similarity of the signs was established "reliably," and for five or more with a probability not lower than 0.80. Later, these pairs were united in the chain of signs shown in Fig. 2.

For the assignment of signs it was natural to choose chains 1a and 2a, which included the largest number of reflections, obtaining the signs in terms of the reflections (15.0.9) and (25.0.4), which (inside the chain) had the largest number of linkages.

---

[5] As shown above, for comparing the signs of the amplitudes F_{h0l}, it was sufficient to make a selection of determining pairs in the plane h0l and afterwards in the plane h1l. For comparing the signs of amplitudes F_{h1l}, the comparison pairs were taken in the plane h1l and the determining pairs one by one from h0l and h1l.

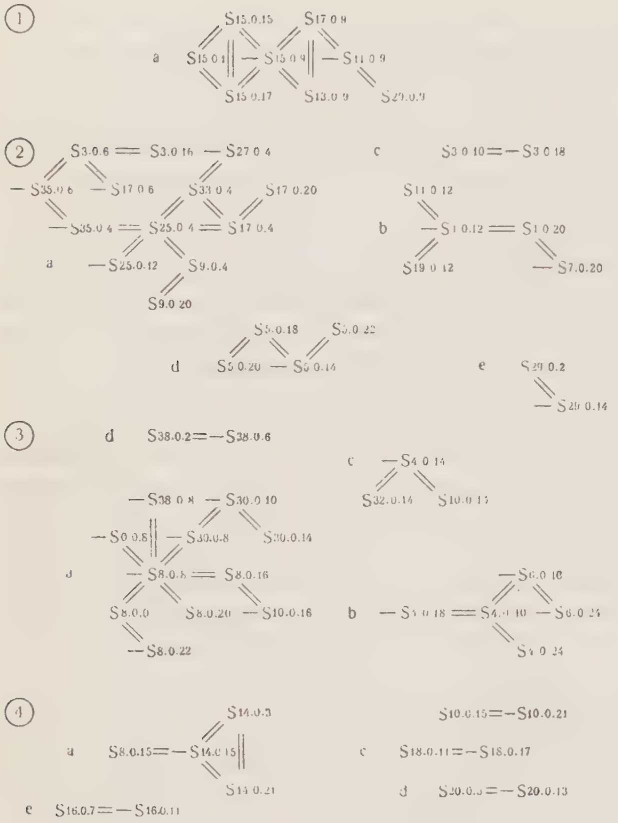

Fig. 2. Chains of signs for h0l reflections.

Putting $S_{15.0.9} = -$, and $S_{25.0.4} = +$, we obtained the signs of 21 amplitudes from chains 1a and 2a. With the help of these signs and relation (1), we successively established signs for (1.0.12), (5.0.14), (6.0.10), (3.0.10), (29.0.2), (38.0.2), (808), and (4.0.14), respectively, entering the chains 2b, 2d, 3b, 2c, 2e, 3d, 3a, and 3c. This extended the number of determined amplitudes from 34 to a total of 55. In the unused chains 4a, 4b, 4c, 4d, and 4e we were unable to determine the sign of a single amplitude by means of these 55.

The 55 amplitudes whose signs were fixed fairly convincingly served to provide a statistical determination of the signs of the remaining amplitudes selected for the key group. First we determined the signs of those amplitudes H for which the greatest number of pairs (K_i, $H + K_i$) could be formed from those already determined. Selection of the pairs was made (in accordance with Vainshtein [2]) by means of movable and stationary networks. After fixing the signs of the whole key group, the sign of each of the 137 was further checked statistically from pairs taken from the other 136.[6] Since, for a large number of determining pairs, the signs of some of the amplitudes were not confirmed, the corresponding reflections were excluded from the key group and not used in establishing the signs of all the amplitudes. In the last stage a sign was considered established if, for 20 to 50 determining pairs, the probability was no lower than 0.66.[7]

Construction and Analysis of Electron-Density Projections

The First xz Projection of Electron Density. In constructing the first electron-density projection, 278 amplitudes F_{h0l} were used, the signs being determined by the statistical method. Identification of the peaks in the numerical table obtained was easy on the basis of the structural link between zoisite and epidote. If we disregard the iron present in epidote (approximately one iron atom for two of aluminum), the zoisite (which does not usually contain iron) is a polymorphic modification of epidote with a similar structure, since two dimensions of the unit cell almost coincide, while between the third ones there is a simple relation $2a \sin\beta = a'$.

Epidote	Zoisite
b = 5.62 kX,	b' = 5.50 kX,
c = 10.23 kX,	c' = 10.14 kX,
a = 8.89 kX,	a' = 16.26 kX
β = 115°24',	($2a \sin 115°24' = 16.06$ kX),
$C_{2h}^{2} = P1\frac{2_1}{m}1.$	$D_{2h}^{16} = P\frac{2_1}{n}\frac{2_1}{m}\frac{2_1}{a}.$

The orthorhombic zoisite is a microtwin of epidote with twinning plane (100). According to analysis of the extinctions (p.), the diagonal glide plane n serves as this twinning plane (100).

In the monoclinic cell of epidote (Fig. 3), one set of four centers of symmetry coincides with the centers of the Al octahedra, and the other set of four inverts the $[Si_2O_7]$ groups at levels b/4 and 3b/4 one into the other (in Fig. 3, pairs of such groups are located in the middle of the a edge). Despite the doubling by the twinning plane, both in volume and in material content, the orthorhombic cell of zoisite is nevertheless primitive, and therefore half of the "epidote" centers of symmetry vanish. Consideration of the epidote cell shows that the Al octahedra (at 0 and c/2) already lie almost exactly in the plane which would correspond to a glide plane passing through them and through the c axis. In zoisite, this plane becomes the actual di-

---

[6] Not strictly from 136, since not all the signs of the 137 were found statistically.

[7] In determining the key group we had no more than 10 to 12 pairs; this also was responsible for the rigorous demands indicated above for this group.

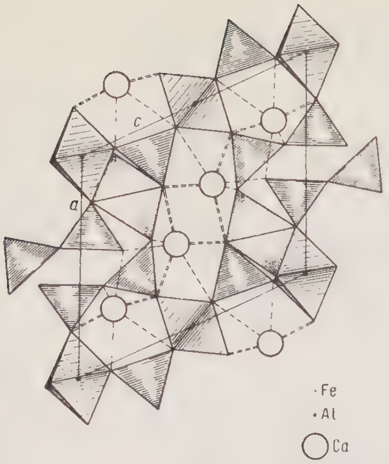

Fig. 3. Structure of epidote in coordination polyhedra. Projection on the xz plane.

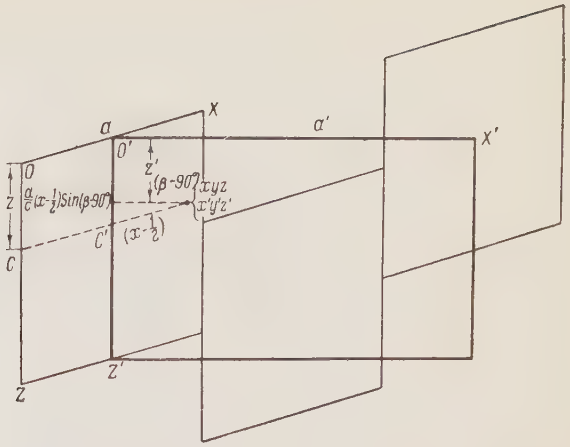

Fig. 4. Scheme of relationships between the monoclinic cell of epidote and the orthorhombic cell of zoisite.

TABLE 4. Coordinates of Atoms in Zoisite from Second Synthesis

Atoms	No. of atoms in cell	Coordinates	
		100 x/a	100 z/c
Al_I	4	25.0	19.05
Al_{II}	4	25.0	19.05
Al_{III}	4	10.7	30.0
Ca_I	4	37.2	43.6
Ca_{II}	4	45.4	11.2
Si_I	4	8.45	10.2
Si_{II}	4	41.2	28.1
Si_{III}	4	16.2	43.5
O_I	8	12.7	15.0
O_{II}	8	10.1	43.1
O_{III}	8	37.5	24.5
O_{IV}	4	22.3	30.4
O_V	4	22.3	30.4
O_{VI}	4	26.85	7.1
O_{VII}	4	−0.2	16.1
O_{VIII}	4	0	29.6
O_{IX}	4	43.5	43.8
O_X	4	26.85	7.1

agonal glide plane, and then the centers of symmetry lying in it should vanish, since, in the group D_{2h}^{16} all the centers of symmetry lie midway between planes.

Thus, in zoisite, the Al atoms do not lie in centers of symmetry, and the latter are retained only between pairs of diorthogroups $[Si_2O_7]$ in the middle of the *a* edge, to which we must also refer the origin of the epidote cell, if we are to calculate the coordinates of zoisite from the coordinates of epidote. The translation reduces all the x coordinates of the epidote by $a/2$, and on taking account of the doubling of the *a* axis in zoisite, the result is further divided in half. Exchanging the oblique-angled cell of epidote for a rectangular cell, according to Fig. 4, reduces all z by

$$\frac{a}{c}\sin 25°24'\left(x-\frac{1}{2}\right)\approx 0.38\left(x-\frac{1}{2}\right).$$

Thus, the formulas for the transformation to the rectangular cell (where the new coordinates of epidote should, to fair accuracy, be the coordinates of zoisite) will be:

$$x'=\frac{1}{2}\left(x-\frac{1}{2}\right),$$
$$z'=z-0.38\left(x-\frac{1}{2}\right),$$
$$y'=y.$$

The coordinates obtained from these formulas for zoisite (Table 4) may be compared with the figures which emerge from the statistical synthesis. Comparison shows that these are in fair agreement. Apart from this, however, the heights of the peaks in the synthesis did not correspond to the atomic numbers. Thus, the peak of the twinned Al was more than three times higher than that of the ordinary Al. Whereas Ca_I had height 451, the height of Ca_{II} was 200. For two of the Si atoms, the heights were over 250, while for the third the height was below 200. The single O_{VII} and O_{VIII} peaks could not be distinguished from "ghost" peaks of similar height.

The reason for this inadequate revelation of the light atoms is clear. Owing to the rapid fall in atomic factor, these only introduce a substantial contribution into amplitudes from planes with large interplanar spacings and small *hkl*. It is the determination of the signs for just these amplitudes which presents greatest difficulty to the statistical method.

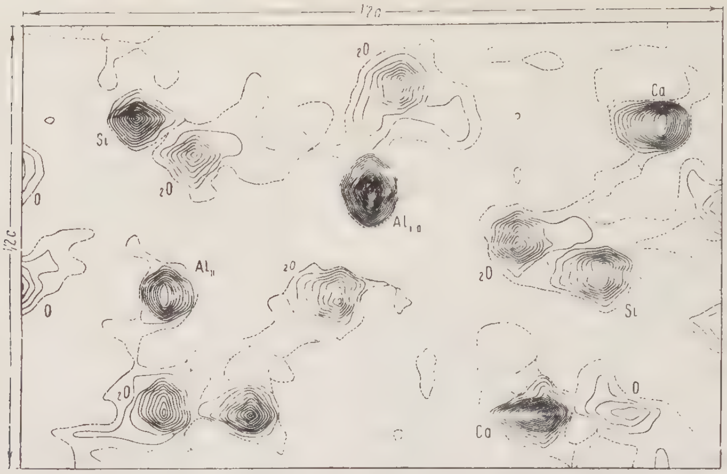

Fig. 5. Electron-density projection of the cell of zoisite on the xz plane (quarter cell).

The Second xz Projection of Electron Density. From the coordinates of the statistical synthesis we calculated the amplitudes whose signs were not given by the statistical method, i.e., 407 – 278 = 129 amplitudes. As indicated, a significant part of them comprised the amplitudes of the fundamental tones. Twenty-two structure amplitudes (all with large indices) were found to be insignificant and changed sign for small changes in coordinates. These were discarded in constructing the second synthesis, presented in contours in Fig. 5. The peaks of the two kinds of Ca became equal in height. The ratio between the heights of the peaks corresponding to the twinned Al_{I-II} and single Al_{III}, and that between the peak of the twinned Al_{I-II} (815) with "atomic number" 2 · 13 = 26 and the peak of Ca (600) with Z = 20, were both well preserved. The three sorts of Si_I, Si_{II}, and Si_{III} have respective heights 512, 425, and 504. The peaks of the twinned O with heights from 362 to 458 decompose into sharp and blurred peaks. The first correspond to pairs of O which are connected by a mirror plane and exactly overlap each other, and the second to pairs of O which are mutually superposed not from the requirements of symmetry but only from the principle of closest packing of atoms in the octahedra around the Al. The single O_{VII} and O_{VIII}, which evaded the first synthesis, are fully revealed. All the single O have maxima from 217 to 274. Not a single side peak ("ghosts") exceeds 160 (background about 100). The coordinates emerging from the second synthesis appear in Table 4.

From these almost-final coordinates we calculated the amplitudes which are compared with experimental values in Figs. 6a to 6i, which show 420 F_{h0l}, including 407 which, from experimental data, were nonzero and 13 zero types with h and l not exceeding 10. The points on the broken line indicate that the sign of the corresponding amplitude was established by the statistical method.

The coefficient of reliability for h0l reflections

$$b = \frac{\Sigma \mid F_{\text{esch}} \mid - \mid F_{\text{calc}} \mid}{\Sigma \mid F_{\text{esch}} \mid}$$

equals 0.22 allowing for zero amplitudes and 0.21 without these.

Construction and Analysis of Conditional Projections

Although there was no doubt as to the y coordinates of the atoms in the zoisite structure, since these corresponded to the heights of the analogous atoms in epidote, we nevertheless verified the horizontal and vertical coordinates by the method of conditional or generalized projections [20]. The corresponding $\int_0^1 \rho(xyz)\sin 2\pi y dy$ function for a structure similar to zoisite with atoms at only four levels, as we can easily see, gives a projection in which atoms at the levels 0 and b/2 vanish, whereas atoms at levels b/4 and 3b/4 are fixed as peaks for the first, and troughs or pits for the second.

The function

$$b\int_0^1 \rho \sin 2\pi y dy = -\frac{1}{S}\left[\sum_{h,\, l=-\infty}^{\infty}\sum F_{h1l} \sin 2\pi (hx + lz)\right]$$

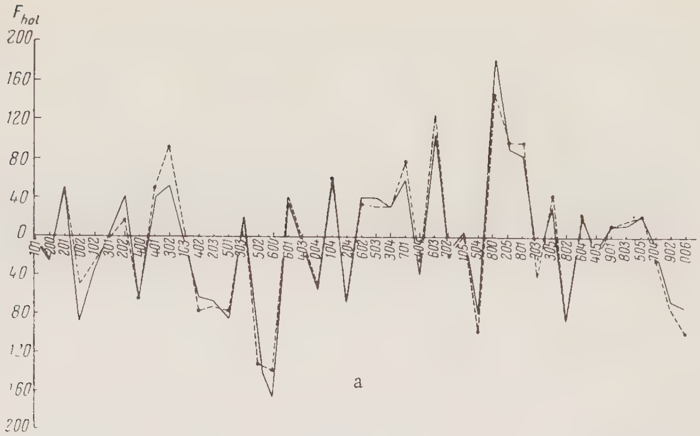
F_{hol}
200
160
120
80
40
0
40
80
120
160
200

a

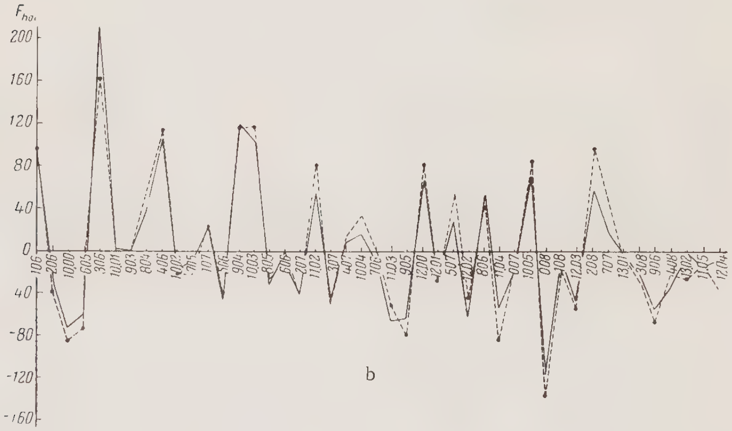
F_{hol}
200
160
120
80
40
0
-40
-80
-120
-160

b

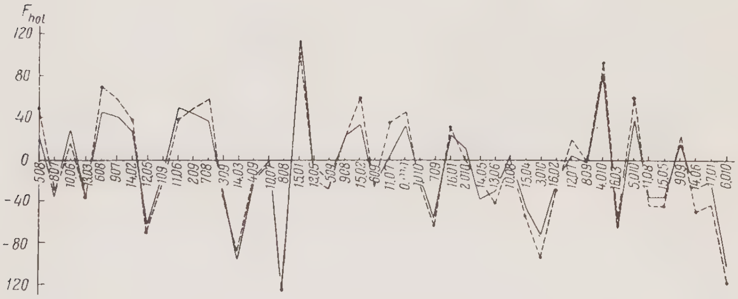
F_{hol}
120
80
40
0
-40
-80
120

c

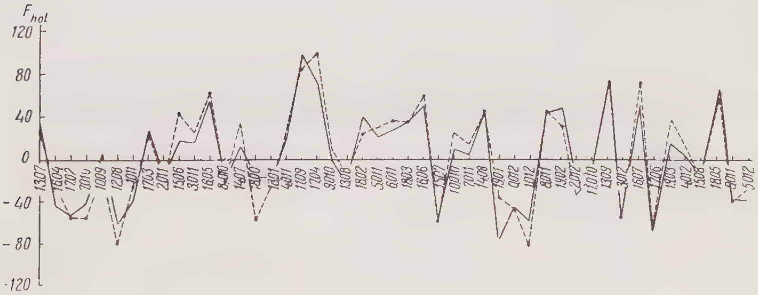
F_{hol}
120
80
40
0
-40
-80
-120

d

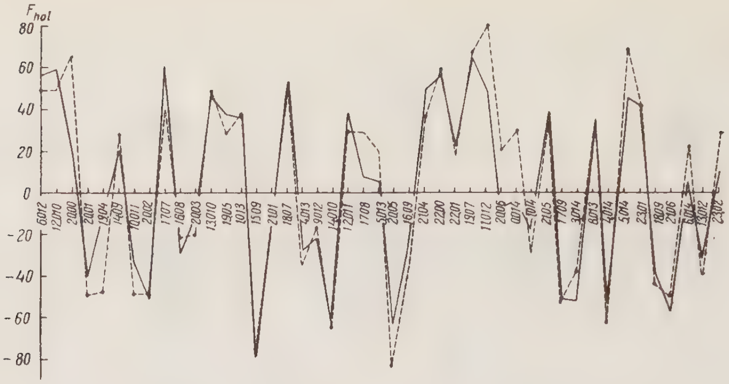
F_{hol}
80
60
40
20
0
-20
-40
-60
-80

e

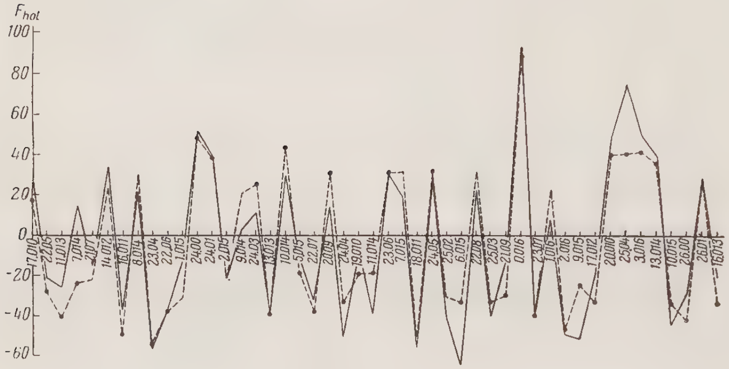
F_{hol}
100
80
60
40
20
0
-20
-40
-60

f

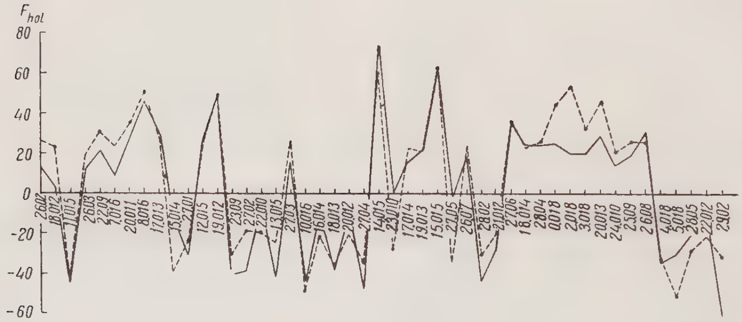
F_{hol}
80
60
40
20
0
-20
-40
-60

g

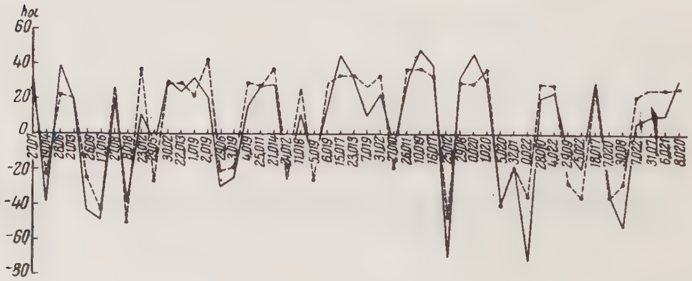
hol
60
40
20
0
-20
-40
-60
-80

h

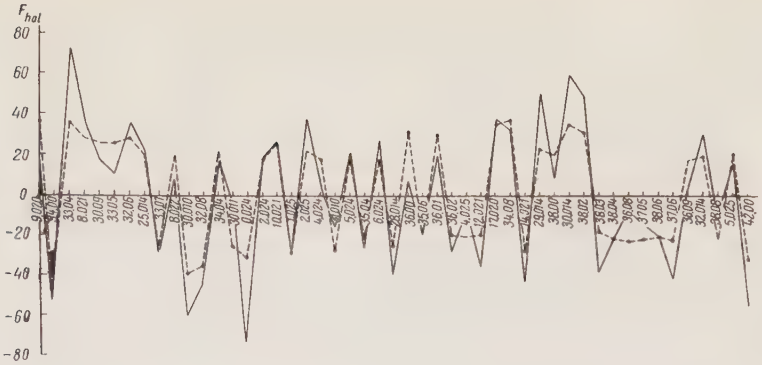

i

Fig. 6. a-i) Graphs showing the correspondence of calculated and experimental values of F_{h0l} (continuous and broken lines, respectively).

takes the following form for calculation:

$$-\frac{1}{S}\left\{2\sum_{h=1}^{\infty}{}' F_{h10}\sin 2\pi hx + 2\sum_{l=1}^{\infty}{}'' F_{01l}\sin 2\pi lz + 4\sum_{h,\,l=1}^{\infty}{}'\sum{}' F_{h1l}\sin 2\pi hx\cos 2\pi lz + 4\sum_{h,\,l=1}^{\infty}{}''\sum{}'' F_{h1l}\cos 2\pi hx\sin 2\pi lz\right\}.$$

The single primes indicate summations referring to F_{h1l} with $h + l = 2n$, and the double primes summations referring to F_{h1l} with $h + l = 2n + 1$.

The Key Group of Structure Amplitudes $h1l$. We used the method of comparing signs and constructing chains which was employed earlier for the F_{h0l}, and in the final stage, relation (1). The problem was made easier by the existence of around 300 amplitudes F_{h0l} with signs determined earlier and confirmed by calculation.

At the first stage (in comparing signs), we used 172 of the greatest amplitudes $\hat{F}_{h0l}$ with reliable signs and 92 $\hat{F}_{h1l}$ which took part in comparing the signs of the $\hat{F}_{h0l}$ (in the determining pairs). The F_{h0l} now entered exclusively into the determining pairs, one in each. The comparison and determining pairs were chosen by the same schemes A and B. Of the comparison pairs, only those which had received the best statistical substantiation were chosen. The chains of signs are given in Fig. 7. The closing of the links enabled us to detect erroneous linkages, for example in chains 4 and 5, where they are shown by broken equality signs.

The x and z coordinates of the origin were fixed by the earlier assignment of signs for two amplitudes. In order to fix the third, the y coordinate, we arbitrarily assign the sign of one of the F_{h1l} amplitudes. Having a large number of rigidly established F_{h0l} signs, and remembering the possibility of undetected erroneous linkages in the S_{h1l} chains, we chose as basis not the longest chain, but only the closed links of chain 4 with amplitudes (517), (717), (13.1.7), (511), and (5.1.17). Setting $S_{517} = -$, we have $S_{717} = +$, $S_{511} = +$, $S_{5.1.17} = +$, and $S_{13.1.7} = -$. With the aid of the five signs so furnished for the amplitudes F_{h1l} and also the 172 F_{h0l}, the signs in the remaining chains were successively found, and then the signs of the key group; after verifying each determined sign by statistics, using all possible pairs from the same key group, we proceeded to apply the statistical equation (1) to the rest of the amplitudes. Altogether, the signs of 218 F_{h1l} amplitudes were established out of a total of 277, i.e., 79%.

Two Conditional Projections. The conditional projection

$$\int_0^1 \rho \sin 2\pi y\,dy$$

was synthesized twice: the first time from 218 F_{h1l} amplitudes with statistical signs, and the second with the addition of amplitudes, the signs of which were calculated from the coordinates. In the second synthesis, we used 273 amplitudes, since, out of the total number of 277 experimental $F_{h1l} \neq 0$ values, six were excluded for the same reasons as in the case of the F_{h0l}, and two, (111) and (211), were added, these being substantial in absolute magnitude, but falling in the "dead zone" of the x-ray photograph. The improved conditional projection is given in contours in Fig. 8. This contains all the peaks of the full projection, except the $\mathrm{Al}_{\mathrm{I-II}}$

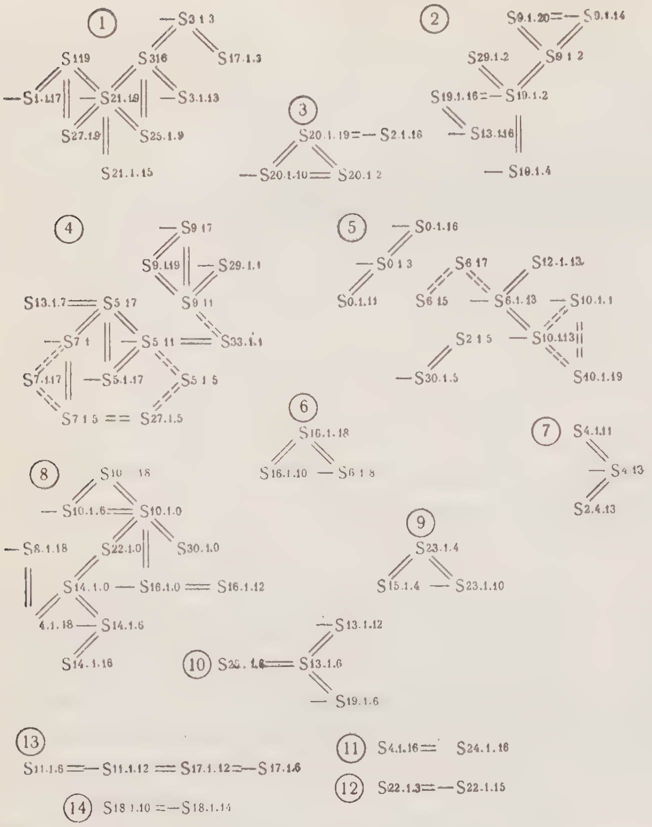
① —S3.1.3 S1.1.9 S3.1.6 S17.1.3 —S1.1.17 —S21.1.9 —S3.1.13 S27.1.9 S25.1.9 S21.1.15
② S9.1.20=—S9.1.14 S29.1.2 S9.1.2 S19.1.16=—S19.1.2 —S13.1.16 —S19.1.4
③ S20.1.19=—S2.1.16 —S20.1.10== S20.1.2
④ —S9.1.7 S9.1.19 —S29.1.1 S9.1.1 S13.1.7== S5.1.7 S33.1.1 —S7.1 —S5.1.1 S7.1.17 —S5.1.17 S5.1.5 S7.1.5 == S27.1.5
⑤ —S0.1.16 —S0.1.3 S0.1.11 S6.1.7 S12.1.13 S6.1.5 —S6.1.13 —S10.1.1 S2.1.5 —S10.1.13 —S30.1.5 S10.1.19
⑥ S16.1.18 S16.1.10 —S6.1.8
⑦ S4.1.11 —S4.1.13 S2.4.13
⑧ S10.1.18 —S10.1.6== S10.1.0 —S8.1.18 S22.1.0 S30.1.0 S14.1.0 —S16.1.0 == S16.1.12 4.1.18— S14.1.6 S14.1.16
⑨ S23.1.4 S15.1.4 —S23.1.10
⑩ S26.1.6== S13.1.6 —S13.1.12 —S19.1.6
⑪ S4.1.16== S24.1.16
⑫ S22.1.3=—S22.1.15
⑬ S11.1.6=—S11.1.12 == S17.1.12=—S17.1.6
⑭ S18.1.10 =—S18.1.14

Fig. 7. Chains of signs for h1l reflections.

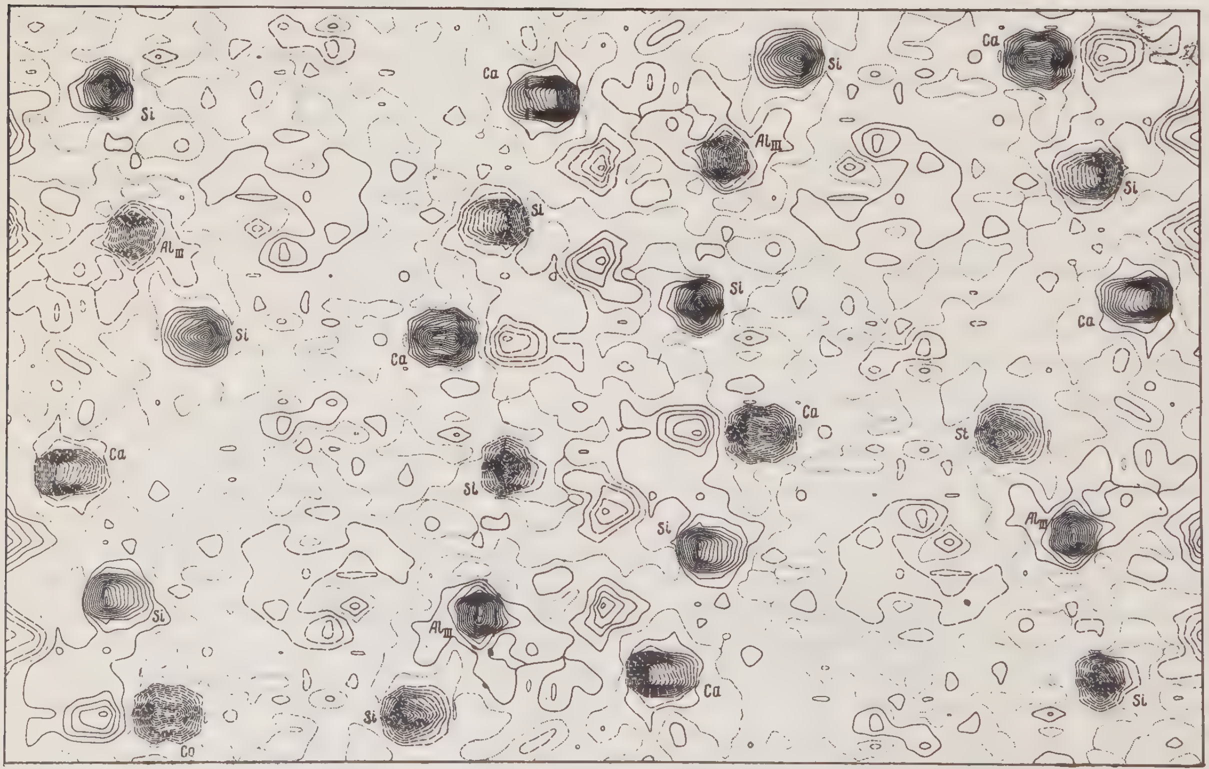

Fig. 8. Conditional projection $\int_0^1 \rho \sin 2\pi y b dy$. Negative signs of the function are indicated by broken contours.

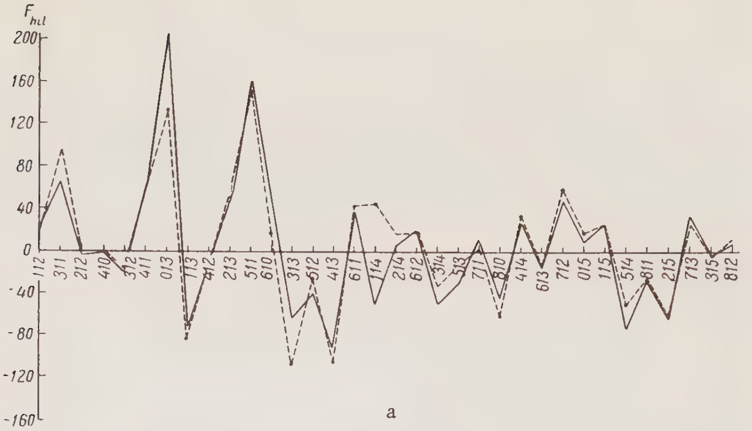
F_{hkl}
200
160
120
80
40
0
-40
-80
-120
-160
112
311
212
410
312
411
013
113
412
213
511
610
313
512
413
611
114
214
612
314
513
711
810
414
613
712
015
115
514
811
215
713
315
812

a

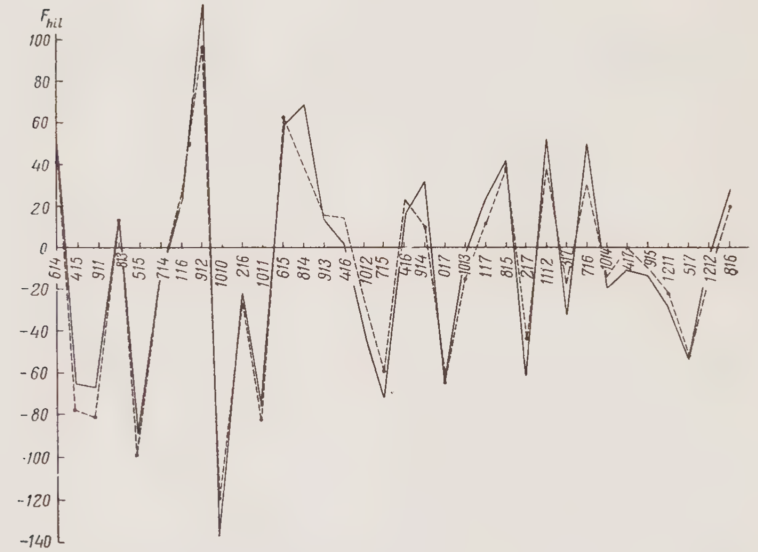
F_{hkl}
100
80
60
40
20
0
-20
-40
-60
-80
-100
-120
-140
614
415
911
813
515
714
116
912
1010
216
1011
615
814
913
416
1012
715
416
914
017
1013
117
815
217
1112
317
716
1014
417
915
1211
517
1212
816

b

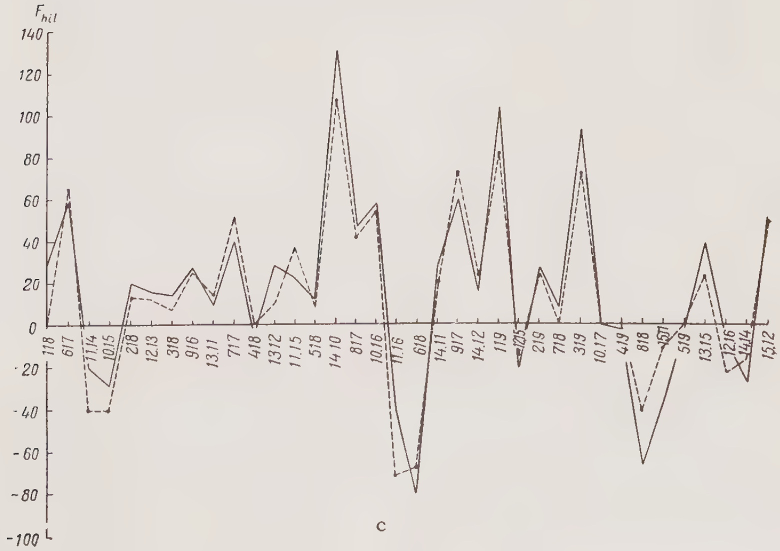
F_{hkl}
140
120
100
80
60
40
20
0
-20
-40
-60
-80
-100
118
617
11.14
10.15
218
12.13
318
916
13.11
717
418
13.12
11.15
518
14.10
817
10.16
11.16
618
14.11
917
14.12
119
12.15
219
718
319
10.17
419
818
15.11
519
13.15
12.16
14.14
15.12

c

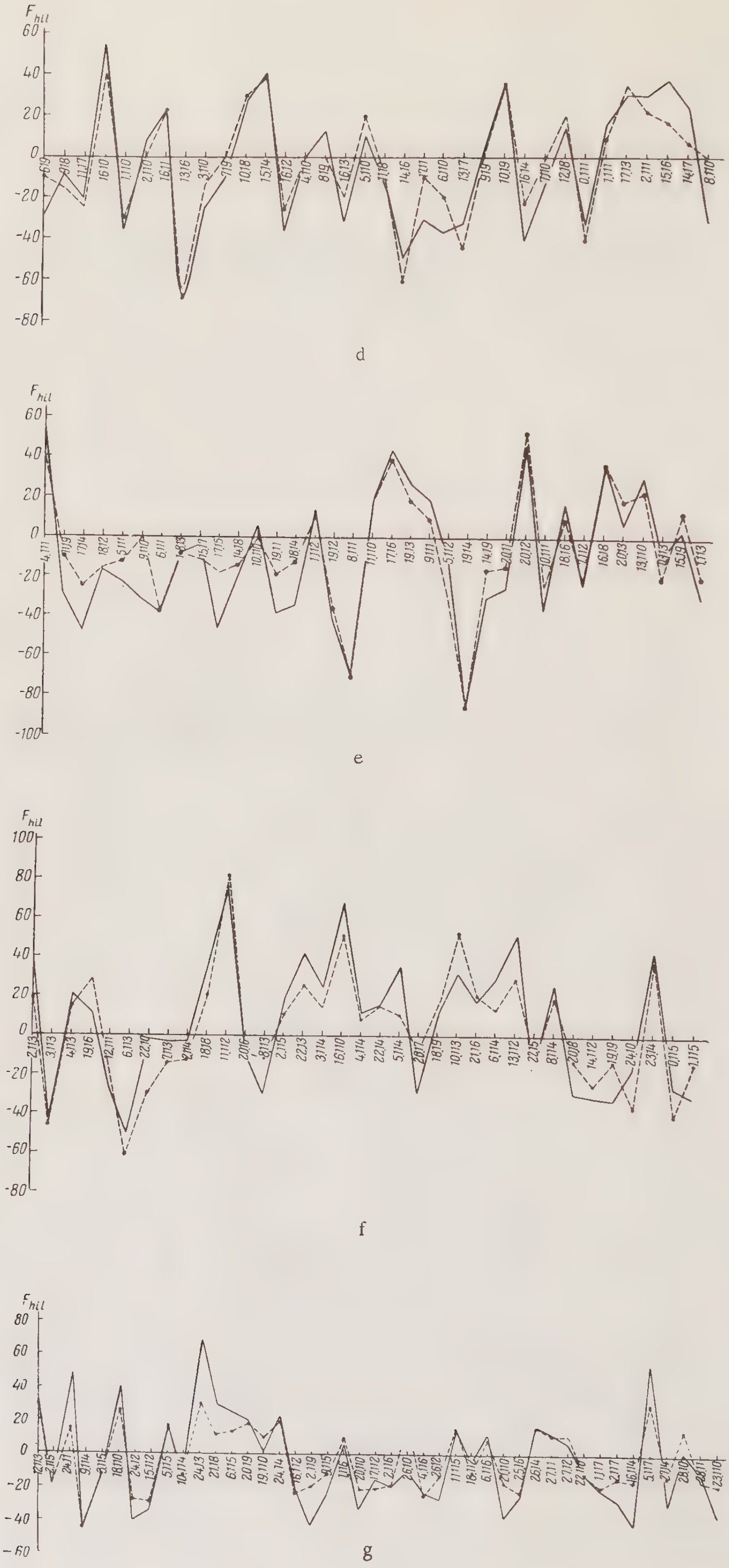
F_{hkl}
60
40
20
0
-20
-40
-60
-80
6.1.9
9.1.8
11.1.7
16.1.10
1.1.10
2.1.10
16.1.1
13.1.6
3.1.10
7.1.9
10.1.8
15.1.4
16.1.2
4.1.10
8.1.9
16.1.3
5.1.10
11.1.8
14.1.6
12.1.1
6.1.10
13.1.7
9.1.9
10.1.9
16.1.4
7.1.10
12.1.8
0.1.11
1.1.11
17.1.3
2.1.11
15.1.6
14.1.7
8.1.10
F_{hkl}
60
40
20
0
-20
-40
-60
-80
-100
4.1.11
11.1.9
17.1.4
18.1.2
5.1.11
9.1.10
6.1.11
1.8.13
15.1.7
17.1.5
14.1.8
10.1.10
19.1.1
18.1.4
1.1.12
19.1.2
8.1.11
11.1.10
17.1.6
19.1.3
9.1.11
5.1.12
19.1.4
14.1.9
2.0.11
20.1.2
10.1.11
18.1.6
7.1.12
16.1.8
20.1.3
13.1.10
0.1.13
15.1.9
1.1.13
F_{hkl}
100
80
60
40
20
0
-20
-40
-60
-80
2.1.13
3.1.13
4.1.13
19.1.6
12.1.11
6.1.13
22.1.0
7.1.13
2.1.14
18.1.8
11.1.12
20.1.6
8.1.13
2.1.15
22.1.3
3.1.14
16.1.10
4.1.14
22.1.4
5.1.14
20.1.7
18.1.9
10.1.13
21.1.6
6.1.14
13.1.12
22.1.5
8.1.14
20.1.8
14.1.12
19.1.9
24.1.0
23.1.4
0.1.15
1.1.15
F_{hkl}
80
60
40
20
0
-20
-40
-60
12.1.13
2.1.15
24.1.1
9.1.14
3.1.15
18.1.10
24.1.2
15.1.12
5.1.15
10.1.14
24.1.3
21.1.8
6.1.15
20.1.9
19.1.10
24.1.4
16.1.12
2.1.19
9.1.15
1.1.16
20.1.10
17.1.12
2.1.16
26.1.0
4.1.16
26.1.2
11.1.15
18.1.12
6.1.16
21.1.10
25.1.6
26.1.4
27.1.1
27.1.2
22.1.10
1.1.17
21.1.7
16.1.14
5.1.17
27.1.4
28.1.0
28.1.1
23.1.10

d

e

f

g

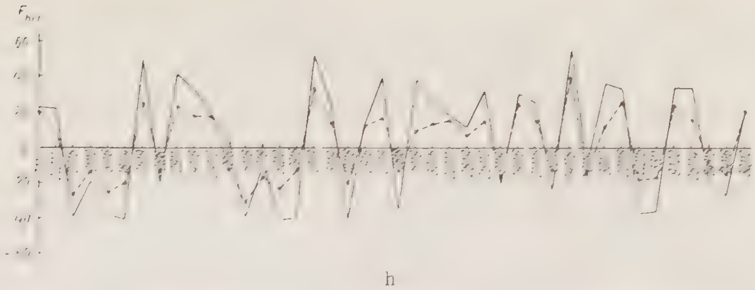

Fig. 9. a-h) Graphs showing the correspondence of calculated and experimental values of F_{h1l} (continuous and broken lines, respectively).

TABLE 5. Coordinates of Basic Atoms of the Zoisite Structure

Atoms		$100\,x/a$	$100\,y/b$	$100\,z/c$
$Al_{I\text{-}II}$	(8)	25.0	0	19.05
Al_{III} (Fe)	(4)	10.7	75	30.0
Ca_I	(4)	37.2	25	43.6
Ca_{II}	(4)	45.4	25	11.2
Si_I	(4)	8.45	25	10.2
Si_{II}	(4)	41.2	75	28.1
Si_{III}	(4)	16.2	25	43.5
O_I	(8)	11.8	0	15.0
O_{II}	(8)	10.1	0	43.1
O_{III}	(8)	37.5	0	24.5
O_{IV}	(4)	22.3	25	30.4
O_V	(4)	22.3	75	30.4
O_{VI}	(4)	26.85	75	5.7
O_{VII}	(4)	—0.3	25	16.3
O_{VIII}	(4)	—0.3	75	29.6
O_{IX}	(4)	43.5	75	43.8
OH	(4)	26.85	25	7.5

and three sorts of O (I, II, III), since, for these atoms, the y coordinates equal 0 or ½. Within the quarter cell the two sorts of Ca occur at different heights. The Si_I and Si_{II} atoms from a single diorthosilicate group and the O_{IX} atoms common to the two Si in fact occurred in a common mirror plane, once in the form of a triplet of peaks and once as a triplet of troughs.

The coordinates of the atoms obtained from the conditional projection, after comparison with the full projection, were used for calculating the structure amplitudes F_{h1l}. Figures 9a-h present graphs comparing $F_{h1l\,\text{exp}}$ with $F_{h1l\,\text{calc}}$ for 295 F_{h1l}, among which 277 are nonzero and 18 are zero with $h, l \leq 10$.

Description of the Structure of Zoisite

Coordinates of the Basic Atoms. Table 5 shows the final coordinates of the basic atoms of the zoisite structure. The four groups of eight in general positions are each characterized by three parameters, and the thirteen groups of four in mirror planes by two. The whole structure is determined by 38 parameters (as against 35 in epidote, where, although there are two kinds of Al atoms, both are in centers of symmetry, i.e., without parameters).

We used Vainshtein's method [13] to calculate the probable error of the coordinates associated with inaccuracy in the intensities. For the case of the projections, the corresponding formula is

$$\Delta r_k = 0.049\,\frac{b}{\sqrt{S}}\cdot\frac{\sqrt{\sum_{i}^{N} Z_i^{2.54}}}{Z_k^{1.35}}, \tag{4}$$

where b is the confidence coefficient of reliability, S the area of the projection, and Z_i, Z_k are atomic numbers. In our case (Mo radiation), the series was broken off at $\sin\vartheta/\lambda = 1.36$, and from the graphs given in [13], $b_{\text{eff}} = 2b = 0.4$. Thus, the probable error in the coordinates introduced by inaccuracy in the intensities is $\Delta r_{Ca} = 0.008$kX, $\Delta r_{Al} = 0.012$ kX, $\Delta r_{Si} = 0.012$ kX, $\Delta r_O = 0.024$ kX, i.e., is considerably smaller than inaccuracy associated with the low resolving power of the 48^2 division of the unit parallelogram.

The sketches in Table 6 indicate the coordination polyhedra for each crystallographically independent Si and Al cation; alongside are indicated the cation–anion distances and the length of the oxygen edges in the polyhedra. The Si–O distances proved to lie within even narrower limits than those of epidote (in zoisite, 1.53 to 1.70 kX; in epidote, 1.51 to 1.73 kX). The Al–O and Ca–O distances were approximately the same in the two structures. The Si–O–Si "valence angle" of the diorthogroup in zoisite, ~161°, is close to the corresponding angle in epidote (158°) and quartz (150°).

Description of the Zoisite Structure. Figure 10 shows the xz projection of the

TABLE 6. Scheme of Environment of Cations and Interatomic Distances in the Structure of Zoisite, in kX

Si_{I}-tetrahedron

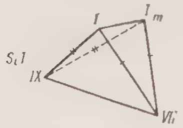

Si — I = 1.61
Si — VII = 1.53
Si — IX = 1.67

I — VII = 2.52
I — IX = 2.73
VII — IX = 2.54
I — I_m = 2.75

Si_{II}-tetrahedron

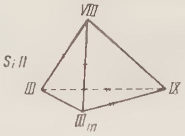

Si — III = 1.68
Si — VIII = 1.61
Si — IX = 1.63

III — VIII = 2.71
III — IX = 2.72
VIII — IX = 2.77
III — III_m = 2.75

Si_{III}-tetrahedron

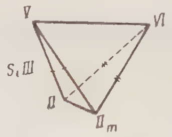

Si — II = 1.70
Si — V = 1.65
Si — VI = 1.67

II — V = 2.73
II — VI = 2.82
V — VI = 2.57
II — II_m = 2.75

$\text{Al}_{\text{I-II}}$-octahedron

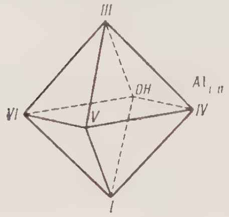

Al — I = 2.02
Al — III = 1.83
Al — IV = 1.87
Al — V = 1.87
Al — VI = 1.93

Al — OH = 1.83
IV — OH = 2.44
V — VI = 2.62
I — VI = 2.82

I — III = 2.91
I — OH = 2.77
$\left.\begin{array}{l}\text{I — IV}\\ \text{I — V}\end{array}\right\} = 2.58$
$\left.\begin{array}{l}\text{III — IV}\\ \text{III — V}\end{array}\right\} = 2.88$
III — OH = 2.80

Al_{III}-octahedron

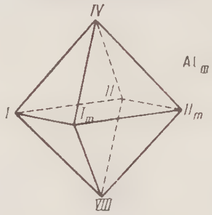

Al — I = 2.08
Al — II = 1.92
Al — IV = 1.87
Al — VIII = 1.79
IV — I = 2.59

I — VIII = 2.93
II — IV = 2.73
II — VIII = 2.57
I — II — 2.88

I — I_m = 2.75
II — II_m = 2.75

1. Roman figures indicate oxygen atoms
2. Atoms I–I_m, II–II_m, III–III_m are connected by mirror plane m.

structure, in which the oxygen tetrahedra around the Si and the octahedra around the two kinds of Al are marked out. The Ca atoms are shown by circles from which bonds pass to the closest O (OH). Figure 11 gives the axonometry of the structure.

The main features of the zoisite structure repeat those characterizing epidote. These include first of all vertical "guide rods," columns of Al octahedra extending along the y axis and passing close to the middle of each quadrant in the xz projection. In contrast to epidote, in the zoisite structure the axis of the columns does not coincide with the 2_1 axis, and the centers of the Al octahedra do not coincide with the centers of symmetry. Along the y axis the octahedra of one column are connected only by mirror planes through a common edge of each two successive octahedra. The neighboring columns of Al octahedra are crystallographically connected by diagonal and parallel glide planes passing through them in the z and x directions, respectively. In epidote, the single Al (Fe) octahedra intimately adjoin one half of the columns of Al octahedra on two sides, in accordance with the law of the two-fold screw axis, and are not connected with the other half of the Al columns. In zoisite the single Al octahedra are attached to both columns from one side only. This is the sharpest difference

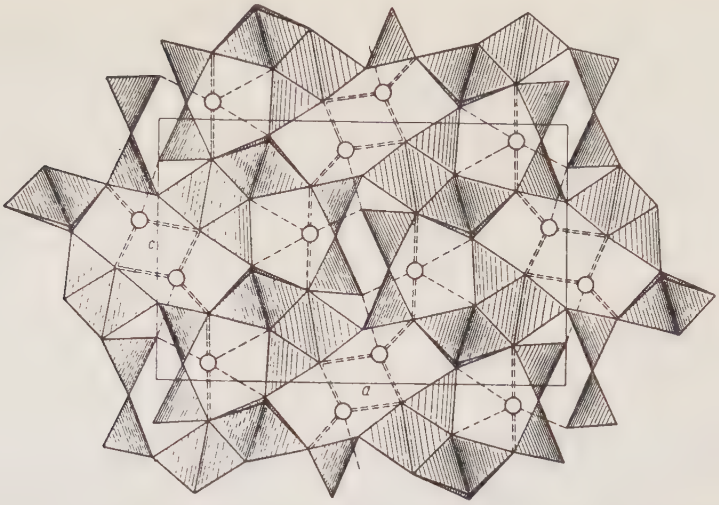

Fig. 10. Structure of zoisite in coordination polyhedra. Projection on the xz plane.

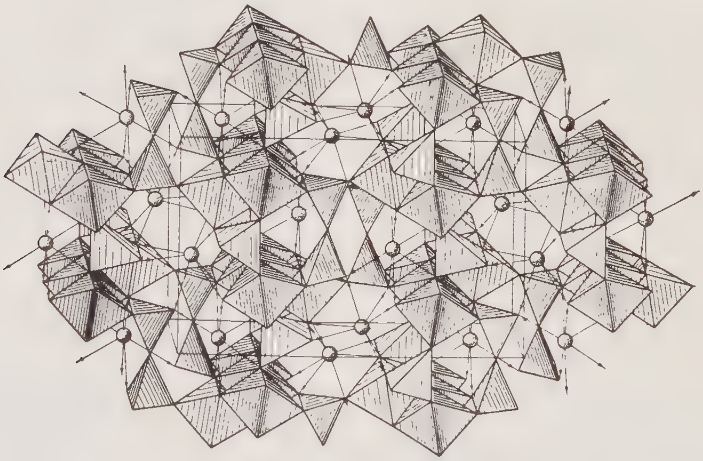

Fig. 11. Structure of zoisite in coordination polyhedra. Axonometry.

between the structures of zoisite and epidote. In epidote, the Al atoms are in the centers of symmetry, and among the vertices of each Al octahedron are either two OH groups (Al_{II}) or none (Al_I). In zoisite, each Al is connected with one OH group.

The Si atoms are of three kinds: Si_I and Si_{II} enter into the diorthosilicate group and Si_{III} into the orthosilicate. All link up with columns of Al octahedra, so that, in the xz projection, we find characteristic pentagons made up of two Al octahedra and three Si tetrahedra (Fig. 10).

Despite the orthosilicate ratio Si : O = 1 : 4 following from the formula, zoisite (like epidote) is nevertheless a silicate of the mixed type with two kinds of silicon–oxygen radicals: $[SiO_4]$ and $[Si_2O_7]$. Of the 12 oxygen atoms in the zoisite formula, 11 take part in the silicon–oxygen radicals; the twelfth O and the OH group are not connected with Si and are only saturated by the Al and Ca cations. In projection, and still better in axonometry, it is clear that there are two kinds of such O atoms: O_{IV} and O_X. According to the balance of valences, the O_X belongs to the OH, since the smallest sum of "cation forces" converges in this atom.

The Ca atoms in zoisite are of two kinds. The coordination polyhedra for both are heptahedra, constituting (as in epidote and ilvaite), the combination of a triangular prism with a hemioctahedron. The Ca_{II} polyhedra "stand" with the triangular base of the prism on the xz plane, while the Ca_I heptahedra "lie" on the same plane with the side edge of the prism. The distances from the Ca to the sever O are from 2.3 to 2.8 kX. For Ca_I we can find two more distant neighbors with distances ~3 kX. The Ca_{II} has three neighbors at a distance rather greater than 3 kX. We find a similar environment

TABLE 7

	Al_{I-II}	Al_{III}	Ca_I	Ca_{II}	Si_I	Si_{II}	Si_{III}	Sum of valence forces
O_I	$^3/_6$	$^3/_6$	$^2/_8$		$^4/_4$			$2^1/_4$
O_{II}		$^3/_6$		$2 \times {}^2/_8$			$^4/_4$	2
O_{III}	$^3/_6$		$^2/_8$	$^2/_8$		$^4/_4$		2
O_{IV}	$2 \times {}^3/_6$	$^3/_6$						$1^1/_2$
O_V	$2 \times {}^3/_6$		$^2/_8$				$^4/_4$	$2^1/_4$
O_{VI}	$2 \times {}^3/_6$		$^2/_8$				$^4/_4$	$2^1/_4$
O_{VII}			$^2/_8$	$^2/_8$	$^4/_4$			$1^1/_2$
O_{VIII}		$^3/_6$		$^2/_8$				$1^3/_4$
O_{IX}			$^2/_8$		$^4/_4$	$^4/_4$		$2^1/_4$
OH	$2 \times {}^3/_6$		$^2/_8$					$1^1/_4$

for Ca atoms in almost all those cases (for example, in apatite, sphene, epidote, and ilvaite), where the Ca occupies positions not in centers of symmetry.

The expanded formula of zoisite may be written as follows:

$$Ca_ICa_{II}(Al_{I-II})_2(Al, Fe)O(OH)[Si_2O_7][SiO_4]$$
$$= Ca_2Al_2(Al, Fe)O(OH)[Si_2O_7][SiO_4].$$

The symbol Al_{I-II} indicates the merging into a single group, in zoisite, of the two kinds of Al which are crystallographically different in epidote:

$$Ca_ICa_{II}Al_IAl_{II}(Al, Fe)O(OH)[Si_2O_7][SiO_4].$$

Balance of Valences. If, in accordance with Pauling's second rule we set up the sum of the valence forces meeting at each O, we obtain Table 7.

According to the table of Si–O distances (Table 6), the too-small sum of forces at O_{VII} is compensated by a reduction in the $Si-O_{VII}$ distance in the tetrahedra. As regards O_{IV}, its location alongside the OH group at a distance of 2.44 kX suggests a hydrogen bond between O_{IV} and O_X(OH), whereby the lack of valence forces at the O_{IV} is also compensated.

Certain Physical Properties of Zoisite. As regards cleavage, the properties of epidote are repeated: perfect along the (001) and imperfect along the (100), the apparent transposition of the cleavage planes causing some surprise. From the structural plan of zoisite and epidote we should have expected better cleavage in the (100) than the (001) plane.

In optical sign, zoisite is opposite to epidote. The negative character in the latter occurs because the Fe and Ca cations, which are energetically the most influential on the optical properties, are linked into plane networks perpendicular to the [010] axis. In zoisite with not more than 2% Fe_2O_3, the role of the networks of Ca and Al (Fe) ions falls into second place, while the first is occupied by the columns of Al octahedra, which determine the positive sign of the crystal. These columns also produce the strongly expressed striation of all the facets of the [010] zone.

Structure of Zoisite According to Ito. A considerable inaccuracy (10 to 12%) in the coordinates of epidote found by Ito was revealed in [2]. We find the same in his coordinates for zoisite [4]. Even for the heaviest atoms (Ca), the discrepancy reaches 0.022 c, i.e., 0.22 kX. For Al (Fe), it is 0.0125 a = 0.2 kX, and for Si_{III} we have 0.025 c = 0.25 kX. The largest are the discrepancies for the O_{IX} atom, which was also inaccurately determined in epidote, namely 0.045 a, i.e., 0.73 kX. For the O_{III} and O_{VII} atoms the discrepancy is around 0.045 c, i.e., 0.46 kX.

Figure 12 shows the structure of zoisite according to Ito. By comparing with Fig. 10 we see its main defects: mutilated Al octahedra and unnaturally featured diorthogroups, caused by the incorrect

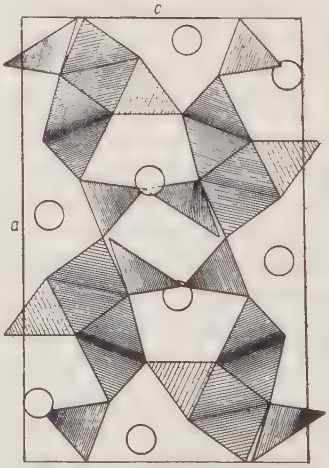

Fig. 12. Structure of zoisite according to Ito.

coordinates of O_{IX}, which for Ito overlaps the Ca atom in the xz projection. The O_{VII} and O_{VIII} overlap in the same way. These defects have a detrimental effect on the interatomic distances in the Si tetrahedra and Al octahedra. Thus, $Si_{I}-O_{IX} = 1.90$ kX, $Si_{III}-O_{VI} = 1.97$ kX, and $Si_{II}-O_{VIII}$ even reaches 2.10 kX. In the Si_{III} tetrahedron there is also a vastly shortened distance of $Si_{III}-O_{V} = 1.45$ kX. The distances between the O atoms vary substantially: the $O_{IX}-O_{VIII}$ edge equals 2.39 kX, and the $O_{IX}-O_{VII}$ edge 3.26 kX. The distances in the Al octahedra are a little better, although even in the Al (Fe) octahedron the Al (Fe) – O_{V} distance falls to 1.63 kX.

LITERATURE CITED

1. N. V. Belov and V. I. Mokeeva, "Crystal structure of ilvaite," DAN SSSR, 81, 581-584 (1951); Tr. Inst. Kristallogr., 9, 47-102 (1954).
2. N. V. Belov and I. M. Rumanova, "Crystal structure of epidote," DAN SSSR, 89, 853-856 (1953); Tr. Inst. Kristallogr., 9, 103-164 (1954).
3. V. S. Sobolev, Introduction to the Mineralogy of Silicates [in Russian] (1949).
4. T. Ito, X-Ray Studies on Polymorphism (1950).
5. B. Gossner and F. Mussgnung, "Über Epidot und Zoisit," Z. Min. Geol. u. Paläont., 369-371 (1930).
6. G. S. Zhdanov and V. A. Pospelov, "Rational tables of extinctions for determining x-ray groups," ZhÉTF, 15, 709-720 (1945).
7. G. S. Zhdanov and V. P. Kotov, "Quantitative determination of the total energies of x-ray interferences in structural analysis," ZhÉTF, 15, 918-921 (1945).
8. E. N. Belova and N. V. Belov, "Simplified methods of calculating the kinematic factor," DAN SSSR, 90, 183-184 (1953).
9. D. Harker and J. S. Kasper, "Phases of Fourier coefficients directly from crystal diffraction data," Acta Cryst., 1, 70-75 (1948).
10. W. H. Zachariasen, "A new analytical method for solving complex crystal structures," Acta Cryst., 5, 68-73 (1952).
11. T. Ito, N. Morimoto, and R. Sadanaga, "The crystal structure of realgar," Acta Cryst., 5, 775-782 (1952).
12. A. J. G. Wilson, "Determination of absolute from relative x-ray intensity data," Nature, 150-152 (1942).
13. B. K. Vainshtein, "Quantitative relationships in the electron-density Fourier series of crystals," ZhÉTF, 27, 44-61 (1954).
14. A. I. Kitaigorodskii, "New method of the direct structural analysis of crystals," DAN SSSR, 102, 519-520 (1955).
15. I. M. Rumanova, "Determining the signs of the 'key' structure amplitudes by statistical equations," DAN SSSR, 98, 395-398 (1954); Tr. Inst. Kristallogr., 10, 59-70 (1954).
16. International Tables (1952), p. 408.
17. H. Hauptman and J. Karle, "Solution of the Phase Problem, I. The Centrosymmetric Crystal (1953).
18. K. Lonsdale and H. J. Grenville-Wells, "Sign determination in crystal structure analysis," Acta Cryst., 7, 490-491 (1954).
19. R. D. Burbank, "The crystal structure of α-monoclinic selenium," Acta Cryst., 4, 140-148 (1951).
20. W. Cochran and H. B. Dyer, "Some practical applications of general crystal-structure projections," Acta Cryst., 5, 634-636 (1952).

AN X-RAY STUDY OF CRYSTALS OF $InF_3 \cdot 3H_2O$

G. B. Bokii and T. S. Khodashova

N. S. Kurnakov Institute of General and Inorganic Chemistry

Translated from Kristallografiya, Vol. 1, No. 2,
pp. 197-204, March-April, 1956
Original article submitted December 28, 1955

Data on the crystal structure of indium fluoride trihydrate $InF_3 \cdot 3H_2O$ are given. It has been shown that the structure is of coordination type without isolated complexes. Two sorts of water molecule are present. Their crystallochemical differences are in agreement with the chemical behavior of the salt.

X-ray structural studies of indium compounds are of interest from the general chemical point of view and because the crystal chemistry of indium has been very little studied. The present paper is concerned with the determination of the structure type of indium fluoride, $InF_3 \cdot 3H_2O$. It is necessary to solve the basic problem of whether the structure is of the coordination type or whether isolated complexes of the type InX_6 exist in crystalline state (X = F or H_2O). The latter appeared to be very probable, because, in most investigated structures of this type, indium has a coordination number of six and an octahedron as its coordination polyhedron.

The second problem to which a structural study could be applied is an explanation of the role of the water of crystallization.

I. Indium fluoride was synthesized by the method of Deichman and Tananaev [1]. The crystals were glistening colorless tetrahedral needles; face development, however, was very irregular. There were vicinals on almost all faces, which made precise geometric measurements very difficult (the precision did not exceed ±10').

From the goniometric data within the limits of precision, the indium fluoride crystals belonged to the tetragonal class. The following simple forms were found: prisms {100} and pinacoids {001}.

The optical studies by É. E. Burova gave the following results: $n_m = 1.450$ and $n_p = 1.425$, straight extinction. A study of the figures in transmitted light showed that the crystals were not strictly uniaxial. When the stage of the microscope was rotated, the cross was always observed to break into two hyperbolic branches; this indicates that the crystals were in fact biaxial, but with a very small angle between the optical axes, i.e., they were only pseudo-uniaxial.

The lattice parameters were obtained from an oscillating x-ray photograph taken in Cu K_α radiation: $a = 7.88 \pm 0.05$ kX, $c = 4.13 \pm 0.05$ kX, density $d = 2.83$ g/cm^3.

Two formula units occur in the unit cell. The most probable space group $C_{4h}^3 - P4/n$ is defined by the following laws of extinction: hkl, all; $hk0$, only with $h + k = 2n$, $00l$, all. Other possible space groups are $C_4^1 - P4$, $C_4^2 - P4/m$, and $S_4 - P\bar{4}$.

II. The F^2-series method was used to discover the basic motif of the atom distribution in the indium fluoride structure.

Two projections of the interatomic functions were constructed from x-ray goniometric data on the zero layer lines. The photographs were taken in a camera which photographed the reciprocal lattice with rotation of the crystals around the x and z axes (Mo K_α radiation). The photographs contained 87 and 126 independent reflections. Intensity estimation was visual. Kinematic and polarization factors were taken into account in constructing the projections.

The two indium atoms can take one of the four twofold positions of the group P4/n: (a) $000, \frac{1}{2}\frac{1}{2}0$; (b) $00\frac{1}{2}, \frac{1}{2}\frac{1}{2}\frac{1}{2}$; (c) $0\frac{1}{2}z, \frac{1}{2}0\bar{z}$.

In the first two cases, the projection of the interatomic function on the plane (100) should have a maximum for In–In at the point $v = \frac{1}{2}$, $w = 0$, while

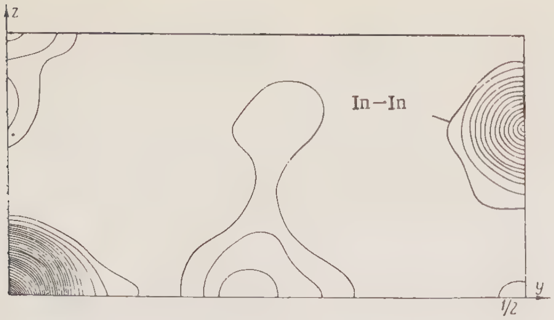

Fig. 1. Projection of the interatomic function on the (100) plane.

in the third case this should be at v = ½, w = 2z. The In–In maximum in the projection (Fig. 1) fulfilled the last requirement.

Thus, the positions of the indium atoms are determined unambiguously; they occupy the (c) positions on the four-fold axis, z ≈ 0.335.

Since fluorine and water have almost the same dispersin power and cannot be distinguished by x-ray analysis, we considered them equal as a first approximation. The following possibilities are then available for the 12 light atoms (6F and $6H_2O$):

(1) they may occupy two of the three four-fold positions (d) $\frac{1}{4}\frac{1}{4}0$, $\frac{3}{4}\frac{3}{4}0$, $\frac{1}{4}\frac{3}{4}0$, $\frac{3}{4}\frac{1}{4}0$; (e) $\frac{1}{4}\frac{1}{4}\frac{1}{2}$, $\frac{3}{4}\frac{3}{4}\frac{1}{2}$, $\frac{1}{4}\frac{3}{4}\frac{1}{2}$, $\frac{3}{4}\frac{1}{4}\frac{1}{2}$; (f) $00z$, $00\bar{z}$, $\frac{1}{2}\frac{1}{2}z$, $\frac{1}{2}\frac{1}{2}\bar{z}$, and two of the three two-fold positions (a), (b), and (c);
(2) all three four-fold positions (d), (e), and (f);
(3) the general eight-fold positions (g): xyz; $\overline{xyz}$; $\frac{1}{2}+x$, $\frac{1}{2}+y$, $\bar{z}$; $\frac{1}{2}-x$, $\frac{1}{2}-y$, $\bar{z}$; $\bar{y}x\bar{z}$; $y\bar{x}z$; $\frac{1}{2}-y$, $\frac{1}{2}+x$; z; $\frac{1}{2}+y$, $\frac{1}{2}-x$, z, and any two two-fold positions;
(4) the eight-fold position (g) and one of the four-fold positions [excluding (f), of which more below].

However, if account is taken of the ionic radii of fluorine and oxygen and the lattice parameter along the z axis (r_F = 1.33 Å, r_{O^2} = 1.36 Å, c = 4.13 Å), the first two variants are immediately rejected, i.e., those in which two fluorine atoms (or two water molecules) lie one upon another along the z direction. The same applies to the four-fold position (f) in variant (4).

An analysis of the projections of the interatomic functions on the (100) and (001) planes showed that they contain only maxima fulfilling the requirements of variant (3) with the two-fold positions (a) and (c) occupied, while the In–F maximum necessary for variant (4) at the point v = ¼, w = ¼ on the (001) projection is not present (Figs. 1 and 2).

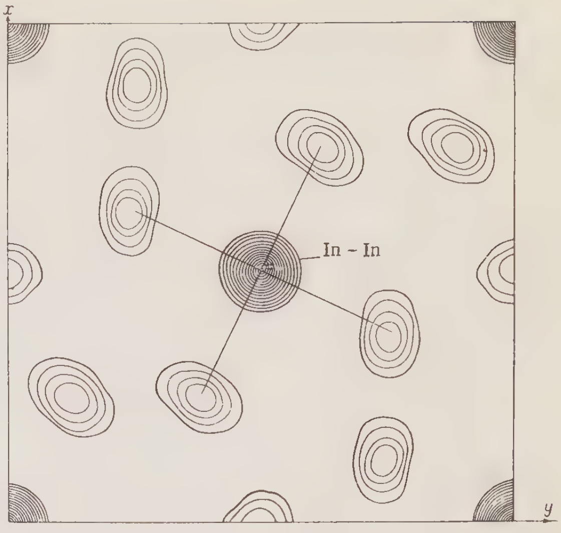

Fig. 2. Projection of the interatomic function on the (001) plane.

The general pattern of atom distribution in the indium fluoride structure is as follows: eight atoms in the general position (g) with coordinates x = = 0.739, y = 0.113, z = 0.335, and two atoms occupying the position (c), z = 0.835, to form an octahedron around the indium atoms (z_{In} = 0.335). The atoms which occupy the vertices (c) of the octahedra belong simultaneously to indium atoms from neighboring cells, so that the octahedra are linked in endless chains parallel to the z axis. The centers of individual octahedra (indium atoms) of neighboring chains are shifted relative to one another by about one-third of the cell edge (c). The chains are interconnected by atoms at the vertices and the center of the unit cell, i.e., the position (a).

A more detailed analysis of the structure based only on x-ray data is impossible because the F and H_2O cannot be distinguished. As shown below, we have been able to do this by crystallochemical analysis. However, the experimental data are sufficient to answer one of the basic questions. The structure is a coordination type and does not con-

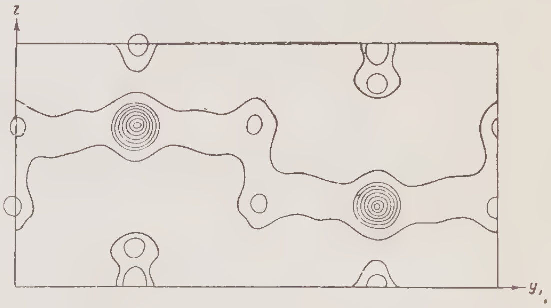

Fig. 3. Projection of the electron density on the (100) plane.

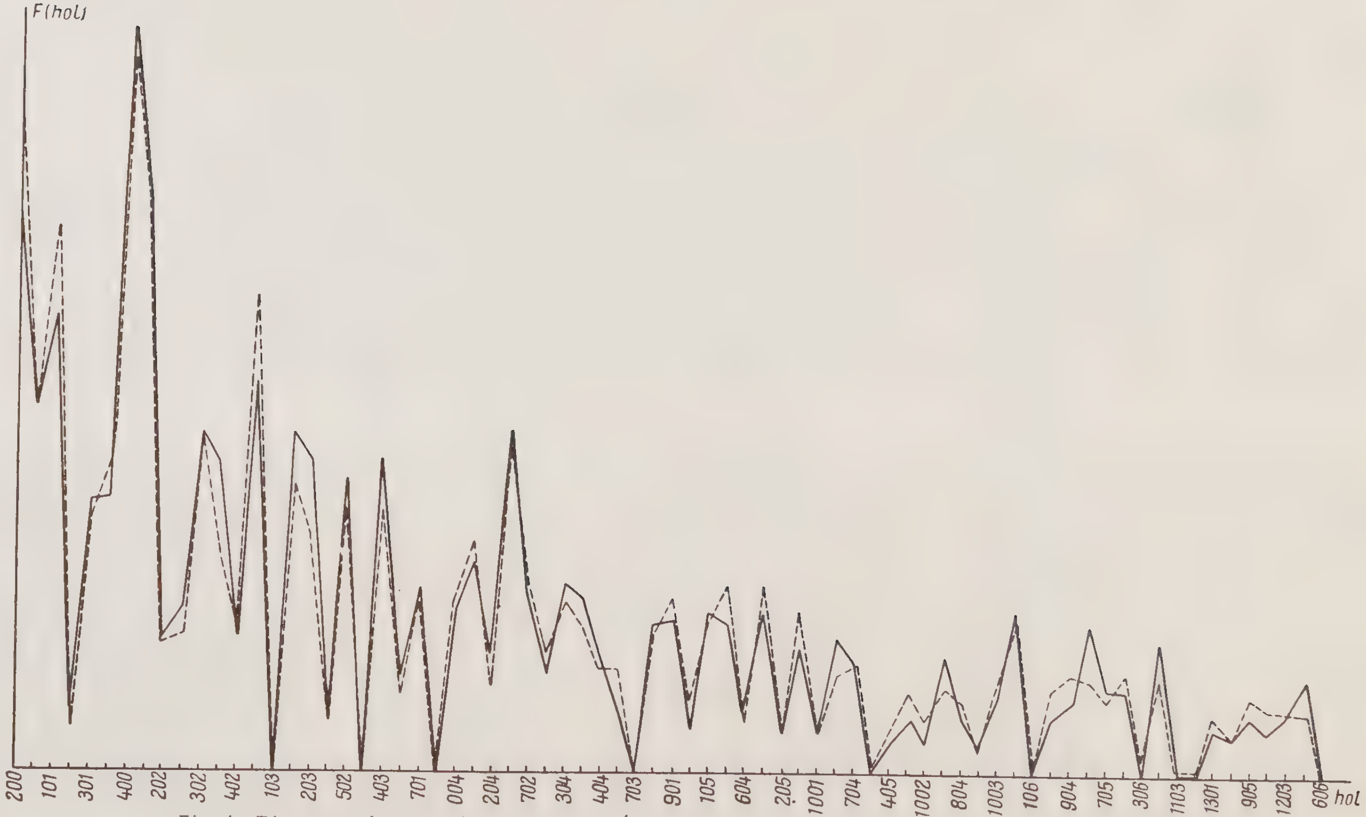

Fig. 4. Divergence between the experimental (solid line) and calculated (broken line) structure amplitudes F(h0*l*).

tain isolated InX_6 complexes, but the coordination number of indium is six.

To confirm the correctness of the chosen structure variant, a projection of the electron density on the (100) plane was constructed (Fig. 3).

Figure 4 shows the agreement between the experimental and theoretical structural amplitudes $F_{0kl} = F_{h0l}$, the values of which were initially related to an absolute scale with the introduction of temperature corrections. Calculation of the coefficient

$$R = \frac{\Sigma \, ||F_e| - |F_t||}{\Sigma \, |F_e|}$$

for the $h0l$ reflections gave a value R = 0.15. The temperature correction constant was B = 2.0.

The atomic coordinates cited in Table 1 were found from the projections of interatomic functions and refined from the electron-density projection.

The probable error in the determination of the coordinates of the indium atoms was 0.01 kX, and for the light atoms, about 0.1 kX.

III. It has been noted already that the x-ray analysis data are insufficient for a complete solution of the indium fluoride structure. The question of which positions in the structure [(a), (c), and (g)] are occupied by which light atoms still remains. By turning attention to the specific crystallochemical peculiarities of water and fluorine, an unambiguous answer can be obtained. Two initial positions arise.

1. The connections between the individual octahedra in a chain are by atoms at position (c) which simultaneously belong to two indium atoms and have a coordination number of two. This position is characteristic of halogen atoms, but is completely excluded for water molecules.

Thus, the (c) positions should be occupied by fluorine atoms (F_I). The $In-F_I$ distance is 2.07 Å, less than the sum of the ionic radii of In and F (2.27 Å), but this is quite natural, because the fluorine atom in this position has a coordination number of two. Similar coordination of fluorine with simultaneous shortening of the M – F distance has been found in a series of fluoride structures, e.g., UF_5, TaF_3, MoF_3, AlF_3 [2,3].

2. The chains of octahedra are interconnected by particles (F or H_2O) in special positions of the inversion axis $\bar{4}$ [position (a)]. That this position is taken by water molecules (H_2O_I) follows from the considerations below: First, the distance to the nearest indium atom (4.18 Å) is much too long for an In – F bond; second, the symmetry of this position indicates a tetrahedral environment which is frequently characteristic for the water molecule.

These two facts determine that the remaining fluorine atoms and water molecules occupy the (g) positions. It is known that the tetrahedral distribution of charge on the surface of water molecules requires definite packing for them in hydrate structures. The latter are stable only if the charge field of the water molecules contacts either ions of opposite charge or the oppositely charged regions of neighboring molecules. According to this, the molecules H_2O_I should be surrounded by two fluorine atoms and two water molecules, oriented with the positively charged regions toward the center of the molecule.

Consequently, each indium atom is surrounded in the plane perpendicular to the axis of the octahedral chain by 2 F and 2 H_2O-F_{II} and H_2O_{II} (Figs. 5 and 6). The water molecules H_2O_I and H_2O_{II} differ crystallochemically, since they occupy different regular systems of points. It was shown above that a strict tetrahedral environment was required for the H_2O_I molecules. We shall now discuss the coordination about the H_2O_{II} molecules and how the compensation of charges is brought about.

The H_2O_{II} molecules form infinite chains extended along the z axis. The chains are connected together by H_2O_I molecules in the corrugated network which consists of the octagonal rings and which is parallel to the (110) plane – the line AB in Fig. 5. This is shown diagrammatically in Fig. 5. One positive and one negative charge of the H_2O_{II}

TABLE 1

Atom	Position	Atomic coordinates					
		in kX			in fractions of cell sides		
		x	y	z	x	y	z
In	(c)	0	3.94	1.38	0	0.500	0.335
H_2O,F	(g)	0.89	2.06	1.38	0.113	0.261	0.335
	(c)	0	3.94	3.45	0	0.500	0.835
	(a)	0	0	0	0	0	0

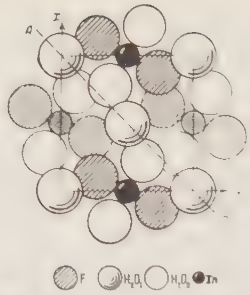

Fig. 5. Crystal structure of $InF_3 \cdot 3H_2O$. View along the z axis (F_I atoms are not shown).

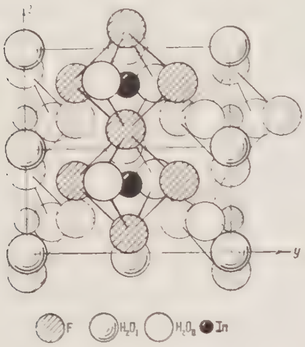

Fig. 6. Crystal structure of $InF_3 \cdot 3H_2O$. View along the x axis.

molecule compensate the opposite charges of neighboring molecules in the chain; finally, there remain a free negative charge caused by the bond to indium and a free positive charge on the H_2O_I molecule.

Thus, both the H_2O_I and H_2O_{II} molecules have tetrahedral coordination.

The presence of two types of water molecules in the structure of indium trifluoride trihydrate (ratio of $H_2O_I : H_2O_{II} = 1 : 2$) with the H_2O_I molecules at a considerably greater distance from the indium atom than the H_2O_{II} molecules is probably the cause for the 5% loss in weight when the salt is dried at 110° [1] (the loss of one molecule of water is 7.8% – a value of the right order); further heating of the salt to 188° caused no further change in weight, i.e., one molecule of water is evidently less strongly bound than the other two.

It is now necessary to return to the following structural peculiarity: Both the indium atoms and the water molecules H_2O_I are placed on the four-fold axes, but each is surrounded by two pairs of different atoms, i.e., we have, in fact, simple diad axes in place of the axes 4 and $\bar{4}$ and, consequently, the space group P4/n must be replaced by P2/n of the monoclinic class. It is true that the monoclinic angle is very small – less than 90°10′ (since the precision of the goniometric measurements was only ±10′, it could not be observed). In all probability, this lowered symmetry explains the pseudomonoaxial nature of the crystal apparent in the optical study. It is possible that this effect is only weakly expressed because of the incomplete order in the positions of the fluorine and water in the actual structure, which leads to an increase in the symmetry. The direct extinction arises because the length of the needles coincides with the direction of the two-fold axis.

The equality of the In – F and In – H_2O distances in the octahedra (2.08 Å), which was obtained on the assumption of a four-fold axis, seems unlikely from a crystallochemical point of view. The same should be said of the somewhat decreased $H_2O - H_2O$ distances (2.64 and 2.56 Å). Since there is some analogy between our structure and that of ice, distances of the order of 2.7-2.8 Å would have been expected.

Bearing in mind the development of a complete analysis of a structure of low symmetry, it seemed to us expedient to take somewhat different values for the coordinates of the water molecules which would eliminate the inconsistencies noted above. The x-ray analysis data permit this because, first, we averaged the intensities of independent reflections, assuming a four-fold axis, when calculating the structure factors F^2_{hk0}; and, second, the (100) electron-density projection appeared imperfect because of strong absorption in the crystal and the water maxima had a diffuse form which hindered the precise determination of their coordinates (this applies particularly to the coordinates of the water molecules).

The final coordinates of the atoms in the structure of indium fluoride trihydrate are given in Table 2.

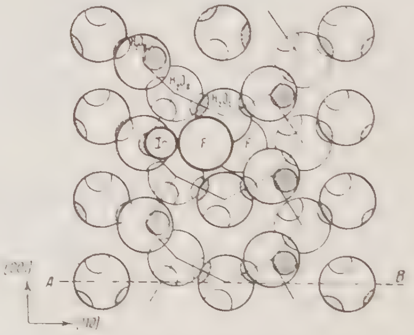

Fig. 7. A layer of H_2O molecules in the $InF_3 \cdot 3H_2O$ structure (section parallel to the line AB of Fig. 5). Small white circles represent (+) charges, hatched circles (–) charges.

TABLE 2

Atom	Position	Atomic coordinates					
		in kX			in fractions of cell edges		
		x	*y*	*z*	*x*	*y*	*z*
In	(*c*)	0	3.94	1.38	0	0.500	0.335
H_2O_I	(*a*)	0	0	—0.25	0	0	—0.061
H_2O_{II}	(*g*)	5.82	0.89	1.38	0.742	0.117	0.290
F_I	(*c*)	0	3.94	3.45	0	0.500	0.835
F_{II}	(*g*)	0.89	2.06	1.38	0.113	0.261	0.335

The interatomic distances (in kX) are given below:

$In-F_I = 2.07$, $H_2O_I-H_2O_{II} = 2.67$,
$In-F_{II} = 2.08$, $H_2O_{II}-H_2O_{II} = \begin{matrix} 2.73 \\ 3.19 \end{matrix}$ (distance, in chains)
$In-H_2O_{II} = 2.13$.

Finally, it is noted that there are some analogies between the structure of indium fluoride $InF_3 \cdot 3H_2O$ and lead oxide PbO (space group D_{4h}^7-P4/nmm) [4].

The structure analyzed here can be considered a complicated form of the PbO type: the Pb positions are taken by the In atoms, while the oxygen positions are taken by those of the H_2O_I molecules. The increased complexity of the composition has led to a decrease in the symmetry in indium fluoride.

Summary

1. The crystals of $InF_3 \cdot 3H_2O$ are pseudotetragonal, space group C_{2h}^4-P112/n. The lattice parameters are: $a = b = 7.88 \pm 0.05$ kX, $c = 4.13 \pm 0.05$ kX, $\beta = 90° \pm 10'$, $N = 2$.

2. The structural coordination does not contain isolated InX_6 groups, but the coordination number of indium is six.

3. A complete structural analysis was accomplished by means of crystallochemical analysis, revealing the different F and H_2O positions and the character of the packing of the water molecules.

4. In agreement with its chemical behavior, the structure of indium fluoride trihydrate contains two types of crystallochemically different water molecules. Both types have tetrahedral coordination.

LITERATURE CITED

1. É.N. Deichman and I.V. Tananaev, "Study of indium fluorides," Khim. Redkikh. Élementov, 1, 95-101 (1954).
2. J.A.A. Ketelaar, "Die Kristallstruktur der Aluminiumhalogenide," Z. Krist., 85, 119-131 (1933).
3. G.B. Bokii, Introduction to Crystal Chemistry [in Russian] (1954), pp. 386-401.
4. G.B. Bokii, Introduction to Crystal Chemistry [in Russian] (1954), p. 359.

METALLOGRAPHIC AND X-RAY-DIFFRACTION STUDY OF ALLOYS IN THE GERMANIUM–RHODIUM SYSTEM

N. N. Zhuravlev and G. S. Zhdanov

M. V. Lomonosov State University, Moscow

Translated from Kristallografiya, Vol. 1, No. 2,
pp. 205-208, March-April, 1956
Original article submitted October 12, 1955

A number of alloys in the Rh–Ge system were studied metallographically and by x-ray diffraction, and the existence of several compounds in this system was established. The unit cell of Rh_3Ge_4 was determined.

Preparation of Alloys

Germanium and rhodium were fused together in various proportions. For preparing the alloys, chemically pure germanium and rhodium were used. The melting was effected in a high-frequency furnace and a resistance furnace in quartz ampoules in an argon atmosphere.

The melting point was determined approximately for a number of alloys. The shape of a section of the melting diagram for the rhodium–germanium system was found on the basis of the melting points of the alloys and from metallographic and x-ray data (Fig. 1).

Metallographic and X-Ray Diffraction Study of the Alloys

Metallographic study of germanium-rich alloys (above the composition Rh_3Ge_4) causes no great difficulty. These alloys are easily etched by nitric acid. The study of rhodium-rich alloys beyond the composition Rh_3Ge_4, however, involves some difficulty, since such alloys cannot be etched by strong acids and alkalis, nor even by mixtures of $HNO_3 + HCl$ and $HNO_3 + HF$. In order to observe the phase composition of such alloys, sections were prepared by the relief-polishing method.

Alloys from germanium to 30% rhodium consist of the eutectic Rh_3Ge_4–Ge and germanium crystals. Figure 2 is[1] a micrograph of the alloy containing 20 wt.% rhodium; etched germanium crystals can be seen on a field of eutectic. Alloys containing 30 wt.% rhodium practically constitute the Rh_3Ge_4–Ge eutectic. Figure 3 is a micrograph of such an alloy. Alloys with germanium content in the range between the eutectic Rh_3Ge_4–Ge and Rh_3Ge_4 are two-phase and consist of crystals of Rh_3Ge_4 and the eutectic Rh_3Ge_4–Ge. Figure 4 is a micrograph of an

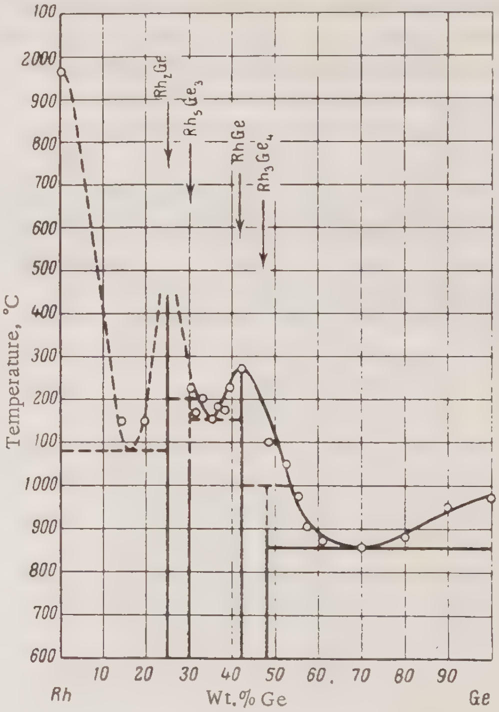

Fig. 1.

---

[1] For Figs. 2, 3, 4, and 5, the magnification is 160; for Figs. 6 and 7 it is 304.

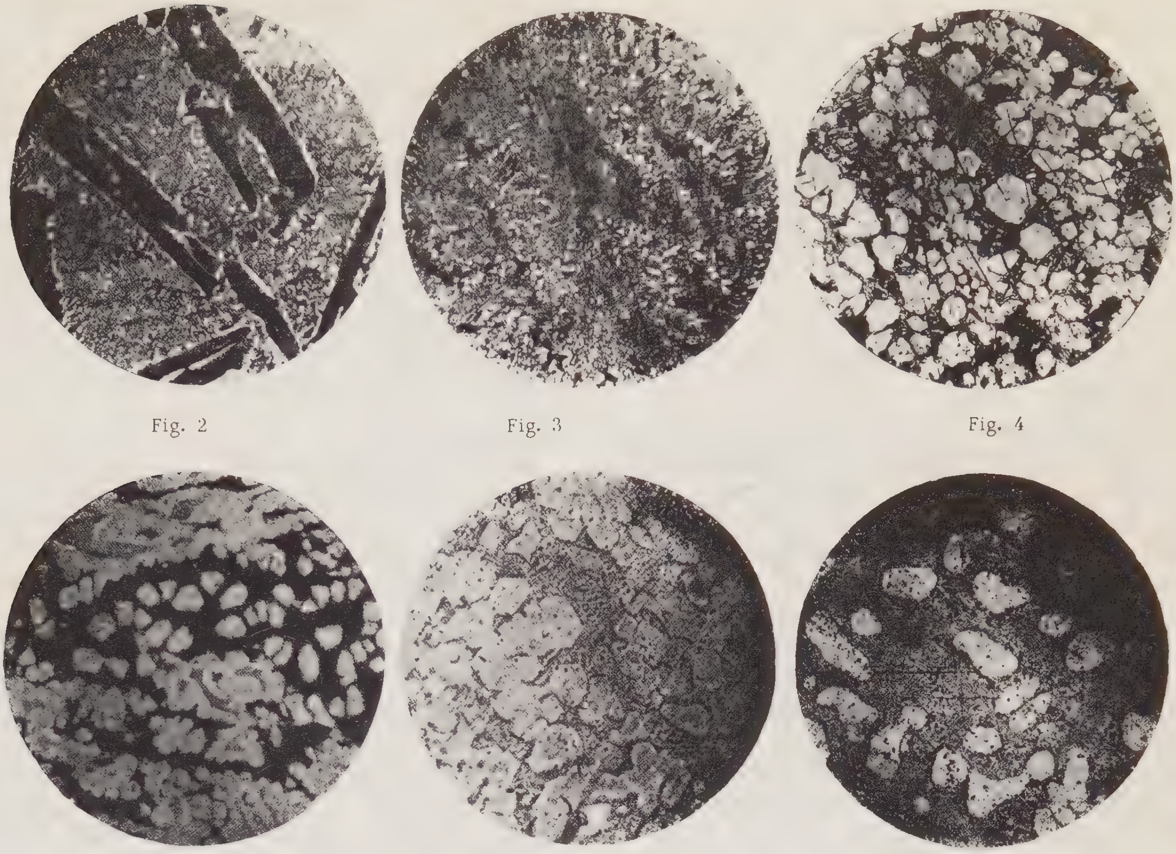

Fig. 2 Fig. 3 Fig. 4

Fig. 5 Fig. 6 Fig. 7

Figs. 2 to 7. Microphotographs of alloys in the germanium–rhodium system.

alloy of composition $RhGe_2$ (58.52 wt.% Ge), in which we see light crystals of Rh_3Ge_4 in a field of eutectic. On an x-ray powder photograph taken in Cu K_α radiation for this alloy, we find lines belonging to Rh_3Ge_4 and germanium.

Annealed alloys of composition Rh_3Ge_4 (48.47 wt.% Ge) are single-phase. On microsections from these alloys we find polyhedral crystals. The x-ray powder photograph obtained for Rh_3Ge_4 crystals has a large number of lines. Alloys of Rh_3Ge_4 cooled in the ordinary way are heterogeneous. We may suppose that the compound Rh_3Ge_4 is formed by a peritectic reaction. In ordinarily cooled alloys of composition Rh_3Ge_4, the reaction does not proceed to completion, and the microsections (Fig. 5) show unconverted crystals of RhGe surrounded by a shell of Rh_3Ge_4 crystals. The space between such grains is filled with Rh_3Ge_4–Ge eutectic. Alloys of composition RhGe (41.36 wt.% Ge), both slowly and rapidly cooled, are single-phase and constitute the compound RhGe. The x-ray powder photographs obtained with slowly and rapidly cooled alloys are identical. This excludes polymorphism of the compound RhGe. Published indications [1] of the existence of a compound with composition Rh_3Ge_2 were not confirmed. The alloys of composition Rh_3Ge_2 which were prepared, both annealed and rapidly cooled, were heterogeneous. These alloys consisted of crystals of the compound Rh_5Ge_3 and a small amount of Rh_5Ge_3–RhGe eutectic. Figure 6 gives a micrograph of an alloy with composition Rh_3Ge_2, in which we see light polyhedral crystals of the compound Rh_5Ge_3 in a field of Rh_5Ge_3–RhGe eutectic. Annealed alloys of composition Rh_5Ge_3 are homogeneous and constitute the compound Rh_5Ge_3.

Alloys of composition Rh_2Ge (26.07 wt.% Ge) are metallographically single-phase and constitute the compound Rh_2Ge. Rhodium-rich alloys consist of crystals of rhodium and Rh–Rh_2Ge eutectic. Figure 7 is a micrograph of an alloy of composition 15 wt.% Ge, in which we see light crystals of rhodium in a field of Rh–Rh_2Ge eutectic.

TABLE 1

Compound	σ_{hyd}, g/cm³	Av. micro-hardness, kg/mm²	Scatter of microhardness, kg/mm²
Ge	5.3	525	420—600
Rh_3Ge_4	8.5	500	420—575
RhGe	9.8	580	470—660
Rh_5Ge_3	10.7	475	420—525
Rh_2Ge	11.0	700	500—900
Rh	12 4	350	320—420

Density and Microhardness of the Compounds

The density σ of the compounds was determined by hydrostatic weighing [2] in carbon tetrachloride (σ = 1.585 g/cm³). The table shows densities σ determined at room temperature. The densities of germanium and rhodium are taken from data in [3,4].

The microhardness of the compounds was measured on the PMT-3 apparatus with a constant load of 10 g on the indentor. Measurements were made on several samples from different melts and the results averaged. The conditions of measurement and surface preparation were as far as possible identical. Table 1 gives the average microhardness and its scatter.

Solubility of Rhodium in Germanium and Germanium in Rhodium

For studying the solubilities of the components in each other we prepared alloys with 10 wt.% of the component being dissolved. After prolonged annealing (50 h), the metallographic alloys showed heterogeneous structures. X-ray powder photographs were obtained in the 114.4-mm diameter RKU camera for these alloys in Cu K_α radiation. On indexing and computing the x-ray photographs it proved that in neither the first nor the second case had the lattice spacings of the rhodium and germanium changed. This indicates that the components have only infinitesimal solubility in each other.

Determining the Unit Cell of Rh_3Ge_4

Crystals of Rh_3Ge_4 were produced by growing in the mother liquor with subsequent separation by dissolution of germanium. The separated crystals mainly constituted concretions and were of irregular form. The most perfect were selected for x-ray study out of a large number of such crystalline concretions. The Laue photographs showed that Rh_3Ge_4 crystals belonged to the tetragonal system. Oscillation x-ray photographs gave the lattice spacings as a = 5.7 ± 0.2 Å, c = 10 ± 0.3 Å.

An x-ray structural investigation of the compounds RhGe, Rh_5Ge_3, and Rh_2Ge was made in [5]. Independent studies of rhodium-rich alloys agreed closely with our own results as regards the composition of the compounds and their densities. The results of this work and Geller's data [5] disprove the existence of the compound Rh_3Ge_2. The temperature of the transformation into the superconducting state (2.12°K) determined by Matthias [1] for alloys of composition Rh_3Ge_2 probably relates to crystals of the compound Rh_5Ge_3.

Conclusions

1. The contours of a section of the melting diagram of the germanium – rhodium system have been marked out.

2. Four compounds are found in the germanium – rhodium system: Rh_3Ge_4, RhGe, Rh_5Ge_3, and Rh_2Ge. It is suggested that the compounds Rh_3Ge_4 and Rh_5Ge_3 are formed by a peritectic reaction. The maxima on the melting diagram relate to compounds RhGe and Rh_2Ge. On fusing the components, these compounds are formed with a considerable evolution of heat.

3. No solubility of rhodium in germanium or germanium in rhodium is found.

4. The density and microhardness of the compounds in the rhodium – germanium system have been determined.

5. Rh_3Ge_4 crystallized in the tetragonal system with lattice spacings a = 5.7 and c = 10 Å.

In conclusion, the authors wish to thank Professor I. E. Alekseevskii for discussing the results and I. I. Lifanov, R. N. Kuz'min, and N. P. Ivanova for help in conducting the experiments.

LITERATURE CITED

1. B. T. Matthias, "Transition temperature of superconductors," Phys. Rev., 92, 4, 874-876 (1953).
2. E. M. Bronshteut-Kupletskaya, Determination of the Specific Gravity of Minerals [in Russian] (1951), pp. 43-55.
3. M. P. Slavinskii, Physicochemical Properties in Elements [in Russian] (1952).
4. M. A. Filyand and E. I. Semenova, Properties of Rare Elements [in Russian] (1953).
5. S. Geller, "The rhodium – germanium system. The crystal structures of Rh_2Ge, Rh_5Ge_3, and RhGe," Acta Cryst., 8, 15-21 (1955).

SOVIET PHYSICS – CRYSTALLOGRAPHY VOL. 1, NO. 2 MAR.-APR., 1956

ELECTRON-DIFFRACTION STUDY OF THE DEGREE OF PERFECTION OF GERMANIUM SINGLE CRYSTALS

S. A. Semiletov and Z. G. Pinsker

Institute of Crystallography, Academy of Sciences of the USSR

Translated from Kristallografiya, Vol. 1, No. 2,
pp. 209-213, March-April, 1956
Original article submitted January 31, 1956

The possibilities of the electron-diffraction method (Kikuchi-line photographs) in studying the degree of perfection of the surface layer in single crystals are examined. The method is used for studying ground and etched single crystals of germanium.

Single crystals of various semiconductors (germanium, silicon, etc.) have in recent years found extremely wide application in electronics and radio technology. The properties of these single crystals apparently depend not only on the insignificant quantity of impurities, but also on the perfection of their structure, in particular that of the surface layer. It is well known that in order to obtain small components for the manufacture of various pieces of apparatus, massive single crystals are sawed or filed. This clearly causes considerable damage to the single crystal structure in the surface layer in contact with the saw or file. In order to remove this layer, grinding and etching are usually employed; the nature of the damage and defects caused in the sawing and grinding operations, however, is not entirely obvious in any specific case, nor is the depth of their penetration into the crystal. It is also not known whether etching removes the whole damaged layer or only part of it.

In view of the above, a study of the structural perfection of such single crystals is, in our opinion, of considerable interest.

In the present investigation, we studied the degree of perfection of germanium single crystals subjected to various forms of treatment by electron diffraction. Before proceeding to a description of the results obtained, we shall briefly discuss the possibilities of the electron-diffraction method in investigations of this type.

In studying massive samples by electron diffraction, the reflection method is used. The diffraction pattern formed by the reflection of an electron beam from the surface of a single crystal must clearly depend a great deal on the degree of perfection of the surface. It is in fact well known that in studying single crystals by electron diffraction, two types of diffraction record, differing in principle, are obtained: photographs formed by a regular network of point reflections and photographs containing Kikuchi lines. As regards the electron-diffraction photographs of the first type, their formation, as we know [1], is associated with the mosaic structure of the sample, i.e., with the presence of individual submicroscopic blocks turned through angles of about 1-3° in all directions with respect to each other. Electron-diffraction photographs of the second type were first obtained by Kikuchi [2] in 1928, when studying the scattering of electrons by sheets of mica. In these photographs, in addition to a small number of point reflections, he found pairs of parallel lines (black and white), subsequently named "Kikuchi lines." The formation of the Kikuchi lines is associated with multiple (dynamic) scattering of electrons, and they can only be completely explained on the basis of dynamic theory; Kikuchi, however, proposed the following elementary explanation for this phenomenon.

When a beam of electrons passes through sheets of mica about 10^{-5} cm thick, intense scattering of the electrons takes place. A considerable proportion of the electrons lose a large part of their energy as a result of multiple inelastic collisions with atoms of the lattice. These electrons form a general background. A certain number of the electrons, however, interact with lattice atoms without seri-

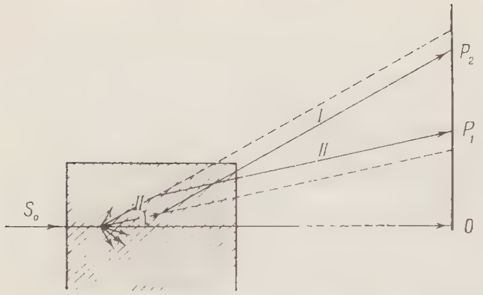

Fig. 1. Formation of Kikuchi lines (schematic).

ous energy loss, although their direction of motion may change quite severely.

As a result of such scattering, a widely diverging beam of electrons capable of interference forms inside the crystal. Meeting a system of crystallographic planes inclined at a suitable angle in the course of their journey, these beams of electrons experience regular reflection and, as a result of this, increased and decreased intensities develop on the background of inelastically scattered electrons.

All this is illustrated by Fig. 1. Here, one of the scattered beams (I) falls on a system of planes at the Bragg angle, undergoes regular reflection, and falls on point P_2 instead of P_1. Thus, at P_1, there is a deficit of electrons as compared with the general background (white point), while at P_2 there is an excess (black point). Among the scattered beams capable of interference there may also (generally speaking) be one (II) which is reflected from the other side of the same system of planes, falling on point P_1 instead of P_2. The reflection of beam (II) would have compensated the excess of electrons at P_2 and the deficit at P_1, were it not for the fact that the intensity of the scattered electrons diminishes with increasing angle of deviation from the original beam ($I_I > I_{II}$), so that compensation does not take place.

In order to obtain a line on the photographic plate, there must be a continuous set of scattered beams over a wide range of angle; the reflection of these beams leads to the formation of diffraction cones, the axes of which are perpendicular to the reflecting system of planes, and the aperture angles close to 180°. The intersection of these cones with the photographic plate leads to the formation of Kikuchi lines.

Electron-diffraction photographs with pairs of lines were obtained by Kikuchi from mica sheets about 10^{-5} cm thick. Elementary consideration of the formation of Kikuchi lines shows that their presence on the electron-diffraction picture is associated not only with the thickness of the sample examined, but also with its degree of structural perfection.

In fact, for Kikuchi lines to be clearly visible on the photographic plate (distinguished from the background), the number of electrons falling on P_2 instead of P_1 must be greater than a certain minimum. This minimum number depends not only on the volume of the crystal in which the scattered beams (I and II) are formed and their reflection from the system of planes, but also on the strictly parallel nature of these planes, one to another, i.e., on the perfection of the crystal structure. If the sample studied consists of individual blocks disoriented with respect to one another, or if in these blocks the planes are not strictly parallel to each other, then each block will reflect beams (I) and (II) into points differing slightly from P_1 and P_2, so that a slight disorientation (of the order of minutes) in the orientation of the blocks will make the Kikuchi lines diffuse, and for a larger disorientation (1-3°) they will become so wide that the contrast between lines and background will entirely vanish, i.e., the lines will not be seen; in this case, the electron-diffraction photograph will only show the point reflections formed by reflection of the primary beam S_0 from various systems of planes.

If the sample being studied has no such blocks, and the reflecting systems of planes are strictly parallel to one another (perfect single crystal), a primary beam S_0 with an extremely small angular divergence has very little probability of falling on several systems of planes at the Bragg angle, and only one or two chance point reflections may form on the diffraction photograph. As regards the scattered beams (I and II), these, according to the foregoing discussion, lead to the formation of patterns with Kikuchi lines on condition that the dimensions of the sample in the direction of the beam S_0 (or the thickness of the blocks protruding from the surface in the case of reflection photographs) are not smaller than a certain critical value. This value may be calculated in any specific case, as was done in [3]. The calculation leads to the value $\sim 10^{-5}$ cm. If the block size is smaller than critical, there will be no high-intensity scattered beams formed in them, or if these are formed they will have little probability of meeting a system of planes at the Bragg angle in the same block and giving reflections at P_1 or P_2. If, however, the block sizes are much greater than critical, the electron beams will experience strong absorption and incoherent scattering, leading to an increase in the general background and a weakening of the Kikuchi lines.

Thus, the presence or absence of Kikuchi lines in the electron-diffraction photograph, as well as their sharpness, depends on the degree of perfection of the crystal: the greater the perfection of the crystal, the sharper and clearer will the Kikuchi lines be, and vice versa.

In one paper [4], photographs with Kikuchi lines were used in studying the plastic deformation of aluminum single crystals.

In the present investigation, the method described was applied to the study of the degree of perfection in ground and etched single crystals of germanium. The samples were ground with corundum powder (120 min) and etched in hydrogen peroxide.

At the initial stage of the work, we made some special experiments with the aim of determining (albeit roughly) the thickness of the layer removed by the etchant. This value was found by weighing the sample before and after prolonged etching. As a result, it was established that, on etching in the peroxide at room temperature, 3 to 4 μ were removed per hour, while on etching in boiling peroxide, 3 to 5 μ disappeared per minute.

In studying germanium single crystals, it was important to obtain an electron-diffraction photograph from the "natural" face, not subjected to any kind of treatment, so as to be able to compare it with photographs from the etched samples. Such an electron-diffraction photograph, obtained from the (111) cleavage face, appears in Fig. 2.

The presence of sharp Kikuchi lines on this photograph, and the absence of a network of point reflections, indicates that, in the sample studied, there was no mosaic structure, but that in its degree of structural perfection it approximated to a perfect crystal. In this connection, it is interesting to note that in one paper [5] the (111) face of germanium was studied microscopically and interferometrically, and that a small number of hexagonal depressions appeared, which the author described as mosaic structure. In our view, the depressions were not the result of mosaic structure, but had a quite different nature.

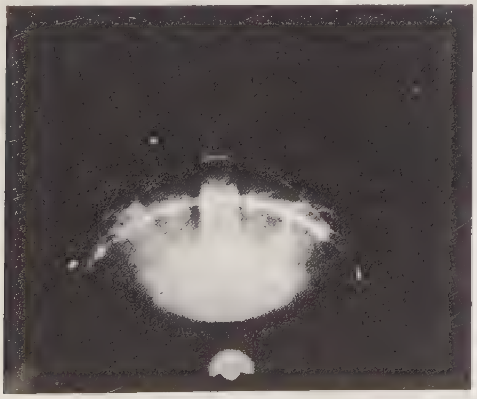

Fig. 2. Electron-diffraction photograph from the cleavage face of a germanium single crystal (L = 250 mm).

Let us turn to an analysis of photographs from germanium samples treated in various ways.

In the electron-diffraction photographs from filed samples, as a rule, there were point reflections (together with strong background) sometimes accompanied by weak, short Kikuchi lines. These photographs led us to conclude that, when germanium was filed or sawed, individual, quite large blocks ($>10^{-5}$ cm) were formed in the layer in contact with the tool, these being turned relative to one another and to the original single crystal. On the photographs from ground samples (Fig. 3) the point reflections are accompanied by Debye half-rings, indicating the presence of polycrystalline dust on the ground surface. Thus, in grinding germanium, tiny crystallites ($\sim 10^{-6}$ cm) are torn out

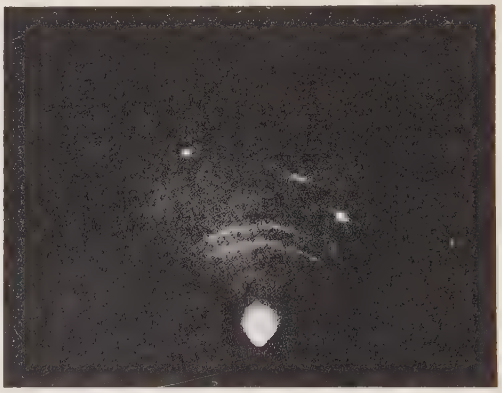

Fig. 3. Electron-diffraction photograph from a ground germanium single crystal (L = 700 mm).

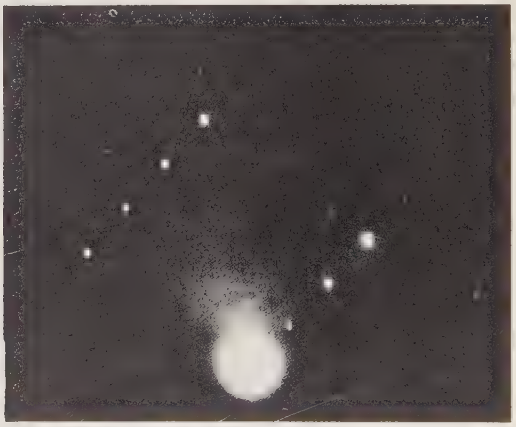

Fig. 4. Electron-diffraction photograph from a germanium single crystal etched for 15 sec (L = 700 mm).

of the crystal surface, together with the formation of mosaic structure. After brief etching (~15 sec) of the ground sample, the electron-diffraction photograph contains only point reflections, forming a two-dimensional network, or else set along straight lines (Fig. 4).

The presence of reflections up to the sixth order from the (111) face on the photograph of Fig. 4 corresponds, according to the Bragg–Wulff formula, to a block disorientation of about 1-3° ($\lambda = 0.05$ Å, $d_{111} = 3.25$ Å).

In the course of later work, we made a more detailed study of the effect of etching time on the degree of perfection of the surface layer of single crystals. This study was made on germanium samples, which after grinding were etched in boiling peroxide several times for 15 sec, each etch being effected in fresh etchant. As a result, it was established that a pattern containing Kikuchi lines appeared after a half-minute etch; at this stage, however, the Kikuchi lines were greatly diffused and accompanied by point reflections, indicating mosaic structure in the surface layer. Increasing the etch time to 1 min led to a slight increase in the sharpness of the Kikuchi lines, without any marked change in the extent of the mosaic structure. An analogous picture was found for samples etched for 2 min. The electron-diffraction pictures of samples etched for 4 min (Fig. 5) showed point reflections up to the fourth order, indicating a block disorientation of ~1°30'. Apart from the reflections mentioned, this photograph also showed fairly sharp Kikuchi lines; comparison of this with the photograph corresponding to the cleavage face, however, showed that even the 4-min etch had not entirely removed the layer damaged in grinding.

The electron-diffraction photograph shown in Fig. 6 was obtained from a sample etched for 10 min (40-μ layer removed). Just as in the case of the cleavage face, this gave sharp Kikuchi lines and bands, indicating a fairly perfect structure for the surface layer.

In some cases it was necessary to increase the etch time to 20 min in order to obtain such pictures; this corresponded to the removal of a layer 80 μ thick.

Thus, for complete removal of the layer with mosaic structure formed on grinding a germanium single crystal, etching in boiling hydrogen peroxide for 10-20 min is required. It also follows from the above data that the structural damage (mosaic) produced in the surface layer of the single crystal on grinding penetrates to a depth of 40 to 80 μ. We note that on the diffraction photographs of germanium samples etched in boiling hydrogen peroxide with added alkali solution (5 drops of a 5% NaOH solution to 10 cm^3 H_2O_2) for 10-20 min, haloes from some kind of amorphous film formed on the surface of the single crystal during etching were system-

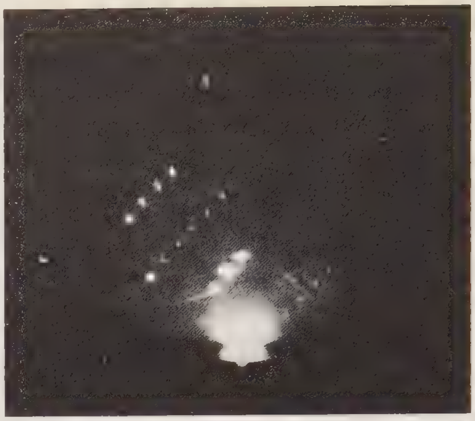

Fig. 5. Electron-diffraction photograph from a germanium single crystal etched for 4 min (L = 250 mm).

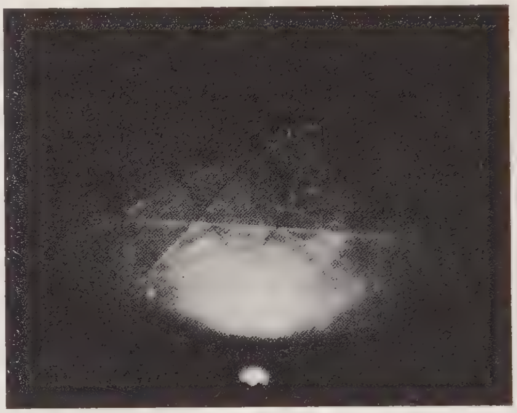

Fig. 6. Electron-diffraction photograph from a germanium single crystal etched for 10 min (L = 250 mm).

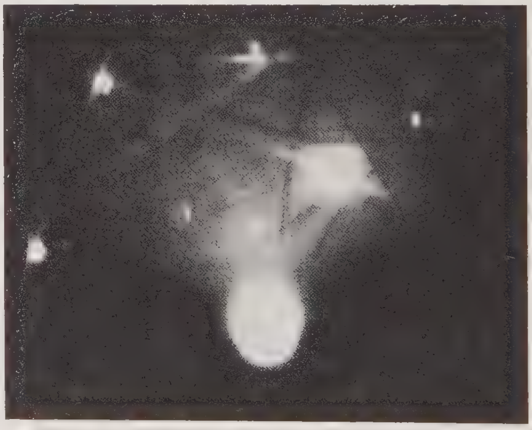

Fig. 7. Electron-diffraction photograph from a germanium single crystal etched for 4 min (L = 700 mm).

atically observed in addition to the Kikuchi lines and bands.

In conclusion, let us examine briefly the method of obtaining the diffraction photographs. In the reflection of an electron beam from the surface of a single crystal with perfect structure, a pattern containing Kikuchi lines is formed, the diffracted beams extending over a large angular range. For a more complete recording of this picture, it is desirable to operate with a small distance between sample and photographic plate. This, however, involves the inconvenience associated with the small scale of the diffraction picture.

In view of this, we took photographs with two different positions of the crystal-holder, with L = 250 and 700 mm, respectively. Comparison of the diffraction photographs shown in Figs. 2 and 7 demonstrates the advantages of this method. In the diffraction picture of Fig. 7 we notice the curvature of some Kikuchi lines, associated with the refraction of the electrons [1], and the extremely high intensity of the "mirror" reflection situated on the Kikuchi line.

LITERATURE CITED

1. Z. G. Pinsker, Electron Diffraction [in Russian] (1949).
2. S. Kukuchi, "Diffraction of cathode rays in mica," Japan. J. Phys., 5, 83 (1928).
3. B. K. Vainshtein, "Kinematic scattering of electrons by an ideal single crystal," DAN SSSR, 104, 537-540 (1955).
4. R. Heidenreich and W. Shockley, "Study of slip in aluminium crystals by electron microscope and electron diffraction methods," Report of a Conference on Strength of Solids (London, 1948), pp. 57-75.
5. A. Verma, "Interferometric observation of mosaic structure on the (111) face of a single crystal of germanium," Proc. Phys. Soc., 67, 359-360 (1954).

AN ELECTRON-DIFFRACTION STUDY OF THE HYDROMICAS

B. B. Zvyagin

All-Union Geological Research Institute

Translated from Kristallografiya, Vol. 1, No. 2,
pp. 214-217, March-April, 1956
Original article submitted December 1, 1955

Unit cells (all monoclinic) are reported for 56 specimens of various hydromicas; the parameters in the basal plane are a = 5.16-5.29 kX, b = 8.90-9.20 kX. Specimens with a repeat consisting of a single three-level silicate layer have c = 10.1-10.3 kX and β = 99.5-101.5°; the two-layer hydromicas have c = 20.0-20.6 kX and β = 93.5-96°. The diffraction patterns and layering allow the specimens to be classed in five groups.

The hydromicas fall between the micas and the montmorillonites as regards structure and physicochemical properties; the amounts of K and H_2O are largely responsible for this. The K cations lie between the silicate layers, and their number controls the adhesion between the layers, which thus is largest in the micas and least in the montmorillonites.

The H_2O in excess of that required by the structural pattern is considered [1,2] to consist of H_3O^+ ions, whose position and role resemble those of K.

Our ideas on the structures of the hydromicas and montmorillonites are rather general, because these minerals are highly variable, as are clay minerals generally. This means that any structural characterization must be based on a large group of specimens, which should include (apart from the various hydromicas) specimens of micas and sericites as being representatives of the layer silicates having the most perfect structures. We have examined specimens previously studied in other ways and also mineralogically identified specimens, mainly from M. F. Vikulova's collections.

Clay minerals lose the interlayer water during examination by electron diffraction, so there is no essential difference in structure between hydromicas and montmorillonites. The diffraction patterns are similar, and the detail is governed by the structural perfection (see Table 1).

The specimens have been arranged in order of the qualitatively evaluated degree of structural perfection. The first 37 have a more or less strict c repeat distance, as the reflections with $k \neq 3k'$ are fairly readily distinguished. The other specimens have only approximate spatial repeats, because only the reflections with $k = 3k'$ are clearly distinguishable [3].

All the patterns have largely the same set of reflections: $13l$, $\bar{1}3l$, $20l$, $\bar{2}0l$ (second ellipse) and $33l$, $\bar{3}3l$, $06l$ (fifth ellipse), which represent periodicity within a single type of layer with three levels. On the other hand, the $11l$, $\bar{1}1l$, $02l$ reflections (first ellipse) show several types of array as regards number and intensity. The reflections with $k = 3k'$ indicate that a monoclinic cell should be adopted for all specimens; then the $k \neq 3k'$ reflections indicate that the layers may have a repeat of one layer or two (see the c repeat distances). The c and β then make the monoclinic cell with a one-layer repeat equivalent to an orthorhombic cell with a repeat of three layers (because $\cos\beta \approx a/3$); and the monoclinic cell with a two-layer repeat is equivalent to an orthorhombic one with a repeat of six layers. These unit cells can be correlated with all the structural modifications of the micas established by x-ray analysis [4], each in accordance with the spatial symmetry of the atomic array, apart from the modification with a 24-layer repeat. This requires analysis of the intensities, of course

A purely qualitative examination of the $02l$, 11 $\bar{1}1l$ reflections shows that there are several different groups, each group having similar intensities

TABLE 1. Unit Cells of Specimens

Experiment No.	Specimen No.	Preliminary identification	a	b	c	β°
			kX			
1	289	Sericites	5.18	8.96	20.3	95.5
2	3050		5.16	8.90	20.3	96.0
3	Zh-14/27 r		5.19	8.96	20.1	96.0
4	Zh-14		5.16	8.92	20.3	96.0
5	Zh-12/6		5.18	8.98	20.3	95.5
6	736	Muscovite	5.16	8.90	20.0	95.5
7		Weathered muscovite	5.17	8.90	20.0	96.5
8		Phlogopite	5.29	9.16	10.3	100.0
9		Biotite	5.28	9.20	10.2	100.0
10		Vermiculite	5.30	9.20	10.4	99.5
11	Zh-12/3	Sericites	5.18	8.96	20.3	94.5
12	756		5.18	8.98	20.3	94.0
13	3060		5.18	8.92	20.3	96.0
14	577	Glauconite	5.22	9.04	10.1	101.5
15	342	Hydromuscovite	5.18	8.95	20.2	95.0
16	Zh-4/2	Sericites	5.18	9.10	10.3	99.5
17	Zh-1/4		5.17	8.95	20.1	95.0
18	L-11	Hydromica	5.18	8.95	10.2	100.0
19	Zh-12/4	Sericite	5.20	9.00	20.2	95.5
20	769	Kaolin clay	5.20	9.00	20.6	94.0
21	420	Hydromicas	5.17	8.94	10.3	100.5
22	118		5.19	8.97	10.2	101.0
23	750	Altered kaolinite	5.16	8.92	20.6	93.5
24	122	Hydromica	5.19	8.96	10.3	101.0
25	T-21	Hydromica or chlorite	5.20	9.00	10.3	100.0
26	S-140	Hydromica	5.18	8.98	10.3	101.0
27	T-19	Chlorite	5.20	9.00	10.2	100.5
28	N-76	Hydromicas	5.20	9.00	10.3	100.5
29	S-150		5.20	8.99	10.2	100.0
30	492		5.18	8.96	10.1	100.5
31	L-9		5.20	9.00	10.0	100.0
32	241	Quaternary hydromica	5.19	8.95	10.2	100.0
33	212		5.18	8.95	10.2	100.0
34	371	Hydromica clays	5.18	8.96	20.0	96.0
35	124		5.17	8.94	20.0	95.0
36	453		5.18	8.96	20.0	95.0
37	475		5.18	8.98	10.2	100.0
38	S-151		5.18	8.98	10.1	100.0
39	134		5.18	8.95	10.2	100.5
40	273	Devonian hydromica	5.17	8.94	10.2	100.0
41	478	Hydromica clay	5.20	9.00	10.0	100.0
42	81		5.16	8.91	10.2	100.5
43	459		5.18	8.95	10.1	101.0
44	375		5.18	8.95	10.2	100.5
45	488	Devonian hydromica	5.20	9.00	10.2	100.0
46	K-110	Hydromica clays	5.17	8.94	10.2	100.5
47	B-564		5.18	8.94	10.3	100.5
48	388		5.17	8.94	10.1	100.0
49	B-541		5.18	8.95	10.3	100.0
50	446		5.20	9.02	10.1	100.0
51	458		5.17	8.95	10.2	100.0
52	569		5.20	9.02	10.0	100.0
53	144		5.18	8.94	10.2	100.0
54	240	Quaternary hydromica	5.16	8.94	10.2	100.5
55	443	Hydromica clays	5.18	8.98	10.2	100.0
56	387		5.17	9.02	10.2	100.0

and positions for the $02l$, $11l$, $1\bar{1}l$ reflections, while groups differ either in intensity or in position.

Group I includes 289, Zh-14/27r, Zh-14, Zh-12/6, 736, the weathered muscovite, 342, and 769. The arc reflections for 289, 342, and 769 are much shorter than those for the others of this group, which indicates that the flakes of these three are isometric, the others being elongated.

Group II includes 3050, 3060, and (perhaps) Zh-12/4 and 750, whose reflections lie roughly as for group I, but which have a distinctive intensity distribution.

Group III consists of the phlogopite, biotite, vermiculite, and Zh-4/2; the patterns demonstrate a strict one-layer repeat. The c and β indicate that the interlayer water is lost from vermiculite as it is from montmorillonite and halloysite [5,6].

Group IV (Zh-12/3, 756, and Zh-1/4) has a distinctive intensity distribution, the reflections being especially uniformly distributed in height above the zero line. The unit cells given in the table could be replaced by orthorhombic ones of c repeat extended to six layers.

Group V is the most numerous and consists of specimens of relatively low structural perfection, which give patterns of glauconite type; 577, L-11, 420, 118, 122, T-21, S-140, T-19, N-76, S-150, 492, L-9, 212, etc.

It is difficult to establish the distinctive features of the specimens Nos. 38-56 because the patterns have either very indistinct $k \neq 3k'$ reflections or ones that completely overlap others.

The patterns indicate as hydromicas some specimens whose preliminary identifications were different (769, 750, T-19).

The a and b parameters of 3050, Zh-14, 736, etc., are somewhat unusual for micas. These are higher or lower than the values given in the literature for phlogopite, biotite, and vermiculite; this is due to the isomorphous replacement within the structures of the particular specimens.

I am indebted to M. V. Vikulova for making available the various materials and for valuable information on the mineralogical characteristics of the specimens.

LITERATURE CITED

1. V. S. Sobolev, Introduction to Silicate Mineralogy [in Russian] (1949).
2. G. Brown and K. Norrish, "Hydrous micas," Min. Mag., 29, 218, 929 (1952).
3. B. B. Zvyagin, DAN SSSR, 97, 2, 251 (1954).
4. S. B. Hendricks and M. E. Jefferson, "Polymorphism of the micas from optical measurements," Am. Min., 24, 12, 729 (1939).
5. B. B. Zvyagin and Z. G. Pinsker, "An electron-diffraction study of the structure of montmorillonite," DAN SSSR, 68, 65-67 (1949).
6. B. B. Zvyagin, "An electron-diffraction study of the minerals of the kaolinite group," DAN SSSR, 96, 809-812 (1954).

THE OPTICAL PARAMETERS OF NEW ULTRAVIOLET POLARIZERS

G. I. Distler

Institute of Crystallography, Academy of Sciences of the USSR

Translated from Kristallografiya, Vol. 1, No. 2,
pp. 218-220, March-April, 1956
Original article submitted January 21, 1956

Optical characteristics are reported for the UFP series of ultraviolet polarizers, which operate between the limits of 240 and 750 mμ.

Polaroid was invented some twenty years ago and has led to rapid extension of the use of polarized light in science and technology. Existing polaroid materials have excellent characteristics in the visible region and equal nicol prisms in this respect, but they absorb strongly in the ultraviolet and are largely useless in that region, although there is a great need for thin film polarizers of high aperture for the ultraviolet.

Research has been done at this institute on ultraviolet polaroids based on polyvinyl alcohol films, which are of adequate transmission in the range 240-400 mμ. These films produce polarized ultraviolet after treatment with suitable reagents. The products are neutral in color and transmit a little blue light in the crossed position. The region of best ultraviolet polarization is dependent on the treatment; some specimens also polarize visible light and so may be used with or instead of ordinary polaroid.

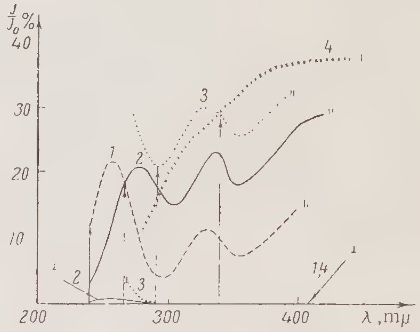

Fig. 1. Dichroism curves for UFP specimens made in various ways.

Methods

All the spectral measurements were made with an SF-4 photoelectric spectrophotometer. All such instruments polarize the radiation to some extent; this is unimportant with ordinary materials, but serious errors can arise with dichroic materials. The simplest method is to use polarized light in all measurements, by inserting a polarizing prism in the system. A polarizing device[1] was used, which consisted of a polarizing prism and a means of rotation. The prism was installed directly behind the exit slit in a support that could be rotated via a gear train through 180° about an axis parallel to the beam; the angular setting could be read to 15'. The specimen was examined with its plane of polarization first parallel to that of the prism and then perpendicular to it. The required orientation was obtained by setting the prism in the position giving minimal transmission; the accuracy was increased by inserting a neutral filter of 1-2% transmission in the reference beam. All specimens were used uncemented and were 0.07-0.08 mm thick. Reflection losses were neglected. The spectral transmission was measured to 0.5%.

Optical Characteristics

The UFP[2] series of ultraviolet polaroids was examined; Fig. 1 shows dichroism curves for four

---

[1] This device was made at the P/Ya 412 plant at our request.

[2] Ultraviolet film polarizers.

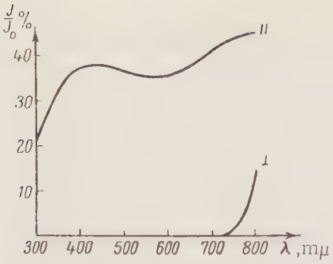

Fig. 2. Dichroism curves for UFP No. 4.

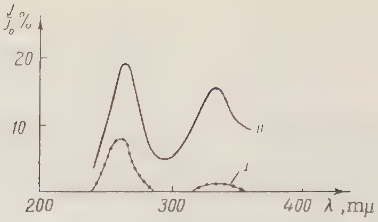

Fig. 3. Dichroism curves for British polaroid.

specimens made in different ways. These differ in properties; each gives the best polarization over some particular range. For instance, No. 1 may be reckoned the best for 240-265 mμ, No. 2 for 265-290, No. 3 for 290-340, and No. 4 for 340-400 mμ. The last is also suitable for the visible region (Fig. 2).

In 1949, Barer [1] reported the ultraviolet transmission of British polarizing films; Fig. 3 shows his results. This material gave complete polarization only over the range 290-300 mμ, and the transmission was very low throughout the ultraviolet.

It is clear that the new polarizers are much more efficient. The set should be used together, each material being employed only in its best range. The set as a whole gives reasonably high transmission and a high degree of polarization over the range 240-750 mμ.

These new materials should find application in optical instruments for many purposes requiring polarized ultraviolet light in science and technology.

Conclusions

1. New ultraviolet film polarizers have been developed.
2. The optical characteristics of these are reported.

I am indebted to E. V. Parvova for preparing the materials and for considerable assistance in the work.

LITERATURE CITED

1. R. Barer, "Some experiments with polarizing films in the ultraviolet," J. Sci. Instr., 26, 10, 325 (1949).

SOVIET PHYSICS – CRYSTALLOGRAPHY VOL. 1, NO. 2 MAR.-APR., 1956

DEVELOPMENT AND TESTING OF HEAT-RESISTING POLARIZERS

G. I. Distler and E. V. Parvova

Institute of Crystallography, Academy of Sciences of the USSR

Translated from Kristallografiya, Vol. 1, No. 2,
pp. 221-227, March-April, 1956
Original article submitted January 21, 1956

Dehydrated films of polyvinyl alcohol have been used in heat-resisting polaroids for the visible region. The dichroism is shown by the infrared spectra to arise from conjugated double bonds.

Introduction

Russian polaroid is made by iodinating films of polyvinyl alcohol and has good optical characteristics [1], the degree of polarization and transmission being high throughout the visible region. The color is almost neutral or very slightly greenish.

Figure 1 shows the dichroism. The molecular compound of iodine with polyvinyl alcohol is thermally unstable; the material is damaged if heated above 80-90°C, which makes it unusable in vehicles, stereoscopic projectors, and in any optical equipment developing much heat.

There is clearly a need for better heat resistance in combination with good optical characteristics. Two reviews by Land, the inventor of polaroid [2, 3] refer to heat-resisting polaroid (type K) for use in vehicles, which is made by thermally dehydrating films of polyvinyl alcohol. Polaroid K is of excellent optical quality; there is some fall in the degree of polarization in the red region, so the material transmits a red color in the crossed position. Figure 2 shows the dichroism. Land's reviews give only the very general statement that polaroid K is made by heating stretched films of polyvinyl alcohol to 160°C in the presence of a suitable catalyst; it is assumed that the dichroism is due to conjugated double bonds.

Ushakov et al. [4], in 1949, made a fairly detailed chemical study of the dehydration of polyvinyl alcohol.

Films of this type have been made in this institute and have been found to be of good thermal stability and to act as polarizers in the visible region. The structural changes during heating are very complicated and are dependent on the pH, degree of stretching, catalyst, and other conditions; they may be followed from the infrared absorption as measured with polarized radiation. It has proved possible to make heat-resisting polarizers with good optical characteristics; the origin of the dichroism has also been established.

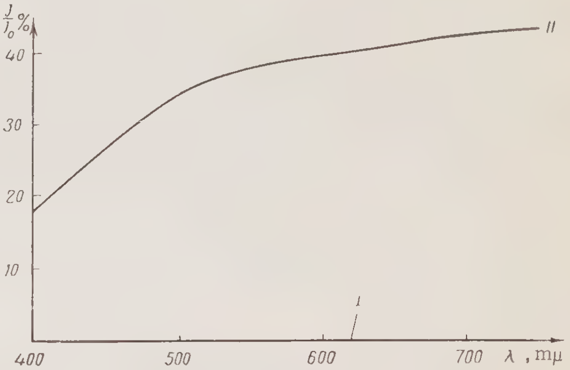

Fig. 1. Dichroism ratio of iodinated polyvinyl alcohol films.

Methods

Alkali-saponification polyvinyl alcohol (made by the Polymeric Products Research Institute, Ministry of the Chemical Industry) was used; films 0.1-0.15 mm thick were made by evaporating 8-10% aqueous solutions on glass. These films are very highly elastic and are readily oriented by stretching, especially when hot. They were stretched to 5-6 times the initial length in a frame with a worm

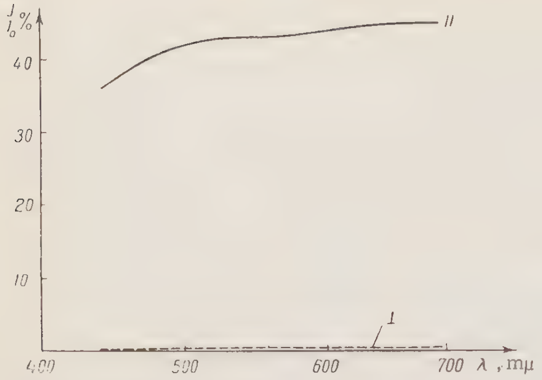

Fig. 2. Dichroism of American Polaroid K, corrected for reflection losses.

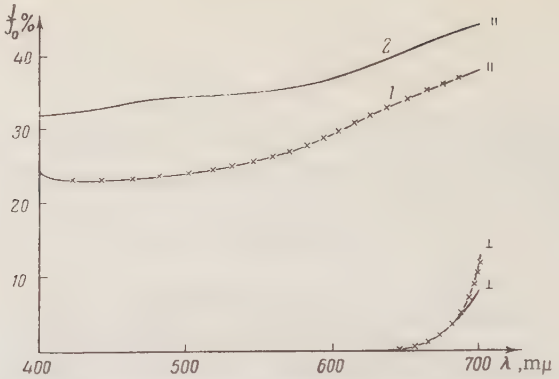

Fig. 4. Dichroism of specimen 64 before and after second stretching.

drive; they were heated in a drying oven to various temperatures and over an electric hotplate, the temperature in the latter case being 100-110°.

Deformation during heat treatment was avoided by clamping the films in holders in the stretched state. The average thickness was 0.07-0.08 mm.

The spectrophotometry was done with an SF-4 (quartz) spectrophotometer fitted with a polarizer. Infrared absorption spectra were recorded with an IKS-1 spectrometer (rocksalt prism), the polarizer being of KRS-5. The spectrum was recorded photographically; spot measurements were also made. The films were measured unmounted; no corrections were applied for reflection. The errors of measurement were 0.5% (SF-4) and 1-2% (IKS-1).

Results

These films were found to be extremely stable on heating; no water was lost unless a special catalyst was added. The optical quality is not good unless the water loss is fairly low and is produced rather rapidly, because numerous oxidation products are readily formed, as can be seen from the C=O absorption (the heating was done in air, not inert gas).

Various catalysts were tried: HCl, HBr, $FeCl_3$, $ZnCl_2$, $AlCl_3$, etc. The best results were obtained with HCl, HBr, and $AlCl_3$.

HCl was used in most cases, this either being added to the solution before the films were poured, or being used as vapor with the stretched film. Temperatures of 110-160° were used, with treatment times of 30-60 sec.

Figure 3 shows the dichroism of specimen 115, which was made at 160° (30 sec) with HCl as catalyst. The dichroism is high, but the overall transmission is poor.

Better characteristics are obtained if the stress in the dehydrated material is allowed to relax, the film then being stretched again. The relaxation may be produced in hot water or in 1-5% aqueous boric acid. The contraction factor is 2-3. Figure 4 shows the improvement (the total transmission shows about 10% increase), which arises because the stretching increases the degree of orientation.

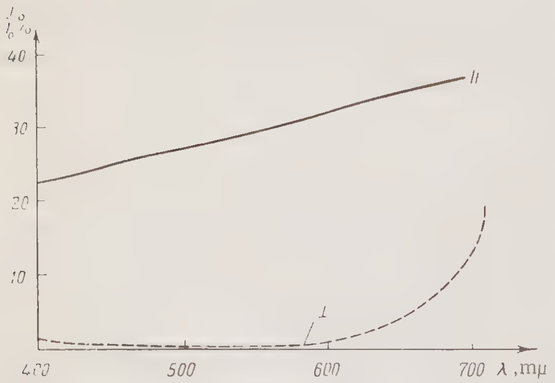

Fig. 3. Dichroism of specimen 115.

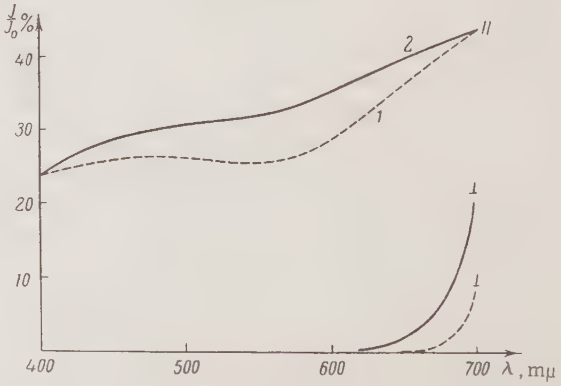

Fig. 5. Dichroism of specimen 80 before (1) and after (2) heating to 130° for 250 h.

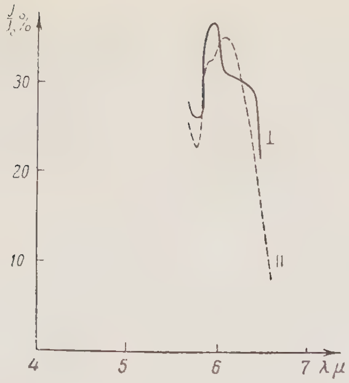

Fig. 6. Dichroism in the range 5.5-5.6 μ of three pieces of specimen 52 set parallel (each pieces 0.03 mm thick).

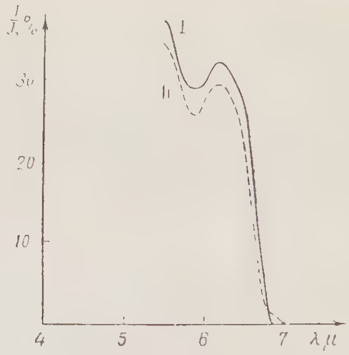

Fig. 8. Dichroism at 5.5-6.5 μ for a 0.03-mm stretched film of polyvinyl alcohol.

This method gives materials of very low degree of dehydration. More prolonged treatment produces a dark material of low transmission, so it is necessary to remove the catalyst and stabilize the material. The following stabilizers were tested: NaCl, Na_2CO_3, $Na_2B_4O_7$, and H_3BO_3 mixed with $Na_2B_4O_7$. Aqueous solutions of these remove the catalyst and enter the film, which relaxes substantially (no special relaxation treatment is needed); the film is then stretched again, the transmission rising.

The products were tested for thermal stability in a thermostat at 125-130°. Figure 5 shows the result for specimen 80 after 250 h; the general transmission was increased, but the degree of polarization in the red region dropped.

The optical parameters change only during the first 20 h and thereafter remain virtually constant.

Infrared spectra reveal the source of the dichroism, as they are very sensitive to the structure of macromolecular films; polarized radiation enables one to determine the orientations of groups and bonds. Dehydration has a complex mechanism very much dependent on the conditions used.[1]

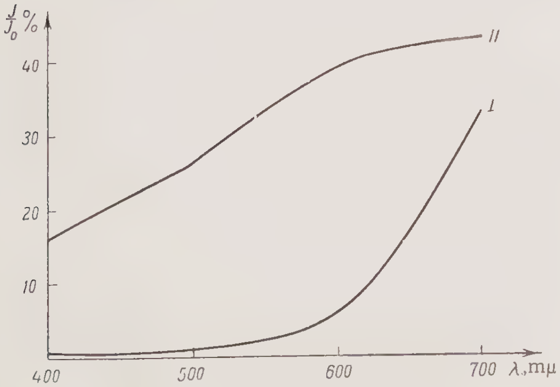

Fig. 7. Dichroism of specimen 52.

Treatment in air at 110-160° always gives rise to double bonds and to the production of fresh carbonyl groups.

Figure 6 shows the dichroism in the range 5.5-7 μ for specimen 52 (dehydrated for 5 min at 160°), which has pronounced dichroism in the visible region (Fig. 7). The infrared absorption is comparatively weak, so three pieces of a specimen were used in the parallel position. Figure 8 gives the

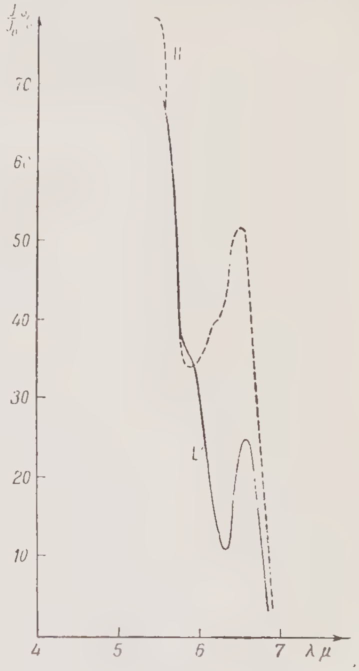

Fig. 9. Dichroism at 5.5-6.5 μ for specimen 70.

---

[1] The detailed mechanism is dealt with in a paper presently in preparation.

curves for untreated film. The band at 5.8-5.9 μ in both spectra indicates that C=O groups are present initially and after treatment, and that these have no obvious preferred orientation. Heat treatment gives rise to a new broad band at 6.1-6.3 μ, which corresponds to double bonds parallel to the stretching direction. Various types of double bond are present.

More prolonged treatment gives a clearer picture; specimen 70 (1 h 40 min at 150°) gives sharp dichroic bands at 5.9 and 6.3 μ (Fig. 9), the latter corresponding to conjugated double bonds of the type −CH=CH−CH=CH−CH=CH−, which lie parallel to the stretching direction. The C=O groups are perpendicular to this direction, which shows that the heat treatment produces crosslinking. The second stretching clearly has the functions of reducing the number of these links and of increasing the degree of orientation parallel to the stretching direction. These conjugated double bonds are thus the chromophore responsible for the dichroism in the visible region.

Conclusions

1. Heat-resisting polarizers have been made from dehydrated polyvinyl alcohol films.
2. A method has been devised for improving the optical parameters and for stabilizing the material up to relatively high temperatures.
3. Infrared spectra show that conjugated double bonds are responsible for the dichroism in the visible region.

LITERATURE CITED

1. D.A. Godina, "Optical parameters of polyvinyl alcohol polarizers," Zh. Tekhn. Fiz., 18 1317 (1948).
2. E.H. Land and G.D. West, "Dichroism and dichroic polarizers," Colloid. Chem., 6, 160 (1946).
3. E.H. Land, "Some aspects of the development of sheet polarizers," J. Opt. Soc. Am., 41, 957 (1951).
4. S.N. Ushakov, R.K. Gavurina, and Kh.V. Tsubina, Studies on Macromolecular Compounds [in Russian](1949), p. 182.

SOVIET PHYSICS – CRYSTALLOGRAPHY VOL. 1, NO. 2 MAR.-APR., 1956

GROWTH OF CRYTALS OF ETHYLENE DIAMINE TARTRATE*

P. G. Pozdnyakov

Division 10, Ministry of the Radio Industry of the USSR

Translated from Kristallografiya, Vol. 1, No. 2,
pp. 228-234, March-April, 1956
Original article submitted January 12, 1956

A description is given of the principal features of a method of growing large crystals of this tartrate, together with a novel method of orienting and mounting seeds; the products are virtually free from inhomogeneity caused by regeneration.

The compound ethylene diamine tartrate (EDT) has crystals that can be cut as crystal filters of low temperature coefficient.

The piezoelectric properties were first examined by Mason in 1947 [2]; EDT crystals are now widely used abroad, and a plant solely devoted to this has been built in the USA [3]. No very extensive use has been made of EDT here, as the material has been rejected in favor of potassium tartrate, which has some advantages in crystal filters. However, EDT has some other uses, and the production of its crystals has not previously been described in the Russian literature, so some details are given here of techniques of value in large scale production. In addition, some new information is presented on the growth of the crystals, which is of interest in relation to the growth of other substances.

The results presented here were obtained by the author jointly with A. A. Shternberg between 1947 and 1952.

The compound is not available for purchase in finished form, so users have to prepare it. I. F. Bogdanov, in 1947, devised methods of making EDT in the form of aqueous solutions and small crystals with ethylene diamine hydrochloride as starting material.

Ethylene diamine tartrate $C_6H_{14}N_2O_6$ is the neutral salt resulting from the interaction of tartaric acid with ethylene diamine. The crystals obtained from aqueous solutions usually contain no water of crystallization, but a monohydrate is also known, and this is deposited from aqueous solutions below 40.6°C.

Only anhydrous EDT crystals are used; the simplest method of preparing the salt is to neutralize tartaric acid with an aqueous solution of ethylene diamine, the latter being available as aqueous solutions containing up to 70% of the diamine of technical purity. The neutralization produces much heat, so the reaction must be carried out by slow addition of the acid to the solution of the base. The temperature must not be allowed to rise above 50-55°C, because the base starts to decompose above this. Some decomposition occurs even below 50°C, but this is relatively slight; the solution becomes progressively more yellow as time passes. The decomposition products are removed by filtering the solution through a layer of activated charcoal, the filtrate being almost colorless. Exposure to heat and light rapidly causes it to turn yellow again.

EDT solutions are highly viscous; the literature gives the viscosity at 50°C for a saturated solution as about 240 millipoises. The salt is very soluble in water, the solubility increasing substantially with temperature; a liter of water dissolves about 1.3 kg at room temperature and about 1.6 kg at 50°C. EDT crystals can thus be grown by cooling the solution, especially since the solubility is a linear function of temperature. The decomposition products tend to reduce the solubility.

Practical purposes are satisfied by the above approximate results, which relate to solutions of pH 7.0-7.2, which corresponds to a slight excess of the base.

---

*Read at the First All-Union Conference on Piezoelectricity, Institute of Crystallography, November 26, 1952 [1].

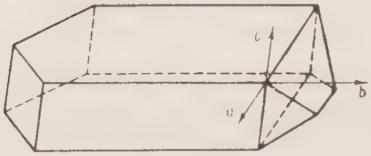

Fig. 1.

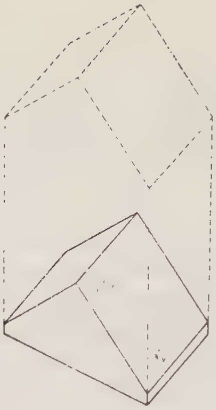

Fig. 2.

EDT will form highly supersaturated solutions, as for many salts that form highly viscous solutions; no crystals are formed even when the solution is supercooled by 12-15°C. Here we disagree with Mason [3], who states that EDT solutions show a considerable tendency to crystallize spontaneously (more so than Rochelle salt or ammonium phosphate); our observations indicate precisely the converse.

EDT crystals fall in the dihedral axial class of the monoclinic system (Fig. 1); β is 105°30'. The density is 1.54, and there is a prominent cleavage on $\{001\}$.

We used small crystals in solutions at rest to establish the main features of the growth. There is a pronounced tendency to preferential growth in the negative sense of the b axis (a diad symmetry axis). The $\{110\}$ faces around the other end of this axis scarcely grow at all, as do the pinacoid faces. EDT resembles ammonium phosphate in usually giving needle crystals, which are of no practical value. Crystals of large cross section require the use of broad seeds, which must also be cut from such large crystals. The best seeds are the heads of broad crystals, which consist of the rapidly growing dihedral faces. These broad crystals were produced by a method previously employed for ammonium phosphate, in which highly supersaturated solutions are employed to produce parallel growths of small crystals on the pinacoid faces, which accentuate the growth of the latter. Several growth cycles based on these heads give reasonably broad crystals with heads suitable for use as seeds. No more effective method of making broad crystals (e.g., adjustment of solution composition, as for ammonium phosphate) is presently known. We initially used heads cut perpendicular to the b axis and attached with cement to a flat horizontal disk. The crystals grew along the b axis (Fig. 2); the effects of supersaturation on the growth were examined on these. Highly supersaturated solutions gave only the $\{001\}$ and $\{100\}$ pinacoid and $\{110\}$ and $\{1\bar{1}0\}$ dihedron faces. The faces of the $\{011\}$ dihedron grew at the positive end. Low supersaturations caused some growth on the $\{101\}$ pinacoid, $\{111\}$ dihedron, and $\{0\bar{1}0\}$ monohedron faces. Some faces of types (hkl) and $(h0l)$ were also observed, especially in impure solutions.

Inhomogeneities are produced within a certain range of supersaturations. EDT crystals were formerly grown at low supersaturations, which fall short of that range, but the growth is then only 0.8 mm/day, so it requires about three months to grow a reasonably large crystal [4, 5]. The lower end of the hazardous range corresponds to a supercooling of 3-4°C. We have found [6] that the upper end of that range corresponds to supercooling by 6-8°C; supercooling by 12-15°C is possible, and this gives growth rates of 5-8 mm/day, which means that a crystal weighing over 1 kg can be grown in about 20 days. Lower supercooling gives inhomogeneity because additional faces arise, these having growth rates sharply dependent on the supersaturation; they give rise to inclusions of solution. In particular, a fast-growing $\{0\bar{1}0\}$ face usually produces cloudy layers parallel to itself; this face is favored by medium supersaturation, and its growth rate increases very rapidly with the latter, which depletes the solution, the residual mother liquor becoming trapped. These additional faces are lost at high supersaturations, so no cloudy inclusions are produced.

EDT crystals regenerate readily, so any accidental damage is healed and does not give rise to large or persistent defects.

We then made tests on the effects of impurities and solution composition generally on the growth.

Neutral solutions gave falling growth rates and tapering crystals, very much as occurs with ammonium phosphate if the solution is too acid.

Alkaline solutions (ones with excess of the base) give higher rates and eliminate taper. We have not tested the effects of other bases, in particular ammonia, which has been recommended by American workers; Walker [5] states that ammonia sufficient to give pH 7.5 eliminates tapering and doubles the growth rate (to 1.5 mm/day). We have produced rates more than three times this, so we did not examine the use of ammonia.

Experience over more than four years has shown that EDT crystals are very insensitive to a great many impurities, whereas the growth rates of ammonium phosphate and potassium tartrate are very sensitive to impurities.

These features make it especially simple to grow large crystals; the initial supersaturation need not be set very precisely, nor need the rate of temperature reduction be kept strictly constant. Also, the solution does not need to be highly pure or of closely controlled composition.

There is no marked effect on the growth rate if the crystal is moved in the solution, on account of the high viscosity; halts in the motion, if not very prolonged, also cause no inhomogeneity (contrast ammonium phosphate and potassium tartrate).

Defects (cloudiness, cracks) arising during growth are very rare in this method of growing EDT crystals, though cracks sometimes arise toward the end, especially while the crystals are being removed. These cracks take a highly characteristic form, being confined entirely to the surface; they arise mainly on the $\{001\}$ cleavage.

Some defects are caused by incorporation of decomposition products; the crystals become yellowish if the solution is so impure as to be brownish and largely opaque. We have no evidence that the properties of the crystal are seriously altered, nor is it clear what products are incorporated. The decomposition products tend to depress the growth rate. It is clearly undesirable to allow excessive contamination by these products, but it is extremely simple to check on this from the color of the solution. Filtration (see above) removes the impurities.

Cylindrical vessels (such as are used for ammonium phosphates) may be employed in large-scale production; these may be of stainless steel and of volume up to 150 liters, with viewing parts, fittings for thermometers and temperature regulators, crystal holder, and close-fitting covers. It is not essential to use a reciprocating crystal holder; continuous rotation can be employed. The holder may be a disk of plastic or stainless steel, with several seeds mounted near the edge. Several disks may be mounted on the same shaft if the crystallizer is of sufficient volume.

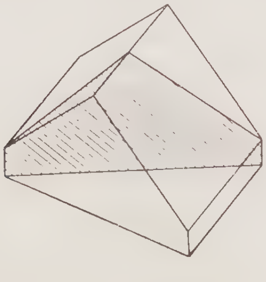

Fig. 3.

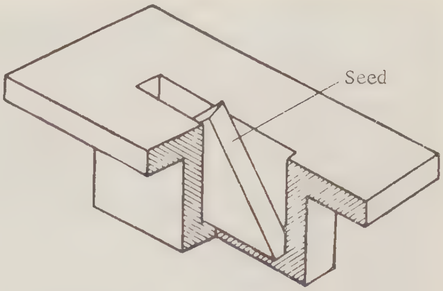

Fig. 4.

Heads of crystals give the best seeds for routine production. The lower end of the crystal (that containing the head) then usually contains defects arising from regeneration, so this part must be discarded.

Tests were done to devise a method of growing EDT crystals free from these defects; a special orientation of the seed may be used together with a particular form of mounting in the holder. These tests showed that large EDT crystals can be grown almost free from these defects arising from regeneration. In addition, the new type of seed requires a much smaller volume of crystal.

New seeds are cut from a head formed by intersection of the faces of the $\{1\bar{1}0\}$ dihedron, which is sliced along a series of diagonal planes parallel to the length of the crystal (Fig. 3). This gives several triangular plates, each of which can act as the seed for a crystal of the same width as the initial one. The plates obtained from the sides of the head are small and are of no real value for growing further crystals.

Defects arising from regeneration are minimized by reducing the surface area of the seed; point seeds would be the best on this basis, but they do not allow one to grow broad crystals. The following method of holding the plate seeds provides essentially growth of the pinacoid faces from a restricted area. The plate is placed in a deep slot closed at the bottom with the vertex upward and slightly projecting from the slot (Fig. 4). The crystal grows outward from the vertex, and the $\{1\bar{1}0\}$ faces that gradually grow out from the slot constantly stimulate the growth of the pinacoid faces,

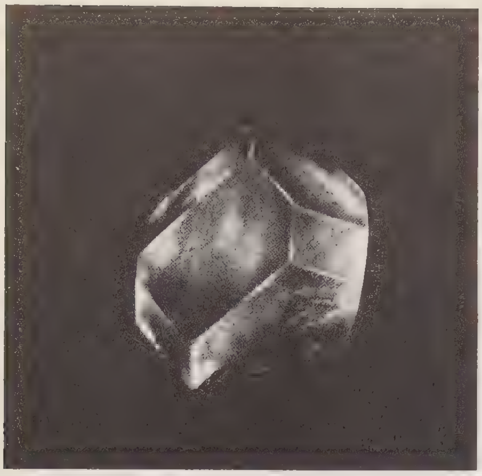

Fig. 5. EDT crystal grown on the vertex of a seed plate (early stages of growth).

which continues until the base of the plate is inscribed within the perimeter of the crystal. The cross section of the finished crystal is thus governed by that of the base.

This method may be used with other substances that show a pronounced tendency to grow in one direction only. Figure 5 shows an EDT crystal in the early stages of growth from a seed plate.

High supersaturations should not be produced until the crystal growing from the seed has reached the required size. This implies special control of the early part of the temperature-reduction curve, if this is the method employed to cause growth.

EDT decomposes rapidly above 50°C, while the monohydrate may be deposited below 40°C, so we made some tests on crystal growth at a fixed temperature of about 45°; the high solubility of EDT makes it quite feasible to produce growth by solvent evaporation.

Solvent removal was effected by a very simple method (layers of filter paper inserted under the edges of the cover). Water condensing on the cover is carried away by the capillary action of the paper. The volume of solution in the vessel is kept constant by adding EDT solution saturated at a lower temperature.

EDT crystals were also grown by reducing the temperature of the supersaturated solution. The initial supercooling was 8 to 12°C. The linear temperature dependence of the solubility makes it very simple to draw up a temperature program, especially since the crystal grows in one direction only. The only quantities that need to be known are the

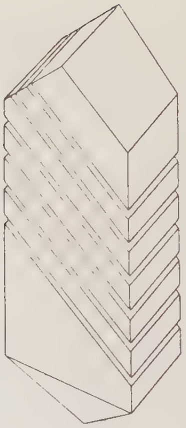

Fig. 6.

volume of solution, number, and cross section of the crystals, and the permissible growth rate. The last was taken as 5 mm/day in our calculations. A fixed rate of reduction is used, apart from the initial stage, where a reduced rate is used until the seeds have grown out to the required cross section. In addition, the fixed rate is exceeded somewhat toward the end of a run in order to compensate for the slight tendency to lateral growth.

We have also used other seed plates for some time. These were cut parallel to the $\{1\bar{1}0\}$ dihedron face as slices 1.5-2.5 mm thick from the entire crystal (Fig. 6). These seeds are held on flat inclined holders mounted on a common base. These seeds regenerate satisfactorily and give large uniform crystals, but they have the disadvantage that the end of the crystal is oblique, i.e., parallel to the $\{1\bar{1}0\}$ face. On the other hand, they are better than plates cut from crystal heads, because there is considerably less waste from cutting. In addition, the complete absence of defects increases the proportion of the crystal that can be utilized. A

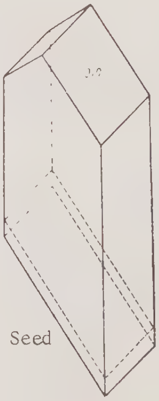

Fig. 7.

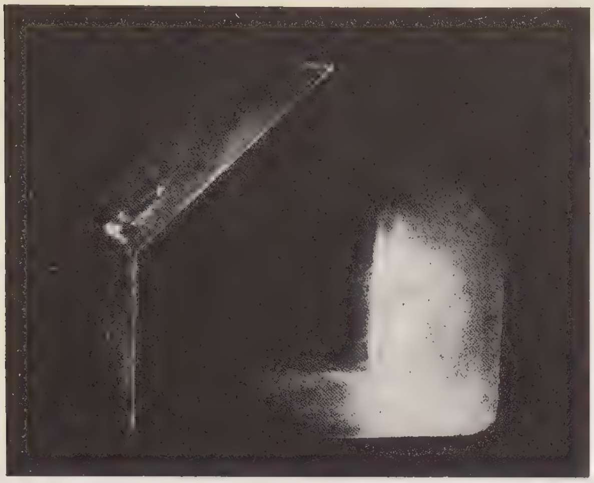

Fig. 8. EDT crystal ($^7/_8$ natural size).

slight difficulty arises over regeneration for seeds of very large area. Figure 7 shows a crystal grown from such a plate; in this case, the temperature may be reduced uniformly, as when complete heads are used.

Although it is possible in principle for the monohydrate to be deposited if the temperature is taken below 40°C (which could bring the run to an end), we have encountered no case in which this occurred, even when the temperature was reduced to 25°C. There may be other reasons for preferring the isothermal method (operated above 40°C).

EDT crystals are very easily grown by simple techniques to be entirely free from defects. Figure 8 shows an EDT crystal at slightly less than natural size. We have produced crystals of slightly over 1 kg, but there appear to be no obstacles to the production of larger ones.

We are indebted to Academician A.V.Shubnikov for comments on the draft of this paper.

LITERATURE CITED

1. Élektrichestvo, No. 6 (1953).
2. W. Mason, Proc. IRE, 35, 1005 (1947).
3. W. Mason, Piezoelectric Crystals and Their Application in Electroacoustics [Russian translation](IL, Moscow, 1952).
4. Walker and Coman, Trans. AIEE, 67, 565 (1948).
5. Walker, J. Franc. Inst., No. 6, 481-524 (1950).
6. Authors Certificate No. 88624, March 13, 1950, in the names of P.G. Pozdnyakov and A.A. Shternberg.
7. Authors Certificate No. 101179, December 2, 1952, in the names of A.A. Shternberg and P.G. Pozdnyakov.

BRIEF COMMUNICATIONS

A NOMOGRAPHIC METHOD OF CALCULATING STRUCTURE FACTORS

N. V. Belov and T. N. Tarkhova

Institute of Crystallography, Academy of Sciences of the USSR
Gor'kii State University

Translated from Kristallografiya, Vol. 1, No. 2,
pp. 235-238, March-April, 1956
Original article submitted January 20, 1956

A new type of nomogram was proposed in [1] for calculation of monoclinic and hexagonal structure factors, as these factors were not reducible to one-term derivatives of the $\cos 2\pi hx \cos 2\pi ky \cdot \cos 2\pi lz$ type. The new method was proved to be very useful in a series of recent structural studies [2-5], carried out with the participation of the present authors; in particular, it has been found worthwhile for orthorhombic structures as well, where, until recently, the logarithmic nomogram method predominated, which was itself proposed by one of the present authors, and "mechanized," as described in [6].

Logarithmic nomograms are inconvenient, because it is necessary to use the same scale for both sines and cosines, and because of the effort involved in remembering the signs corresponding to a given quadrant.

By using nomograms of the type described in [1], the need no longer arises to bring the structure factor formulas to the "logarithmic" form, which takes up considerable space in the new edition of the International Tables. Groups with their origin at a center of symmetry contain no sines at all. Let us examine the structure factor calculation for the following symmorphic groups:

$$D^1_{2h} = Pmmm,\ D^{19}_{2h} = Cmmm,\ D^{23}_{2h} = Fmmm,\ D^{25}_{2h} = Immm.$$

$$A = n\{\cos 2\pi(hx + ky + lz) + \cos 2\pi(h\bar{x} + ky + lz) + \cos 2\pi(hx + k\bar{y} + lz) + \cos 2\pi(hx + ky + l\bar{z})\}.$$

As is usual in structure analysis, we begin with the structure factors for the hk0 reflections, i.e., with the expression $A = n\{\cos 2\pi(hx + ky) + \cos 2\pi(hx - ky)\}$. Let $x = 0.35$ and $y = 0.21$. On millimeter graph paper (Fig. 1) we chose a central bold line, on which we place a cosine scale (twice), at a scale of 1 = 20 cm. On one of the bold lines to the left of the central scale we plot the values of hx on a 1 = 40 cm scale, writing h = 1,2,... at the ends of the segments. If hx is more than one (40

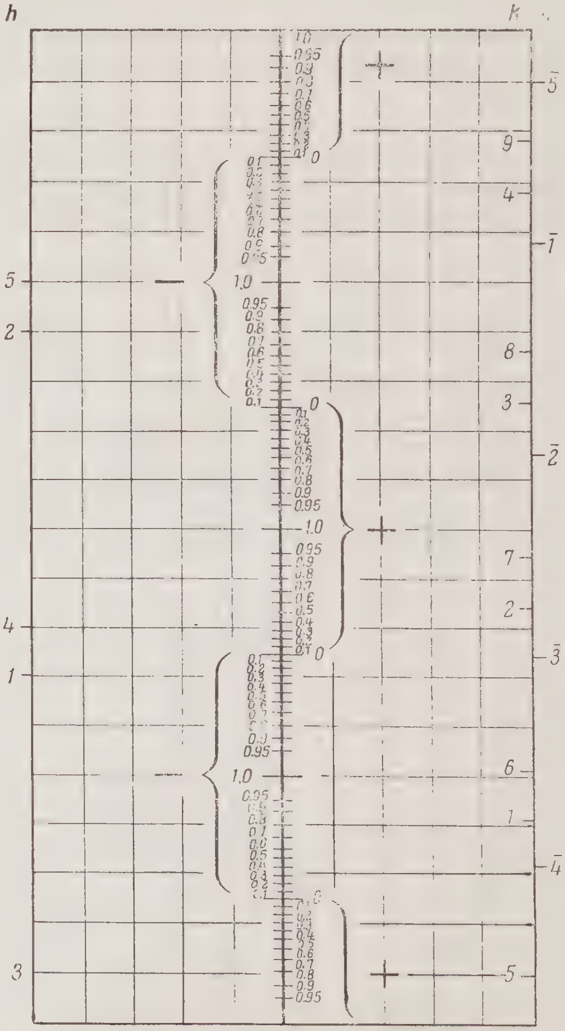

Fig. 1.

cm), the corresponding fractional part is plotted. On the symmetrically opposite bold line (on the right), the values of ky are put but, in this case, twice; once counting from the bottom of the 40-cm scale, and once from the top (again, only fractional parts). In the second case, the figures are marked with minus signs ($\bar{1}$, $\bar{2}$, $\bar{3}$, . . .).

A straight line (drawn on tracing paper), which connects a given h on the left-hand scale with a given k on the right-hand scale, cuts the central line at the value of $\cos 2\pi(hx + ky)$. The straight line h to $\bar{k}$ gives the second term, $\cos 2\pi(hx - ky)$.

If a group is not symmorphic, then, depending on whether there is an even or odd number of halves involved in the argument of the second term in the structure factor expression, the corresponding cosine will be either added or subtracted. Thus, for the group D_{2h}^{16} = Pnm*a*, and for the hk0 reflections, the structure factor will be

$$A = 4\cos 2\pi(hx + ky) + 4\cos 2\pi(hx + \overline{ky})$$

for even k, and

$$A = 4\cos 2\pi(hx + ky) - 4\cos 2\pi(hx + \overline{ky})$$

for odd k (h is always even for D_{2h}^{16}, according to systematic absence rules).

The structure factors are usually calculated according to the layer lines. For the *l*-th line, the corresponding expression (starting off with the group D_{2h}^{1} = Pmmm), is:

$$2\{\cos 2\pi(hx + ky + lz) + \cos 2\pi(\overline{hx} + ky + lz) + \cos 2\pi(hx + \overline{ky} + lz) + \cos 2\pi(hx + ky + \overline{lz})\},$$

which is rewritten in the form

$$2\{\cos 2\pi(lz + hx + ky) + \cos 2\pi(lz + \overline{hx} + ky) + \cos 2\pi(lz + hx + \overline{ky}) + \cos 2\pi(lz + \overline{hx} + \overline{ky})\}.$$

On the left-hand scale we fix the value of *l*z, and we begin to plot the values of hx only from this point, with, as before, the counting starting at the bottom when the 40-cm scale is run over. From the same *l*z point, we plot the values of $\overline{hx}$ along the opposite direction, marking them $\bar{1}$, $\bar{2}$, $\bar{3}$, . . .

On the right-hand scale, in the same order as previously, we mark off k and $\bar{k}$. A line from h to k cuts the central scale at the value of the first cosine: $\bar{h}$ to k, h to $\bar{k}$, and $\bar{h}$ to $\bar{k}$ give the second, third, and fourth cosines. With nonsymmorphic groups, the second, third, and fourth terms may have either plus or minus signs, depending on whether there is an odd or even number of translational halves in the argument, for example, for the group D_{2h}^{16} = Pnm*a*, there are four possible cases:

$$\begin{cases} h + l = 2n \\ k = 2n \end{cases} \quad + + + +$$

$$\begin{cases} h + l = 2n \\ k = 2n + 1 \end{cases} \quad + - - +$$

$$\begin{cases} h + l = 2n + 1 \\ k = 2n \end{cases} \quad + - + -$$

$$\begin{cases} h + l = 2n + 1 \\ k = 2n + 1 \end{cases} \quad + + - -$$

For the group D_{2h}^{7} = Pnm*a*, with the general structure factor expression

$$A = 2\left\{\cos 2\pi(hx + ky + lz) + \cos 2\pi(\overline{hx} + ky + lz) + \cos 2\pi\left(hx + \overline{ky} + lz + \frac{h+l}{2}\right) + \cos 2\pi\left(hx + ky + \overline{lz} + \frac{h+l}{2}\right)\right\}$$

there are, in all, two possible cases:

$$h + l = 2n \qquad + + + +,$$

$$h + l = 2n + 1 \qquad + + - -.$$

If the group is not centrosymmetric, it is necessary to separately calculate the cosine part (A) and the sine part (B) of the structure factor. The first part is calculated by the method already described, and the second part by raising the central scale a distance of 5 cm. It is convenient to have the central scale movable (compare [1]), not only for changing from cosines to sines, but also so that, instead of marking the value of *l*z on the left-hand scale, the central scale can be simply moved by the distance *l*z, working to a scale of half the size.

For the group D_2^1 = P222,

$$A = \cos 2\pi(hx + ky + lz) + \cos 2\pi(hx + \overline{ky} + \overline{lz}) + \cos 2\pi(\overline{hx} + ky + \overline{lz}) + \cos 2\pi(\overline{hx} + \overline{ky} + lz),$$

$$B = \sin 2\pi(hx + ky + lz) + \sin 2\pi(hx + \overline{ky} + \overline{lz}) + \sin 2\pi(\overline{hx} + ky + \overline{lz}) + \sin 2\pi(\overline{hx} + \overline{ky} + lz),$$

which can be rewritten as

$$A - \cos 2\pi(lz + hx + ky) + \cos 2\pi(lz + \overline{hx} + ky) + \cos 2\pi(lz + hx + \overline{ky}) + \cos 2\pi(lz + \overline{hx} + \overline{ky}),$$

$$B = \sin 2\pi(lz + hx + ky) - \sin 2\pi(lz - \overline{hx} + ky) - \sin 2\pi(lz + hx + \overline{ky}) + \sin 2\pi(lz + \overline{hx} + \overline{ky}),$$

i.e., the cosine sequence is++++;the sine sequence, +− − +.

For the group P$ca2_1$, with the origin on the 2_1 axis, the general structure factor expression is

$$A = \cos 2\pi(hx + ky + lz) + \cos 2\pi\left(h\bar{x} + ky + lz + \frac{h+l}{2}\right) + \cos 2\pi\left(hx + k\bar{y} + lz + \frac{h}{2}\right) + \cos 2\pi\left(h\bar{x} + k\bar{y} + lz + \frac{l}{2}\right);$$

$$B = \sin 2\pi(hx + ky + lz) + \sin 2\pi\left(h\bar{x} + ky + lz + \frac{h+l}{2}\right) + \sin 2\pi\left(hx + k\bar{y} + lz + \frac{h}{2}\right) + \sin 2\pi\left(h\bar{x} + k\bar{y} + lz + \frac{l}{2}\right),$$

and we have the four sign sequences:

$h = 2n,$	$l = 2n$	A	+	+	+	+
		B	+	+	+	—
$h = 2n,$	$l = 2n + 1$	A	+	–	+	—
		B	+	[illegible]	+	[illegible]
$h = 2n + 1,$	$l = 2n$	A	+	–	[illegible]	+
		B	+	—	—	+
$h = 2n + 1,$	$l = 2n + 1$	A	+	+	—	—
		B	+	+	–	–

It is easy to make up similar sequences for all the 230 space groups.[1]

LITERATURE CITED

1. N. V. Belov, "Nomographic methods of calculation in x-ray structure analysis," Tr. Inst. Kristallogr., 9, 277-286 (1954).
2. N. V. Belov and I. M. Rumanova, "The crystal structure of epidote," Tr. Inst. Kristallogr., 9, 103-164 (1954).
3. E. G. Fesenko, I. M. Rumanova, and N. V. Belov, "The crystal structure of zoisite," DAN SSSR, 102, 275-278 (1955).
4. R. F. Smirnova, I. M. Rumanova, and N. V. Belov, "The crystal structure of cuspidine," Zap. Min. Obshch., ch. 84, 159-169 (1955).
5. N. I. Golovastnikov, "The crystal structure of eremeyevite," Zap. Min. Obshch., ch. 84, 405-414 (1955).
6. Yu. T. Struchkov and B. V. Nenart, "A nomogram for calculating structure amplitudes," Tr. Inst. Kristallogr., 9, 317-320 (1954).

---

[1] These can be obtained, ready for use, from the X-Ray Laboratory, Gor'kii State University.

AN ELECTRON-DIFFRACTION STUDY OF Bi AND Sb ALLOYS AND CERTAIN OF THEIR OXIDES

Z. G. Pinsker, O. S. Orekhvo, and A. I. Miller

Faculty of X-Ray and Crystallographic Studies and Institute
of Physicotechnical Studies, Gor'kii State University
Institute of Crystallography, Academy of Sciences of the USSR

Translated from Kristallografiya, Vol. 1, No. 2,
pp. 239-240, March-April, 1956
Original article submitted January 25, 1956

Some very full x-ray studies [1] of alloys from the Bi – Sb system have shown that these components form a continuous series of solid solutions, with an unlimited range of solubilities. It appeared of interest to investigate the thin layers obtained by simultaneous condensation of the vapors of these two components in a vacuum, since these layers actually demonstrate a continuous change in the concentration of each of the metals.

The films were condensed either on celluloid or on a fresh sliver of rocksalt crystal. The temperature of condensation or subsequent annealing was varied from experiment to experiment, from room temperature up to about 100°C for the celluloid, and up to 300-350°C for the rocksalt. As the condensation and annealing temperatures were increased, the degree of orientation of the film crystallites was improved. At a 50 : 50 composition, several diffuse reflections were observed.

Over the whole range of concentrations studied by the electron diffraction method, an identical structure was observed, corresponding to that of antimony or bismuth, with continuously variable unit cell constants; a was equal to 4.53 ± 0.01 Å (on the Bi side) and 4.29 ± 0.01 Å, and c was equal to between 11.88 ± 0.02Å and 11.24 ± 0.02 Å.

The films prepared on celluloid had their crystallites oriented with their basal faces parallel to the substrate and in a random azimuthal arrangement. By annealing at 100°C it was possible to obtain good orientation with any composition.

The films prepared on NaCl, particularly those subjected to annealing after condensation, did show azimuthal orientation. From each of the hki0 ring cleavages, 12 point reflections were observed, indicating two equally probable dispositions; any vector of the [100], [110], [010] type in the metal lattice could be parallel to the [110] and [$\bar{1}\bar{1}$0] directions in NaCl.

A series of specimens on NaCl crystals, representing the whole range of concentrations, was annealed at t = 200°C for 15 h. No changes were observed in the diffraction patterns as a result of this annealing.

The formation of well-oriented films, even when condensing on substrates at room temperature, shows that the Bi and Sb atoms are quite mobile on these substrates under the experimental conditions used. We therefore assumed that the fact that 15 h of annealing at 200°C had no effect on the diffraction pattern was proof that these alloys could not attain an ordered arrangement of their Bi and Sb atoms.

Experiments were carried out on the oxidation of films of the pure components and of their alloys. An Sb film on rocksalt oxidized on heating to t = 180°C in air at a pressure of 10^{-1}-10^{-2} mm Hg. In this case, senarmontite, Sb_4O_6, was invariably formed, this having a cubic lattice with a = 11.14 Å. In all cases, the senarmontite crystallites were oriented with their (111) planes parallel to the substrate. If the antimony specimen was azimuthally oriented, then the Sb_4O_6 crystals repeated this orientation. The relative orientations of the Sb and its oxide are a reflection of the well-known relationship between cubic and hexagonal lattices: $[111]_{cub} \parallel [001]_{hex}$ and $[110]_{cub} \parallel [100]_{hex}$.

When Bi films were oxidized, or Bi vapor was condensed under preliminary vacuum conditions (at 200-250°), oxide phases were apparently observed; these had cubic lattices with a_1 = 4.65 Å (I) and a_2 = 5.49 Å (II). The crystals of these phases were

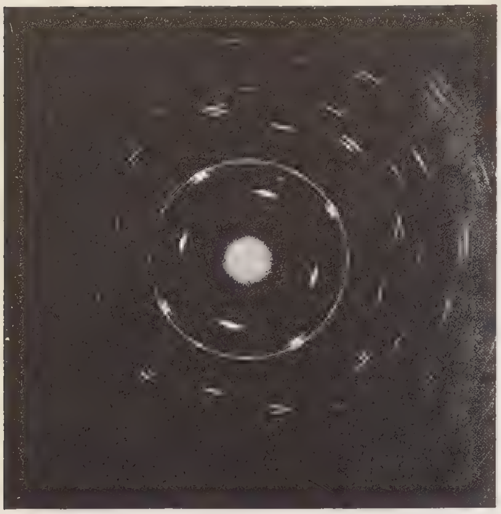

Fig. 1. Electron-diffraction pattern from a Bi film containing a cubic oxide phase with a = 4.65 A.

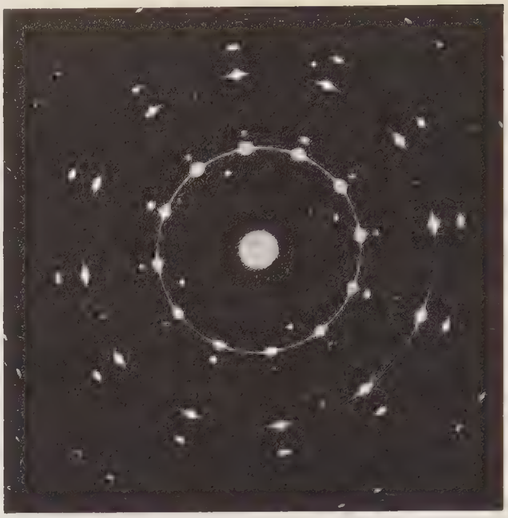

Fig. 2. Electron-diffraction pattern from a film of azimuthally oriented Bi, containing a cubic oxide phase with a = 5.49 and NaCl.

regularly oriented (Figs. 1 and 2).

In Bi specimens without azimuthal orientation, the crystallites of (I) were oriented with their cube faces parallel to the substrate, forming a mosaic crystal. In specimens of azimuthally oriented Bi, the crystallites of (II) were also oriented with their cube faces parallel to the substrate, and with their [100] or [010] directions parallel to the [100] or [010] vectors of the hexagonal Bi. The oxide phase (II) which we detected, with a cell constant of 5.49 Å, is evidently identical to a phase described in [2].

LITERATURE CITED

1. W. F. Erhet and M. B. Abramson, "The nature of the solid phase in the system antimony–bismuth," J. Am. Chem. Soc., 56, 385-388 (1934).
2. S. A. Semiletov and Z. G. Pinsker, "Oxidation of Bi_2Se_3 and Bi_2Te_3 specimens on heating in air," Zh. Tekhn. Fiz., 25, 2336-2338 (1955).

THE ORIENTED CRYSTALLIZATION OF POTASSIUM IODIDE AND BROMIDE ON MUSCOVITE

I. E. Kamentsev

Crystallography Faculty, A.A. Zhdanov University, Leningrad

Translated from Kristallografiya, Vol. 1, No. 2,
pp. 240-243, March-April, 1956
Original article submitted December 3, 1955

The question of the manner in which the ability of crystals to form regular overgrowths depends on the relative difference in parameters of the overgrowing flat networks has been considered by Yanulov [2]. He quotes some old experiments by Frankenheim [4] on the preparation of growths of various halide salts (NH_4I, KI, KBr, KCl) on the (001) cleavage planes of biotite and muscovite.

On the basis of experimental studies, Yanulov came to the conclusion that the relative number of oriented crystals forming on the mica was a simple linear function of the relative difference between the parameters of the flat networks growing together (Fig.1). The substances were crystallized by evaporating drops of solution on freshly cleaved flakes of the mica. Excess solution was removed with a filter paper. In Yanulov's opinion, this excluded the possibility of nonoriented growth being obtained through precipitation of crystals from the upper layers of the drop.

The present study was to investigate the possibility of deriving quantitative relationships between the overgrowth behavior of KI and KBr on muscovite and the degree of similarity of their parameters.

The process of crystallization of KI and KBr from solution onto muscovite can be represented as follows. When the drop of solution is placed on the surface of the crystal, evaporation of the liquid takes place, leading to the formation of two kinds of crystals. One of these arises in the immediate vicinity of the substrate, and is oriented[1]; the other is formed outside the zone of influence of the crystal substrate surface; these latter very fine crystals, when "their weight is sufficient, fall onto the surface, where they may lay in any position" [5]. This type of crystal generates nonoriented overgrowths.

Yanulov's conclusion that there was a linear relationship between the formation of regular overgrowths and the degree of similarity of the crystal parameters does not seem to be very likely to us, because, in his experiments, he did not completely eliminate the causes of crystals precipitating from the upper layers of the liquid.

In order to avoid crystals precipitating from the upper layers of the drop, we used a vertical, flat crystallization vessel, with the mica plate placed in it in a vertical position also. On this, under the action of surface forces, only oriented crystals arose. The observations were made using a microscope.

The solution with the mica plate immersed in it was either left several days to stand or was cooled rapidly with dry ice. In the latter case, growths were obtained after 10-15 min. The experiments were carried out in the KI–muscovite and KBr–muscovite systems. During the crystallization of KBr on muscovite, when the relative difference between the network parameters was 11.4%,

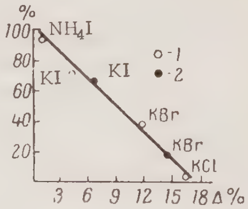

Fig. 1. Relationship between the difference in parameters of intergrowing flat networks (Δ %) and the percentage orientation of crystals (%). 1) Crystallization on muscovite; 2) crystallization on biotite (after K.P. Yanulov).

---

[1] Bradley [3] has established that the zone of surface forces of mica extends to 10^{-5} cm when NH_4I is crystallized onto its surface.

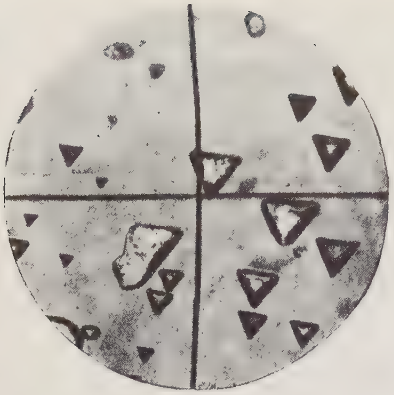

Fig. 2. Oriented crystallization of KBr on muscovite. Magnification 120×.

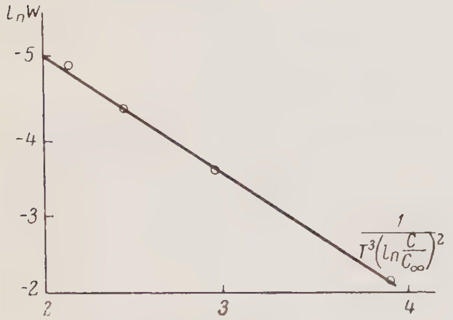

Fig. 3. Graph of $\ln w$ against $\frac{1}{T^3\left(\ln\frac{c}{c_\infty}\right)^2}$ for the KI–muscovite system.

Yanulov obtained only 39% of oriented crystals (Fig. 1), while in this case we found complete orientation of all the 500 KBr crystals studied (Fig. 2).

Thus, where in crystals the relative difference between their parameters and that of muscovite is increased from 11.4% (crystallization of KBr on muscovite with full orientation) to the values permitted by Royer's limit rule (about 15%, for example as in KCl), there must be an abrupt change in their ability to form regular overgrowths.

In our view, therefore, it would be wrong to assume that there is a gradual change in percentage orientation, depending on the relative difference between the parameters of the flat networks growing together. Our experiments indicate, rather, that the proportion of oriented crystals varies in stepwise fashion.

As the quantity which varies according to the difference in network parameters, we can examine the value of the "limiting" supercooling [1], i.e., that value of solution supersaturation at which precipitation of crystals onto the support occurs. The supersaturation of the solution may be expressed by the quantity ($\ln(c/c_\infty)$), where c is the equilibrium concentration, and c_∞ is the concentration at which precipitation of crystals begins.

TABLE 1

Saturation temp., °C	Temp. at start of crystal separation, °C	Time of appearance of crystallization centers (av. of many measurements),* sec
20	10.5	150
20	10.0	100
20	9.0	50
20	8.5	10

---

* The time of appearance of crystallization centers is the reciprocal of the probability of their formation, T = 1/w [1].

In this connection, a relationship of considerable interest is the straight-line graph obtained by plotting the logarithm of the probability of formation of crystallization centers ($\ln w$) against a quantity inversely proportional to the square of the supersaturation,

$$\left[\frac{1}{T^3\left(\ln\frac{c}{c_\infty}\right)^2}\right].$$

This relationship was first established by Ovsienko [1] for the crystallization of aqueous NaBr and NaCl solutions on the surface of galena. Our experiments on the KI–muscovite and KBr–muscovite systems confirm this relationship.

Part of the experimental data on the KI–muscovite system is given in Table 1.

From the results obtained, a graph was constructed (Fig. 3). The results obtained by Ovsienko and by us allow conclusions to be drawn as to the change in the value of the "limiting" supercooling with change in the difference between the parameters of the flat networks.

Thus, in the case of the NaCl–PbS system (Δ = 5.7%), precipitation of crystals of the dissolved substance takes place on the PbS at a degree of supersaturation one quarter of that pertaining before the introduction of the PbS crystal, while with NaBr solutions (Δ = 0.2%), the supersaturation is reduced by a factor of 10 [1].

As the probability of appearance of the crystals is related to the supersaturation of the solution, it might be considered that changes in the parameters of the intergrowing flat networks would have a direct effect on the probability of appearance of crystal growth nuclei. Table 2 shows how the time of appearance of crystallization centers alters depend-

TABLE 2

System	Δ %	Saturation temp., °C	Temp. at start of crystal separation, °C	Time of appearance of crystallization centers, sec
KI—muscovite	3.81	20	10	100
KBr—muscovite	11.4	20	10	Crystals did not appear
KI—muscovite	3.81	40	20	Crystals appeared momentarily
KBr—muscovite	11.4	40	20	30

ing on the relative difference between the network parameters (Δ %).

Conclusions

1. The percentage of oriented crystals depends, above all, on the experimental conditions. It is possible to obtain complete orientation of one substance growing on another even when a considerable difference exists between the parameters of their flat networks.

2. The percentage orientation does not change gradually, but abruptly, close to a limiting value.

3. The drop in the value of the "limiting" supercooling is due to the reduction in the relative difference between the parameters of the two flat networks concerned, which in its turn affects the probability of the appearance of crystal growth nuclei.

The author is grateful to V.A. Frank-Kamenetskii for his guidance in this investigation.

LITERATURE CITED

1. D.E. Ovsienko, "The crystallization kinetics of NaCl and NaBr solutions on galena surfaces," Vopr. Fiz. Metal. i metalloved., No.4 (1953).
2. K.P. Yanulov, "The law of epitaxial growth limits," DAN SSSR, 62 (1948).
3. R.S. Bradley, "Experiments on the range of surface forces," Z. Krist., 1, 96 (1937).
4. L. Frankenheim, "Über die Verbindung verschiedenartiger Kristalle," Ann. Phys. Chemie, 37, 520 (1836).
5. M.L. Royer, "Recherches experimentales sur l'epitaxie ou orientation mutuelle des cristaux des espèces differentes," Bull. Soc. Franc. Min., 51, 7-159 (1928).

A SIMPLE METHOD OF OBSERVING A PHASE TRANSITION IN QUARTZ SINGLE CRYSTALS

V. G. Zubov

M. V. Lomonosov State University, Moscow

Translated from Kristallografiya, Vol. 1, No. 2,
pp. 243-245, March-April, 1956
Original article submitted January 24, 1956

It is well known that α- and β-quartz, in the immediate vicinity of the phase transition point, have a rapid temperature variation of the index of refraction. Consequently, if the phase transition is not completed simultaneously throughout the entire volume of the crystal, but is gradually propagated from several centers of formation of the new phase, under certain conditions it is evidently possible to observe an intense and almost regular reflection of light at the α- and β-phase boundaries, and a redistribution of light in regions adjacent to these boundaries.

This circumstance has been used for carrying out the following simple method of observing the entire process of phase transition in large single crystals of quartz.

The quartz specimens, in the form of cubes with the linear dimensions 20-25 mm, were placed in a parallel beam of light, as shown in Fig. 1. In Fig. 1, A is a light source, B a condenser, C a circular point diaphragm, D a collimator lens, E a cylindrical vacuum furnace, F the specimen, and K a screen or photographic plate.

With such an arrangement, the shadow image of the specimen, shown in Fig. 2a, was obtained on the screen.

The furnace construction ensured uniformity of the temperature field, necessary for accomplishing a phase transition in large quartz specimens without damaging them. Slight temperature gradients of the order of 0.1-0.2°C/cm in the cross section of the furnace enabled phase transition fronts to be obtained parallel to the light rays.

The apparatus was used for following the phase transition processes in a free crystal, in a crystal exposed to the action of a strong dc field, and also in a high-frequency field. The entire phase transition was photographed on a motion picture film.

Figure 2b shows the occurrence of centers of formation of α-quartz in a single crystal of high-temperature β-quartz. When a center of the new phase was formed, temperature redistribution occurred in its immediate vicinity and large gradients of the indices of refraction were produced, resulting in distortion of the outline of the shadow of the specimen, a redistribution of the light flux, and the appearance of a dark area around the place of formation of the new phase. The center of formation of the new phase itself was revealed in the photograph (Fig. 2b) in the form of a bright spot. The centers produced on the lateral boundaries were concealed by the mounting and are not visible. Their presence may be judged only by the distortions of the contour and the occurrence of a dark region.

In Figs. 2c-2l are shown the photographs of different successive stages of development and movement of the phase transition fronts. The contours of the part of the front which is almost parallel to the light rays are revealed in the form of a bright line in the photograph.

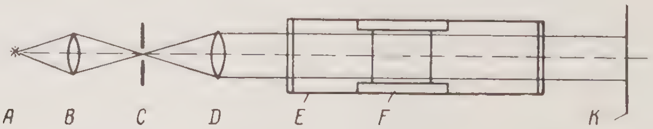

Fig. 1.

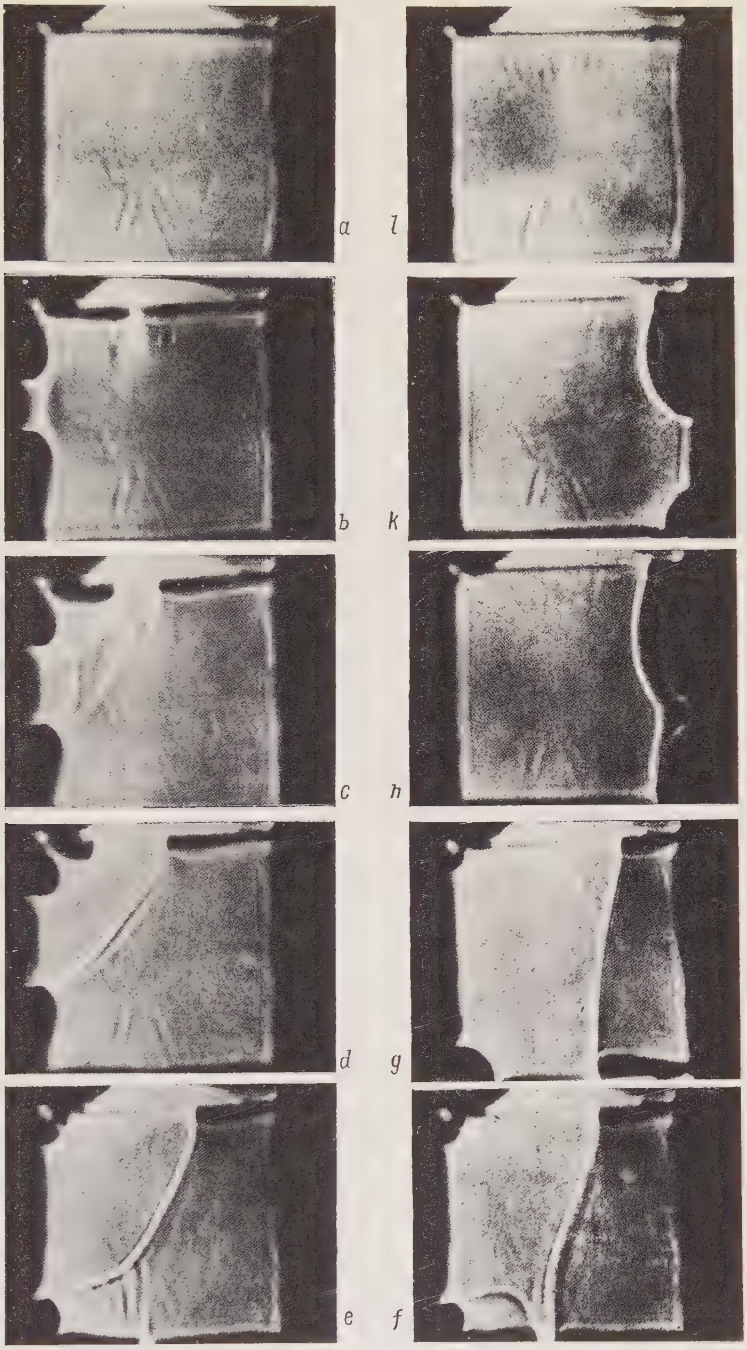

Fig. 2.

Observation of the character of movement of the front showed that the sites of origin of the centers of formation of the new phase were determined entirely by the temperature field of the furnace. The time required for the complete accomplishment of the phase transition was determined by the rate of supply of heat to the specimen, and could be indefinitely increased by the choice of suitable heat-supply conditions. In the case of slow conduct of the phase transition, the specimen retained its single-crystal structure even in repeated transitions, despite the fact that the formation of the new phase always commenced simultaneously at a number of points in the specimen. In the case of rapid transitions, of the order of 2-3 min, the specimens sometimes twinned. On approaching the phase-transition temperature, the boundaries of the twins were clearly observed in the form of thin bright lines. Distortion of the front of formation of the new phase occurred at the boundary of twins, and the passage of the front across a twin boundary appeared to be difficult. The velocities of the front were different in different stages. A sharp increase in velocity was observed at moments preceding the joining together of a number of fronts.

In the case of sufficiently uniform external temperature field and slow heat supply, the form and direction of movement of the phase-transition fronts were determined basically by the character of anisotropy in thermal conductivity of the quartz. The patterns of development of the phase transition were different when observed along different crystallographic axes. For each of the axes, the character of these patterns remained the same in all the specimens.

If no twinning of the specimen occurred in the process of the $\alpha-\beta$ transition, the $\beta-\alpha$ transition repeated strictly all the stages of the first transition in the reverse order.

It should be mentioned that a number of rapidly moving dark bands were always formed in front of the phase-transition front.

The method described enables one to follow quite reliably not only the phase-transition process itself, but also the character of the variation of the temperature field in the specimen during phase transition, and it may be used in work on the exact determination of the phase-transition temperature.

SOVIET PHYSICS – CRYSTALLOGRAPHY VOL. 1, NO. 2 MAR.-APR., 1956

LETTER TO THE EDITORS

ON THE ABSENCE OF A DEFINITE CONNECTION BETWEEN THE HOMOLOGY OF THE EXTERNAL FORM OF CRYSTALS AND THAT OF THEIR OPTICAL INDICATRICES

A. V. Shubnikov

Institute of Crystallography, Academy of Sciences of the USSR

Translated from Kristallografiya, Vol. 1, No. 2,
pp. 246-247, March-April, 1956
Original article submitted February 14, 1956

In a recently published paper by V.I. Mikheev [1], it was asserted that we, as it were, "had expressed the opinion that the phenomenon of the dispersion of the optical indicatrix... was incompatible with the homology of crystals." In fact, in our earlier papers on homology [2,3,4], we denied the possibility of a definite connection between the homology of the external form of crystals and that of the indicatrices of their physical properties, in particular, their optical indicatrices. Considered individually, the external form and optical indicatrices can and do possess properties of homology, but not a single operation of form homology (apart from those simultaneously constituting symmetry operations) enters into the group of operations for the homology of the optical indicatrices.

As we see it, our actual opinions and those ascribed to us do not quite coincide. This, however, is not the point.

In the paper cited, V.I. Mikheev tries to refute our assertion in the following way. He takes a polyhedron of the tetragonal system with an optical indicatrix for two wavelengths inscribed in it (the indicatrix is laid out quite incorrectly, but this is not important in the present case). He then subjects this model of a tetragonal crystal to extension along some direction and finds, as we should expect, a model of a monoclinic crystal possessing the properties of homology which he (the author) wished to obtain. In this discussion, however, V.I. Mikheev makes the great mistake of arbitrarily assuming that the particular deformation (in this case, extension) whereby the tetragonal form of the crystal may be imagined to be converted into monoclinic and the deformations whereby the optical indicatrices of the tetragonal crystal are simultaneously transformed into indicatrices of a monoclinic crystal are one and the same. It is in fact quite well known that these deformations cannot be identical.

If we take V.I. Mikheev's point of view, then we deduce that, on subjecting crystals of the cubic system to uniform elastic compression along one of the normals to the cube and octahedral faces, the crystals must necessarily acquire optical properties of a uniaxial-negative crystal, since the spherical optical indicatrix of such crystals should under these circumstances always transform into an oblate ellipsoid of revolution. In fact, in such cases, as shown by direct experiment, very different results may be obtained. Rocksalt, for example, on compression along the normal to the (100), becomes optically uniaxial-negative, while sylvine under the same conditions becomes uniaxial-positive. On compression of fluorite along the normal to the (111), the crystal becomes optically uniaxial-positive, while under the same conditions sylvine becomes uniaxial-negative ([5], p. 481).

Analogous phenomena are found for crystals of all other systems, not only for mechanical, but also thermal deformation. If we are to be guided by V.I. Mikheev's views, then for all crystals of the cubic system the spherical optical indicatrix should expand uniformly in all directions on thermal expansion, i.e., the refractive index should increase. Actually, the thermal expansion of such crystals as rocksalt, sylvine, fluorite, and aluminum–potassium alum leads to a fall in refractive index, while in other crystals (diamond, zinc blende) under the same conditions the refractive index increases [5], p.451).

The lack of agreement between the thermal deformation of a crystal and that of its optical indicatrices is found not only for cubic crystals but for crystals of all systems. It is well known, for example, that, on heating, a calcite crystal expands along the optical axis and contracts in a perpendicular direction, whereas the optical indicatrix under the same conditions expands in both these directions ([5], p. 452).

V.I. Mikheev asserts that on elongation of a crystal its optical indicatrix should also expand, but then one can assert with equal justification that the Fresnel ellipsoid should do likewise. This, however, would contradict common sense, since the elongated indicatrix should correspond to an oblate Fresnel ellipsoid.

It is perfectly clear from our discussion that no definite connection exists or can exist between the homology of the external form of crystals and that of their optical properties.

In V.I. Mikheev's article one may also find a whole series of "errors" naively imposed upon us. For example, Mikheev asserts that we ascribe some "spherical indicatrix of electric charge distribution" to a monoclinic crystal. In fact, in our earlier paper [3] we were considering not the spherical indicatrix, but a sphere ground out of a crystal. Our other "errors" are of the same nature. There is no need to discuss them.

LITERATURE CITED

1. V.I. Mikheev, "Possible connection between the dispersion of the disposition of optical indicatrices and the homology of crystals," Zap. Min. Obshch., Part 84, 170 (1955).
2. A.V. Shubnikov, "On the so-called homology of crystals," DAN SSSR, 83, 453 (1953).
3. A.V. Shubnikov, "What the homology of crystals is," Tr. Inst. Kristallogr., 9, 35 (1954).
4. A.V. Shubnikov, "On the absence of a definite connection between the homology of the external form of crystals and that of the indicatrices of their physical properties," Zap. Min. Obshch., Part 84, 121 (1955).
5. F. Pockels, Lehrbuch der Kristalloptik, pp. 451, 452, 481.

REVIEW

APPLICATION OF COMPUTERS TO X-RAY STRUCTURAL CALCULATIONS

M. A. Porai-Koshits

N.S. Kurnakov Institute of General and Inorganic Chemistry

Translated from Kristallografiya, Vol. 1, No. 2,
pp. 248-263, March-April, 1956
Original article submitted November 9, 1955

I. The mechanization of computing processes in x-ray structural analysis is one of the most pressing problems in x-ray instrument making. Naturally, the main subjects for mechanization are those calculations which are most laborious to execute, most urgently required, and most standard in form. In the field of x-ray structural analysis, this category, above all, includes the solution of problems arising in the study of atomic structure in crystals of complex composition.

Three main factors govern the difficulty of structural investigations: (1) the so-called "initial-phase problem" (the absence of any direct experimental data on the phases of diffracted rays); (2) the duration of the experiment and the preliminary analysis of experimental data; (3) the difficulty of the computing operations involved in the determination of atomic coordinates.

The statistical method of determining the coordinates of atoms, developed and successfully applied in recent years (especially in the Soviet Union), solves the first (and most basic) of these difficulties, at least as far as centrosymmetrical crystals are concerned. The construction of diffraction cameras with ionization recording of the rays and automatic adjustment of the crystal and receiver makes the actual experiment much faster. Mechanization of the main computing processes solves the third problem. Taking all together, we may well expect soon to witness a radical change both in the speed and volume of structural investigations, and hence also in the very position of x-ray structural analysis in relation to fields of science constituting the "clientele" of structural studies, chemistry, geology, physics, biology, etc. The hundredfold increase in the speed of calculations achieved with the help of electronic computers constitutes a powerful stimulus to reinforced efforts toward the perfection of experiment and the development of methods of structural investigation. It is thus clear that the maximum acceleration of computing operations in the analysis of crystals, complex in structure, is important in principle as well as technologically.

II. The main computing problems in the field of atomic structural analysis are the following.

1. Finding the distribution of electron density over the cell (or the interatomic function in interatomic vector space), i.e., summing the two- and three-dimensional Fourier series, in general of the type

$$\rho(xyz) = \frac{1}{V} \sum_{hkl \atop -\infty}^{\infty} \{F_A(hkl) \cos 2\pi(hx + ky + lz)$$

$$+ F_B(hkl) \sin 2\pi(hx + ky + lz)\}.$$

2. Calculating the structure amplitudes (or unitary structure amplitudes) of the diffracted rays from the coordinates of the atoms and the atomic amplitudes (per-unit coefficients), i.e., calculating a sum of type

$$F_A(hkl) = \sum_{j=1}^{N} f_j \cos 2\pi(hx_j + ky_j + lz_j),$$

$$F_B(hkl) = \sum_{j=1}^{N} f_j \sin 2\pi(hx_j + ky_j + lz_j).$$

3. Refining the coordinates of the atoms by successive approximations to the electron-density distribution and the initial phases of the reflections. The most convenient form of this refinement is the method of differential synthesis, at each stage of approximation requiring the solution of the system of equations:

$$A_{hh}\,\Delta x + A_{hk}\,\Delta y + A_{hl}\,\Delta z + A_h = 0,$$
$$A_{hk}\,\Delta x + A_{kk}\,\Delta y + A_{kl}\,\Delta z + A_k = 0,$$
$$A_{hl}\,\Delta x + A_{kl}\,\Delta y + A_{ll}\,\Delta z + A_l = 0,$$

where Δx, Δy, Δz are unknown corrections to the coordinates, and A_h, A_{hh}, A_{hk}, etc., are Fourier expansions of the corresponding derivatives of electron density at a point corresponding to the original coordinates of the atoms:

$$A_h = \left(\frac{\partial\rho}{\partial x}\right)_{x_j y_j z_j}, \quad A_{hh} = \left(\frac{\partial^2\rho}{\partial x^2}\right)_{x_j y_j z_j},$$

$$A_{hk} = \left(\frac{\partial^2\rho}{\partial x\,\partial y}\right)_{x_j y_j z_j}, \text{ etc.}$$

4. Determining the signs of the structure amplitudes in a centrosymmetric crystal by the statistical method. In the simplest form, this problem reduces to the setting up of all possible combinations of reflections hkl, $h'k'l'$ and $h+h'$, $k+k'$, $l+l'$ belonging to a group of strong reflections, then to a wider group of strong and medium, and, finally, to all reflections including the weak (but of course existing) ones.

In its more complex setting, this problem includes the calculation of the probability of satisfying the sign relationship $s(hkl) \cdot s(h'k'l') = s(h+h', k+k', l+l')$, where s is a symbol for the sign of the structure amplitude, i.e., +1 or −1.

5. Calculating the quadratic form, i.e., finding $1/d^2$ or $(\sin\vartheta/\lambda)^2$ from the lattice parameters and diffraction indices. In the general case, the problem reduces to solving the equation

$$Q_{hkl} = Ah^2 + Bk^2 + Cl^2 + Dhk + Ehl + Fkl$$

for all necessary combinations of hkl.

In recent years, a great deal of attention has been paid abroad to mechanization of the main computing operations of structural analysis. Many machines and mechanisms have been developed for solving the first three of the problems just listed. The largest laboratories have in some way or other been provided with the necessary computing devices.

In the Soviet Union, also, considerable work has been done on constructing computers for structural analysis. At a conference on the use of computing techniques called by the Commission for X-Ray Diffraction at the Institute of Crystallography, Academy of Sciences of the USSR in Moscow, on April 14-15, 1955, six contributions were devoted to the construction of computers, either in service or being developed.

III. Before passing on to a description of various types of machines, it is useful to give some classification as regards their main features.

All machines may be roughly divided into two groups: on the one hand, none-too-complex specialized machines intended for use universally in x-ray and crystallographic laboratories (these we shall subsequently call "laboratory" machines) and, on the other hand, high-speed (specialized or universal) machines, automating the computing processes to the highest possible degree, and intended mainly for large computing centers.

It must be emphasized that machines of the first type will answer their purpose only on satisfying certain conditions as regards dimensions, cost, and simplicity of servicing, and machines of the second type are conditioned by the accessibility of the computing center for systematic and "inertia-free" fulfillment of the demands of the structural laboratories.

In principle, the operation of all computing machines may be divided into two groups: (1) continuous-action machines or analog computers, in which the computing operations are imitated by certain physical processes, and, (2), discrete-action machines (i.e., finally, digital computers).

Analog machines may be used on mechanical motion, electrical, electromagnetic, optical, and other processes. Present-day digital machines may be separated into four main groups: purely mechanical, electromagnetic pulse, electronic, and magnetic machines.

Analog machines are in all cases specialized, intended for the solution of definite particular problems; digital machines may be either specialized or universal.

Below are listed the main types of computers applicable to structural analysis. The letter L indicates laboratory types and LS denotes large-scale machines.

Machines acting continuously:

1. Mechanical (L)
2. Electrical (L)
3. Optical:
    - fly's eye (L)
    - x-ray microscope (L)
    - photo-adder (L)
4. Electronic Pepinsky (LS)

Discrete-action machines:

1. Mechanical (L)
2. Electromagnetic:
    - specialized (L, LS)
    - universal (LS)
3. Electronic:
    - specialized (LS)
    - universal (LS)
4. Magnetic:
    - specialized (LS, L)
    - universal (LS)

Continuous-acting machines are mainly of the laboratory type. An exception is the electronic machine of Pepinsky. Discrete-action machines, apart from mechanical, are mainly large scale. Specialized electromagnetic machines may be considered as intermediate between laboratory and large-scale (see below); in the field of magnetic specialized machines we may expect the creation of laboratory-only desk computers (see below).

IV. The least perfect, until recently, were the purely mechanical continuous-action machines. Quite a number of mechanisms simple in principle have been proposed ("hand" machines) both for calculating structure amplitudes and for summing series. The first group includes the machines of Evans and Peiser [1], Cox,[1] Booth [3], Bragg [4], Vand [5], and Clastre and Gay [6]. The main failing in all these machines is evidently the slowness of the computing process, associated either with the fact that calculations are made for each reflection separately and often even for each term in a summation one after the other, or else with the fact that the initial parameters are given in too complex or inconvenient a form. Another failing in most of the machines mentioned is their low accuracy.

Mechanical computers for summing Fourier series have failings of a somewhat analogous kind; these include those of Brown and Wheeler [7], Robertson [8], Shilton [9], McLachlan and Champaygne [10], Rose [11], Vand [12], and Beevers and Robertson [13].

In all probability, however, the failings of the mechanical computers (constructional rather than matters of principle) can be overcome. Purely mechanical or electromechanical machines also have a number of advantages over any others as regards reliability of operation, compactness, and possibly cost.

Deserving of attention is the general idea of Booth's second machine, which solves the problem of calculating structure amplitudes completely and simultaneously with respect to all the terms of the summation (described in Booth's monograph [14]), and Robertson's discrete-action machine for the summation of series which, judging from a short communication [15], constitutes an arithmometer, an analog of the ordinary method of strips. The machine accelerates the work by roughly a factor of ten, with a considerable increase in accuracy. The details of its construction have not yet been described.

V. Among the constructionally simplest, high-speed, compact, and inexpensive systems for finding two-dimensional electron-density distributions in two-dimensional assemblies of structure amplitudes F_{hk} are those based on an optical analogy.

The optical analogy enables either the direct or the inverse Fourier transformation to be made at will (the crystal cell transforming into a distribution of structure amplitudes in reciprocal space or, conversely, the reciprocal lattice into a distribution of density in the crystal cell).

The following systems described in the literature (especially in a series of monographs [16,17] and also Eller's review [18]) are well known: (1) an apparatus for finding structure amplitudes based on the method of modeling the projection of the structure (fly's eye); (2) a machine of the "x-ray microscope" type solving the inverse problem, i.e., transforming a two-dimensional reciprocal lattice into a density distribution; (3) a photographic device for summing Fourier series acting on the principle of the superposition of sinusoidal black–white two-dimensional distributions on the same photographic plate.

Among this group of machines, we must give more detailed attention to that of Eller, belonging to the third group and manufactured in France by the Baudouin company [19]. The principle of action is shown in Fig. 1: S is a linear light source, A a screen with vertical "columns" of sinusoidally varying blackening, and P a photographic plate. Variation in the orientation of the sinusoidal waves representing the individual terms of the Fourier series is achieved by rotating the photographic plate in its own plane, variation in the frequency of the waves by moving the screen A toward or away from the photographic plate, variation in the initial phase of the wave by moving the screen A in a horizontal direction in its own plane. A general view of the machine is given in Fig. 2. A cassette with photo-

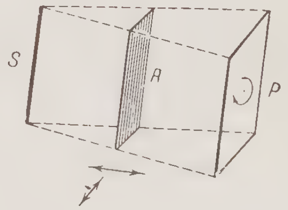

Fig. 1. Principle of construction of the photographic device of Eller.

---

[1] Described in Booth's monograph [2].

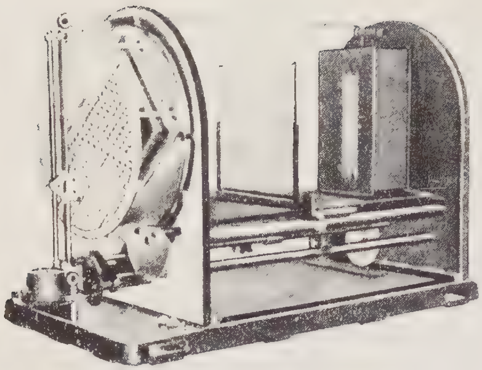

Fig. 2. Eller's machine.

graphic plate P is rigidly connected to a disk to which is attached a graphical representation of the reciprocal lattice network; the screen S is connected by a system of blocks to an indicator which can move along a vertical rod situated in front of the reciprocal lattice network. On rotating the disk with the network, the orientation of the cassette changes; on moving the indicator along the rod, so does the screen–cassette distance. The adjustment of the apparatus consists of two operations: (1) a reciprocal lattice point is brought onto the vertical diameter of the disk, (2) the indicator is set opposite to the point. The first operation gives the orientation of the sinusoidal distribution, and the second its frequency. Thus, the adjustment process in the apparatus is extremely simple.

The projection is obtained on a photographic plate 17 × 23 cm in size, and the indices of the terms being summed may lie between 0 and 100. The time needed for a complete projection with 100 coefficients of the series is 30 min.

The machine has very varied applications. Apart from the calculation of ordinary and various kinds of complex projections (in particular the minimalized projection of Burger [20]), it can be used to give pictures of the Fourier transformations of any system of points, the values of structure amplitudes [21], and even to solve the problem of the refinement of coordinates by the method of differential series [22].

The rapidity of obtaining results, together with simplicity of equipment, is the main advantage of the photographic method. A failing is its low accuracy, difficulty of assigning numerical characteristics to the results obtained and, in all probability, insufficient sensitivity when the structure contains atoms with sharply differing scattering powers. The use of optical machines is apparently most widespread in France and Italy [23,24,25]. In the Soviet Union, unfortunately, hardly anyone has been engaged in the construction of optical computing systems. Only by V.A. Shamburov at the Institute of Crystallography, Academy of Sciences of the USSR, have any developments been made. At the Institute of the Chemistry of Silicates, a machine acting on a similar principle has been made for the solution of rather different problems.

VI. Certain electrical and electromagnetic machines acting on the analog principle are described in the literature. Except for the machine of Maxwell [26], all the rest are very similar in concept and differ mainly in constructional details (Rymer and Butler [27], Hägg and Laurent [28], Beevers and McEvan [29], Ramsay, Lipson, and Rogers [30], and Azároff [31]). In all the machines listed, which are intended for summing one-dimensional Fourier series, the values of the trigonometric function are obtained by the sinusoidal subdivision of resistances or transformers (voltage taken off $\cos 2\pi x$ or $\sin 2\pi x$); multiplication by F_h is effected by potentiometric variation of the voltage, and summation by the addition of currents or voltages in corresponding circuits.

Machines of this type are mechanized analogs of Robertson's method of strips, since the electrical circuits only give the function $F \cos 2\pi x$ directly at certain points: $x = 1/n,\ 2/n,\ 3/n \ldots h/4n \ldots$ Transformation from $F \cos 2\pi x$ to $F \cos 2\pi hx$ is effected by a corresponding change in the order of connecting the sections to the commutation panels. Each coil (or resistance) is joined to its own panel, and the order of connecting its sections corresponds to a definite h (for example, for $h = 2$, the zeroth, second, fourth, etc. sections are connected one after the other). Passage from one terminal to the next in turn is effected simultaneously and automatically on all the panels by means of the standard walking mechanism of a telephone apparatus. In this way, currents (or voltages) corresponding to $F_h \cos 2\pi hx$ for various h and given x are summed in a common circuit.

The group of electrical analog machines for summing one-dimensional Fourier series includes one developed by engineers A.L. Dvorkin and E.G. Lipshtein for the X-Ray Laboratory of the INEOS, Academy of Sciences of the USSR. In this machine, the coefficients of the series are introduced by means of telephone dials; the maximum h index is 24, and the period is divided into 96 parts. The introduction time for calculating a one-dimensional series is a minimum of 5 min, while operation and calculation of the results takes 15 min. Corresponding to this, calculation of a two-dimensional series, in the simplest case of a projection with two lines of symmetry, with separation into 48 × 48 parts and 100 coefficients, requires approximately 10 h which, generally speaking, is only a little less than the time required to make an analogous calculation by the hand method of strips. Undoubtedly, a change in the system of assigning the initial data and the attachment of a printing device at the output will enable the operating time to be reduced at least by a factor of two.

VII. The second group of computers applicable to x-ray structural analysis is made up of automatic systems which, according to their fundamental parameters (rapidity of action, scale, complexity of servicing, and cost), are certainly intended only for the largest structural laboratories or computing centers. Before passing on to a description of individual types of machines, it is appropriate to discourse on some general principles of their construction [32-37].

All these machines are of the pulse type: each single-digit number is assigned in the form of a corresponding number of electrical impulses passing successively through the circuit. The main operating units of the machines are automatic relays. Each relay can exist in two states, excited and quiescent, depending on whether it has received an impulse or not. Corresponding to this relay, an output circuit (or several of these) closes or opens and hence either directs pulses or prevents their direction into other parts of the machine. Thus, each relay fulfills a definite logical operation, answering the question "yes" or "no" and conveying this reply further.

The relays of automatic machines are joined in individual groups or registers, playing the part of receivers or stores for the numbers. A number of pulses falling on a group of relays connected into a register bring it into a definite state "imaging" the corresponding digit. The single-digit registers are connected into groups for representing multidigit numbers. The connection is effected in such a way that, on completing a full "ten" in one register, a single pulse is developed and sent into the register of the following digit, all the units of the first register returning to the zero state.

Clearly, questions of economy in the number of relays frequently compel one to change from the ordinary "scale-of-ten" to other systems. The most suitable (though not most economical) is the binary system of counting, which is widely used, especially in electronic machines; in this, each "ten" contains only two digits, 0 and 1, and hence requires only one relay (having two states).

The successive direction of two groups of pulses into the same counters leads to the addition (or, if desired, subtraction) of the numbers applied to them. The pulses stored by the counters may be "held" in them for as long as required. In this respect, the counters play the part of memory cells. By feeding in a special group of pulses equal to a whole number of tens, hundreds, etc., the number stored in the counter may be taken from it and passed to any other counter.

The memory may be either temporary or permanent, i.e., the counter can be cleared after operation, or the stored number can be preserved indefinitely. In machines intended for structural analysis, the permanent "memory" cells are used to establish the values of the trigonometric functions.

Thus, the counters may be used for logical operations, arithmetical operations, or as memory cells. Hence, the machine can carry out any instructions in an assigned sequence. The problem consists only in decomposing a complex procedure into simple acts and in setting up a program of operations most suited to a machine of the particular type.

The introduction of numbers into a computer is usually effected by means of punched cards or tapes.

On passing the cards (tapes) through the machine, electrical contact is made only in places where there is a perforation, so that the corresponding circuit is closed and the right number of pulses is fed into the machine.

As regards the physical principles of the operation of the basic elements (relays), all impulse machines can be divided into three types: electromagnetic, electronic, and magnetic. In the first, the instructions of the operator are carried out by electromagnetic relays opening or closing certain contacts; in the second, switching in the circuits is effected by feeding pulses to a network of electronic tubes connected in smallish groups (the so-called trigger circuits); in the third, the same operation is effected by changing the magnetic state of a certain magnetic element. Since the operation of electromagnetic relays is associated with mechanical motion, while that of electronic and magnetic devices involves merely a change of field, the computing speeds are very different. In electromagnetic machines, the elementary operation takes fractions of a second, and in electronic machines fractions of a microsecond.

The memorizing of numbers in pulse counters demands a very large number of relays. Hence, electronic machines use other means of memorizing; these are also based on electronic processes (cathode-ray tubes or mercury delay lines) and have a large capacity, together with a rapidity of action adequate to the computing speed of the electronic machine. In order to increase the memory of electronic machines further, recording can be made on magnetic tapes or drums.

Electromagnetic machines do not have this kind of memory structure. Hence, their capabilities are comparatively limited. Extra memory devices can be provided in the form of punched cards, punched by the machine itself at intermediate stages of the calculation.

The transfer of such cards into the input device of the machine, however, demands the intervention of an operator, so that the whole process of calculation is split into several stages and cannot be fully automated.

VIII. Universal electromagnetic computers are known under the name of computer-analyzers. The genus of computer-analyzers includes not only the fundamental counting mechanisms or tabulators, but also a whole series of auxiliary devices: punchers, reproducers, controllers, sorting machines, and multipliers.

The first paper on the application of computer-analyzers to x-ray structural investigations was published in 1946 (Shaffer, Schomaker, and Pauling [38]), and further progress in computing processes was made, mainly in the United States and England, in 1946 to 1953 [39,40].

A general advantage of computer-analyzers is the possibility of using them for solving all three fundamental problems of structure analysis: the summation of Fourier series, the calculation of structure amplitudes, and the calculation of differential series for improving the coordinates.

The simplest method of calculating Fourier series on computer-analyzers reduces in essence to the mechanization of the Beevers – Lipson strip summation. Each strip is replaced by a punched card containing the same data. Selection of the punched cards from the whole pack, their restacking, and the checking for correctness of choice are effected by hand. The tabulator only carries out the operation of adding the one-dimensional series. Two-dimensional and three-dimensional syntheses reduce to the successive calculation of one-dimensional series. In the Crystallographic Laboratory of Cambridge University, a block of punched-card strips has been prepared; this provides for the separation of a period into 120 parts and contains values of F_h with two significant figures, and values of $F_h \cos 2\pi hx$ with four. The pack contains 2460 different cards and, in all, including the necessary number of duplicates, 18,860 cards, disposed in eight boxes 60 × 19 × 10 cm in size.

According to the data of this laboratory [40], for the calculation of a two-dimensional series containing 200 terms, with division of a centrosymmetric cell into 60 × 60 parts, seven hours (for two operators) are required, i.e., roughly 7 sec per point; in calculating a three-dimensional series of 1000 terms some 50 sec per point are needed.

This computing speed is quite inadequate for the systematic calculation of three-dimensional distributions. An advantage of this very simple method, however, is that it requires only one basic machine, the tabulator, which considerably broadens the practical possibility of setting up calculations and even the direct acquisition by the structural laboratory of a ready-made machine, requiring no new development.

Analysis shows that more than half the time required for calculating a series by the method described goes into the hand selection of the punched cards and their return to the pack, and also into the checking for correct choice. Other, more complex methods of using computer-analyzers make it possible to shorten this time substantially, and simultaneously to reduce the required number of cards. In this case, however, practically the whole gamut of machines is required: puncher, controller, reproducer, multiplier, and sorting machine. Hence, the calculations can only be made in a computing center.

For the calculation of structure amplitudes and the refinement of structures by differential synthesis, the whole set of machines is required in all cases, the procedure for their use being quite complex and split into several stages.

Despite the fact that the application of computer-analyzers to problems of structure analysis has become quite widespread in the United States, and especially in England, the method as a whole cannot be regarded as entirely satisfactory. Its chief disadvantages are: (1) relatively low gain in time (completely insufficient for three-dimensional calculations); (2) the need for a qualified operator (qualified as regards structural analysis) working in a general-purpose computing center; (3) insufficient automation of the calculation for the complexity of its procedure, bringing with it the possibility of operator error.

The method could be considerably improved by supplementing the computer-analyzer with electronic control for the sequence of operations.

IX. Considerably more successful in the solution of structural questions are specialized electromagnetic-impulse machines, made up mainly of standard parts from computer-analyzers and telephone apparatus.

In the Soviet Union, a machine of this type is being developed in the Physics Faculty of Moscow State University (under Professor A. N. Tikhonov and Engineers B. V. Sokolov and A. V. Luk'yanov). The machine is intended to sum Fourier series. The main unit of the machine (making it specialized) is a set of a special kind of electrical strips or permanent memory cells storing values of the trigonometric functions for the first four periods.

The second important element specializing the machine is a set of telephone walking mechanisms effecting simultaneous switching on the commutation panels and transforming functions $\cos 2\pi x$ into $\cos 2\pi hx$.

The coefficients of the series are given in the form of four-figure numbers. The period is divided into 48 parts, the maximum index being 48. The authors estimate the machine time for calculating a one-dimensional series as 2 min, the time for putting out in the form of punched cards 1.5 min, and the printing time, 2 min. Thus, the total time is of the order of 3.5 to 4 min, which means that a two-dimensional series (given in the form

$$\sum_{hk} F_{hk} \cos 2\pi\, hx \cos 2\pi ky)$$

could be calculated in approximately 50 to 70 min. To this we must add the time for preparing the punched cards with the F_{hk} coefficients. Since a series consisting of 100 terms requires in all 10 to 20 punched cards, this time is in general insignificant (a trained operator can punch 250 cards per hour).

The whole machine consists of puncher, reading mechanism, main computing mechanism, automatic puncher, and printing system.

The machine as a whole is to be considered as intermediate between a laboratory-only machine and one belonging to a computing center. In this lies its main defect. For a laboratory-only machine it is too cumbersome, and probably too expensive; in relation to machines of the second type, it is insufficiently versatile (solving only one problem), and gives altogether too low a computing speed. Further development of the machine is to be desired, since the general advantage of electromagnetic over electronic computers is in reliability of operation, lower cost, and relative simplicity of servicing. Improvements should be directed toward increasing the field of problems which the machine can solve, and also the computing speed. There are certainly possibilities in this direction, as can be seen from the example of another specialized impulse machine constructed by Beck and Cormarie in France, using more fully the operating principles of automatic telephone exchanges. The machine simultaneously gives the values of ρ(xyz) at all (64) points x for given values of y and z.

X. For all their advantage in reliability of operation, relative simplicity of servicing, and relative cheapness, electromagnetic computers cannot emulate electronic types in computing speed and flexibility in setting up problems.

All the demands of the most laborious and variegated structural calculations can be completely met, given the existence of a universal high-speed electronic computer running continuously and accessible for the customers of the computing center.

Much has been said of the applications of universal electronic computers [50-58], in particular in contributions to the International Congress of Crystallographers in Paris in 1954 [54-57]. The possibilities of electronic machines may be judged from the data presented by Cruikshank [57]: for a total machine time of 290 h, the Manchester University machine made calculations for 18 structures, including 56 calculations of structure amplitudes and 50 differential syntheses.

The application of a universal electronic computer for solving structural problems in Moscow was effected by Fellow of the Faculty of Computer Mathematics, Moscow State University, N. P. Trifonov (Faculty Head Academician S. L. Sobolev) in collaboration with others of the Crystallochemical Laboratory, Institute of General and Inorganic Chemistry, Academy of Sciences of the USSR.

The main preparatory work connected with the setting up of structural problems on the universal electronic computer is the programming of the problem, i.e., finding the most convenient and economical sequence of operations and writing this in the form of coded machine orders. Programming must take into account not only the possible economy in machine time, but also the loading of the machine "memory," the control of calculations at various stages, and the suitability of the setting up of the problem in view of its possible modification or complication at later stages, etc.

N. P. Trifonov set up and solved the following problems: (1) calculation of structure amplitudes from "trial" coordinates of the atoms and atomic factors; (2) calculation of electron-density distributions; (3) linking the two problems into a single cycle to be carried out automatically, i.e., finding F_{calc} from x_j, y_j, z_j, and f_j, transferring the sign of F_{calc} (or in general the initial phase D_{calc}) to the experimental F_{exp}, and calculating the electron-density distribution; (4) refining the coordinates of the atoms by the method of differential synthesis, uniting all the successive-approximation cycles into a single automatically executed process.

With respect to the two-dimensional problem, programs were created for all plane symmetry groups; with respect to the three-dimensional problem this was done for space groups C_{2h}^5 and D_{2h}^{16}. The programming of the problem for the other space groups, however, does not now present any technical difficulties.

Let us consider a few details.

1. The calculation of structure amplitudes is effected with allowance for the dependence of the atomic factors on the hkl indices. The atomic factors are given to the machine in the form of a table of values of f_j as a function of $\sin\vartheta/\lambda$ with a 0.1 interval in $\sin\vartheta/\lambda$. The machine is also given the parameters of the quadratic form $(\sin\vartheta/\lambda)^2 = Ah^2 + Bk^2 + Cl^2 + Dhk + Ehl + Fkl$, and it calculates $\sin\vartheta/\lambda$ for each hkl reflection and then finds the value of $f_j(hkl)$ by interpolation of the tabulated data. Thus, another problem of independent interest is solved in passing: the calculation of the quadratic form.

2. In the calculations of electron-density distributions made on the machine, the period was divided into 60 parts. In principle, however, the electronic machine, not being connected with strips, can just as easily effect division into arbitrary parts, and in practice the most convenient are hundredths of the period.

3. The solution of problems on the universal machine is so flexible that it permits any auxiliary calculations to be included at will. Thus, at any stage in the refinement of coordinates by the method of differential synthesis one has the possibility of switching in a program for calculating the whole electron-density distribution in order to inspect the general picture. It is possible to include in the process of successive refinements not all, but only some of the atoms, leaving the coordinates of the rest unchanged or disregarding them entirely, only including them in the general process at some intermediate stage, when the process of refinement has reached the required level (this operation does not require a halt in the operation of the machine).

The machine solves in passing the problem of comparing F_{calc} and F_{exp}, and reducing F_{exp} to the absolute scale.

At the concluding stage, a calculation is made for the "theoretical series" in order to find the correction for the breaking off [of the series] (Booth) and to calculate the functions $\Sigma_{hkl}\, h\,(F_{exch} - F_{calc})$, $\Sigma_{hkl}\, h^2\,(F_{exch} - F_{calc})$, etc., which are needed in order to estimate the accuracy of determination of the coordinates from the well-known computing formulas.

For the characteristics of the machine time necessary, it is most convenient to take specific examples.

In studying crystals of $Ni(NH_3)_3(SCN)_2$, a universal electronic computer was used to calculate the ordinary and weighted projections on the XY plane. For 250 independent hk0 reflections and a plane group of electron density pgg, calculation of the projection by the hand method of strips would require approximately 30 h. Roughly the same time would go into calculating the signs of the structure amplitudes from tables or nomograms. Thus, a single cycle of refinement by hand operation would require around 60 h. On this problem the universal electronic computer spends 50 min machine time if the programs for calculating the structure amplitudes and electron density are not connected together, and in all, 30 min on joining these into a single cycle (structure-amplitude values not printed). Use of the electronic machine, however, requires preliminary treatment of the initial data: transforming the data to the binary system and putting it on punched tape. Some 2 h are spent in this operation for a problem of the size in question. Furthermore, for nine independent atoms in the cell, not less than an hour is spent on interpolation calculations for finding the coordinates of the maxima. Hence, in all, the first cycle of refinement requires some three and a half hours. On using the method of differential synthesis, as a result of the curtailment of print-out operations, the machine time for one cycle of the present problem is reduced to 5 min. The elimination of the interpolation work and administrative operations in transferring the material for analysis to the laboratory after each cycle of refinement reduces the whole working time to simply that of the machines, plus the time required for preliminary preparation of the initial data. In the present problem, eight cycles of refinement were used, and these took the machine 40 min.

The whole calculation thus required 2 h 40 min instead of the 14 h needed when the F-series method was used in the same machine, or 480 h when using strips and nomograms.

The refinement of atomic coordinates in the Cs_2CoCl_4 structure was effected by the differential-synthesis method, applied to a three-dimensional density distribution. The number of independent hk*l* reflections was 950; the space group was D_{2h}^{16} = Pn*a*m. The number of structurally independent atoms was six. The computing time for one cycle was 30 min. Three cycles of refinement were needed in all. In an hour and a half, this gave results which would have called for months by the method of strips and at least a week on any of the other machines mentioned above.

Work on broadening the field of problems soluble on the universal machine is continuing. At the present time work is proceeding with the setting up of another of the most important structural problems: the choice of combinations of reflections hk*l*, h'k'*l*', h + h', k + k', *l* + *l*' for determining the signs of the structure amplitudes by the statistical method. The same problem has been set up in England by Cochran and Douglas [58], but the solution is very cumbersome and not entirely convincing. The setting up of the sign relationships on a different machine is also occupying a group of engineers associated with the x-ray laboratory of the INEOS, Academy of Sciences of the USSR.

It follows from this discussion that the use of universal electronic computers has great possibilities, especially with the continually changing demands of x-ray structural analysis, with the development of new methods of solving structural problems, and with modifications of old ones.

A fundamental failing in the use of universal electronic computers is the time occupied by the preparatory operations in setting the initial data and the final operations in printing the results, this being because the standard auxiliary apparatus of the universal machine used for these purposes cannot take account of the specifications of the problem (such as the fact that F_{exp} is given to two or at most three significant figures, and that the results, the coordinates of the atoms, require no more than three places of decimals).

In this respect, as in certain others, specialized discrete-action electronic computers should be more suitable. Specialization of the machine should substantially reduce its size and cost, and gain time mainly in the preparatory and final operations. The capabilities of such a machine will however fall significantly below those of the universal type. Machines of this type have evidently not been developed abroad.

In the Soviet Union, on the initiative of G. S. Zhdanov, it is proposed to construct a machine for solving three problems: finding the electron-density distribution in two-dimensional cross sections, finding F(hk*l*) for a given *l*, and calculating the quadratic form.

XI. Another type of specialized electronic machine is the Pepinsky X-RAC [59], an analog machine having in principle much in common with the photographic systems based on the superposition of two-dimensional sinusoidal distributions. The idea of the machine arose from considering the mechanism for the transmission of television signals: that of converting the picture into electrical signals and conversely, the signals into an image. Since the taking of a motionless image constitutes a periodically repeatable process, the electrical signal produced may be represented as a function of time in the form of a double Fourier series, and its transformation into an image on the screen as a translation of a function of time into a function of the coordinates of a point on the screen. The beam of an oscilloscope oscillates in two directions, vertical and horizontal, at constant frequencies ω_{vert} and ω_{horiz}, where $\omega_{horiz} \gg \omega_{vert}$. The unmodulated beam will trace out a continuous band on the screen of the cathode-ray tube; this moves along the horizontal and is displaced along the vertical.

If a modulated sinusoidal voltage at frequency $h\omega_{horiz}$ is applied to the grid of the CRT, the screen shows vertical bands (h bands over the width of the screen). If the frequency of the applied field equals $k\omega_{vert}$, horizontal bands develop (k bands over the height of the screen). On applying frequency $h\omega_{horiz} + k\omega_{vert}$, corresponding inclined bands are obtained. The contrast of these will depend on the amplitude of the applied field. Clearly, on applying a field equal to $\Sigma_{hk}F_{hk}\cos 2\pi \cdot (h\omega_{horiz} + k\omega_{vert})$, the oscilloscope screen will give an image of the electron-density distribution. Thus, the main problem lies in obtaining an electrical signal constituting the sum of a double Fourier series. This calls for the generation of the necessary set of frequencies in two ranges (low-frequency $k\omega_{vert}$ and high-frequency $h\omega_{horiz}$), the assignment of their amplitudes and initial phases, and then their superposition. In this review, the technical details of constructing such a complex machine cannot be given; the size would be very great and so, undoubtedly, would be the cost.

The combination of the basic X-RAC machine with the auxiliary system S-FAC [60] for calculating structure amplitudes [61] makes the Pepinsky machine certainly the most flexible of all the specialized machines. Such a machine can solve any structural problems, beginning with the summation of series and finishing with minimization of the interatomic function and the calculation of sign relationships.

At the same time, one cannot fail to note the economic unsuitability of manufacturing such a specialized machine. Its cost and servicing approach those of the universal machine; its functions are substantially narrower; it would be very problematical to ensure constancy of loading for the enormous operating speeds. One may well suppose that the correct way toward the coordinated solution of structural problems lies not in the creation of electronic machines such as the X-RAC, but in the development of specialized discrete-acting magnetic systems [63-65] which in the near future should compete substantially with electronic machines.

XII. The first communication regarding the application of a magnetic machine of the universal type, MAGYC, to the solution of structural-analysis problems was given by Booth at the Paris Congress [62].

The replacement of electronic trigger circuits by magnetic devices evidently enables the scale and cost of machines to be sharply reduced and the reliability of the work to be increased. Reducing the size and cost in turn makes it possible to raise the number of computing units and modify the general structure of the machine, i.e., to construct specialized machines having almost the same capabilities, as regards modification and broadening of the field of problems soluble, as those of a universal electronic computer.

It is also not excluded that table machines for the solution of the simplest structural problems (summation of one-dimensional series) will prove most compact, inexpensive, and reliable on using magnetic counting units. So far, however, there are no real data on this.

XIII. By comparing all the available data on computers for the structural analysis of crystals, we may draw the following conclusions.

1. As comparatively cheap and compact mechanisms, suitable for use in laboratory conditions, the most appropriate are: (a) purely mechanical machines for summing one-dimensional series; (b) an optical machine of the Eller type for rapid (but not exact) calculation of two-dimensional density distributions and for computing structure amplitudes.

2. For the solution of complex problems of structural analysis, it is appropriate either to use universal electronic machines in a general-purpose computing center, or to create specialized but fairly versatile machines for the structure-computing center, based on electronic trigger circuits or magnetic counting units.

LITERATURE CITED

I. Mechanical Systems

1. R.C. Evans and H.S. Peiser, "A machine for the computation of structure factors," Proc. Phys. Soc., 54, 457 (1942).
2. A.D. Booth, Fourier Technique in X-Ray Organic Structure Analysis (1948), p. 67.
3. A.D. Booth, "Two calculating machines for x-ray crystal structure analysis," J. Appl. Phys. 18, 664 (1947).
4. W. L. Bragg, "A device for calculating structure factors," Acta Cryst., 5, 4, 474 (1952).
5. V. Vand, "A simple mechanical structure-factor computing aid," Acta Cryst., 5, 3, 390 (1952).
6. L. Clastre and R. Gay, "Machine a calculer les facteurs de structure," Acta Cryst., 7, 10, 623 (1954).
7. S. L. Brown and L. L. Wheeler, "The use of a mechanical synthesizer to solve trigonometric equations," J. Appl. Phys., 14, 30 (1943).
8. M. J. Robertson, "A simple harmonic continuous calculating machine," Phil. Mag., 13, 413 (1932).
9. A. Shilton, "A machine for harmonic synthesis," Proc. Phys. Soc., 56, 130 (1944).
10. Dan McLachlan, Jr., and E.F. Champaygne, "A machine for the application of sand in making Fourier projections of crystal structures," J. Appl. Phys., 17, 1006 (1946).
11. A.J. Rose, "Machine à calculer permettant la determination de fonctions periodiques et leur introduction dans des calculs," Centre Nat. Recherche Sci. Lab. de Bellevue (Paris, 1950), Vol. 7.
12. V. Vand, "A Fourier electron-density balance," J. Sci. Instr., 29, 118 (1952).
13. C.A. Beevers and J.M. Robertson, Collection: Computing Methods and the Phase Problem in X-Ray Crystal Analysis (X-Ray Crystal Analysis Lab., Pennsylvania State College, 1952), p. 119.
14. A.D. Booth, Fourier Technique in X-Ray Organic Structure Analysis (1948), p. 76.
15. J.M. Robertson, "A desk computer for Fourier analysis," Acta Cryst., 7, 624 (1954).

II. Machines Based on an Optical Analogy

16. C.W. Bunn, Chemical Crystallography (Oxford, 1946), p. 271.
17. H. Lipson and W. Cochran, The Determination of Crystal Structures (1953), pp. 140, 236.
18. C.R. Eller, "Le photosommateur harmonique et ses possibilités," Bull. Soc. Franc. Min. Crist., 78, 157 (1955).
19. C.R. Eller, "Sur un nouvel appareil pour le developement par voie optique des series de Fourier," Compt. Rend. Acad. Sci., 232, 1122, 2333 (1931).
20. L. Bru, M.P. Rodriguez, and M. Cubero, "Application of Eller's optical machine to the determination of crystal structures by the direct method," Acta Cryst., 7, 625 (1954).
21. L. Bru, M.P. Rodriguez, and A.L.L. Castro, "Application of Eller's optical machine to the determination of crystal structures by the trial-and-error method," Acta Cryst., 7, 625 (1954).
22. L. Bru, M.P. Rodriguez, and M.G. Gea, "Application of Eller's optical machine to the refinement of crystal structure," Acta Cryst., 7, 625 (1954).
23. M.M. Wolfson, "A photoelectric structure-factor machine," Acta Cryst., 4, 3, 250 (1951).
24. W. Hughes and C.A. Taylor, "Apparatus used in the development of optical-diffraction methods for the solution of problems in x-ray analysis," J. Sci. Instr., 30, 4, 105 (1953).
25. R. Fürth and R.W. Pringle, "A new photoelectric method for synthesis and analysis," Phil. Mag., 35, 643 (1944).

III. Electrical Analog Machines

26. L.R. Maxwell, "An electrical method for compounding sine functions," Rev. Sci. Instr., 11, 47 (1940).
27. T.B. Rymer and C.C. Butler, "An electrical circuit for harmonic analysis and other calculations," Phil. Mag., 35, 606 (1944).
28. G. Hägg and T. Laurent, "Machine for the summation of Fourier series," J. Sci. Instr., 23, 155 (1946).
29. C.A. Beevers and D. McEvan, "A machine for the rapid summation of Fourier series," J. Sci. Instr., 19, 150 (1942).
30. I.W. Ramsay, H. Lipson, and D. Rogers, Collection: Computing Methods and the Phase Problem in X-Ray Crystal Analysis (X-Ray Crystal Analysis Lab., Pennsylvania State College, 1952), p. 119.
31. L.V. Azároff, "A one-dimensional Fourier analog computer," Rev. Sci. Instr., 25, 471 (1954).

IV. General Reviews on the Principles of Constructing Pulse Computers

32. H.H. Aiken and G.M. Hopper, Automatically Controlled Calculating Machine [Russian translation from the English by M.A. Bykhovskii, Usp. Mat. Nauk, 4, 119 (1948)].
33. M.L. Bykhovskii, "Fundamentals of electronic mathematical discrete-counting machines," Usp. Mat. Nauk, 3, 69 (1949).
34. L.D. Kudryavtsev, "Principles of producing arithmetical operations on calculating machines," Usp. Mat. Nauk, 3, 104 (1950).
35. Murray, Theory of Mathematical Machines [Russian translation] (Inizdat, 1949).
36. Hartree, Modern Development of Computing Machines [Russian translation] (GNB).
37. I. Ya. Akushskii, "Brief sketch of computer-analyzers," Izv. otd. Tekh. Nauk AN SSSR, 8, 1081 (1946).

V. Application of Computer-Analyzers

38. P.A. Shaffer, V. Schomaker, and L. Pauling, "The use of punched cards in molecular structure determinations," J. Chem. Phys., 14, 648 (1946).
39. E.G. Cox, L. Gross, and G.A. Jeffrey, "Use of punched-card tabulating machines for crystallographic Fourier syntheses," Nature, 159, 433 (1947).
40. M.L. Hodgson, C.J.B. Clew, and W. Cochran, "A punched-card modification of the Beevers–Lipson method of Fourier synthesis," Acta Cryst., 2, 113 (1949).
41. E.G. Cox and G.A. Jeffrey, "The use of 'Hollerith' computing equipment in crystal-structure analysis," Acta Cryst., 2, 341 (1949).
42. J. Donohue and V. Schomaker, "The use of punched cards in molecular structure determinations. III. Structure-factor calculations of x-ray crystallography," Acta Cryst., 2, 344 (1949).
43. M.D. Grems and J.S. Kasper, "An improved punched-card method for crystal-structure factor calculations," Acta Cryst., 2, 6, 347 (1949).
44. E.G. Cox, L. Gross, and G.A. Jeffrey, "A Hollerith technique for computing three-dimen-

sional differential Fourier syntheses in x-ray crystal-structure analysis," Acta Cryst., 2, 351 (1949).

45. E. Cox, Collection: Computing Methods and the Phase Problem in X-Ray Crystal Analysis (X-Ray Crystal Analysis Lab., Pennsylvania State College, 1952), p. 132.
46. E.W. Hughes, Collection: Computing Methods and the Phase Problem in X-Ray Crystal-Analysis (X-Ray Crystal Analysis Lab., Pennsylvania State College, 1952), p. 141.
47. N. Kitz and B. Marchington, "A method of Fourier synthesis using a standard Hollerith senior rolling total tabulator," Acta Cryst., 6 , 325 (1953).
48. C.R. Hudgexs and A.M. Ross, "Computing Fourier syntheses in x-ray crystal-structure analysis," Anal. Chem., 25, 734 (1953).

VI. Application of Universal Electronic Computers

49. J.M. Bennett and J.C. Kendrew, "The computation of Fourier syntheses with a digital electronic calculating machine," Acta Cryst., 5, 109 (1952).
50. F. Ordway, Collection: Computing Methods and Phase Problem in X-Ray Crystal Analysis (X-Ray Crystal Analysis Lab., Pennsylvania State College, 1952), p. 148.
51. S.W. Wayer and K.N. Trueblood, "Three-dimensional Fourier summations on a high-speed digital computer," Acta Cryst., 6, 427 (1953).
52. F.R. Ahmed and D. Cruickshank, "Crystallographic calculations on the Manchester University electronic digital computer," Acta Cryst., 6, 765 (1953).
53. T. Thompson and D. Caminer, "The use of a high-speed automatic calculator in the refinement stages of crystal-structure determination," Acta Cryst., 7, 260 (1954).
54. A.S. Douglas, "The use of digital computers in structure analysis," Acta Cryst., 7, 624 (1954).
55. A.S. Douglas,"Application of the EDSAC to structure determination by a direct method," Acta Cryst., 7, 624 (1954).
56. M.M. Woolfson and W. Cochran, "Some experience of direct methods of Fourier structure determination," Acta Cryst., 7, 624 (1954).
57. D.W.J. Cruickshank,"The use of Manchester University electronic digital computer in detailed structure refinement," Acta Cryst., 7, 624 (1954).
58. W. Cochran and A.S. Douglas, "The use of a high-speed digital computer for the direct determination of crystal structures," Proc. Roy. Soc., A227, 1171, 486 (1955).

VII. Pepinsky Machine

59. R. Pepinsky, Collection: Computing Methods and Phase Problems in X-Ray Crystal Analysis (X-Ray Crystal Analysis Lab., Pennsylvania State College, 1952), p. 167.
60. R. Pepinsky, "R-PAC: Analog recorder-playback computer for crystal analysis," J. Appl. Phys., 24, 663 (1953).
61. R. Pepinsky, "Letters to the Editor," J. Appl. Phys., 24, 1520 (1953).

VIII. Magnetic Machines

62. A.D. Booth, "The application of MAGIC to the determination of crystal structures," Acta Cryst., 7, 626 (1954).
63. An. Vang, "Static magnetic storage and delay line," J. Appl. Phys., 21, 49 (1950).
64. An. Vang, "Magnetic delay-line storage," Proc. Inst. Radio Eng., 38, 626 (1950).
65. An. Vang, "Magnetic triggers," Proc. Inst. Radio Eng., 39, No. 4 (1951).